Finding Periods in the High Mass X-Ray Binary Stars of the Magellanic Clouds.

A Thesis Submitted to the
College of Graduate Studies and Research
in Partial Fulfillment of the Requirements
for the degree of Master of Science
in the Department of Physics and Engineering Physics
University of Saskatchewan
Saskatoon

By
Lorin Briand

Permission to Use

In presenting this thesis in partial fulfilment of the requirements for a Postgraduate degree from the University of Saskatchewan, I agree that the Libraries of this University may make it freely available for inspection. I further agree that permission for copying of this thesis in any manner, in whole or in part, for scholarly purposes may be granted by the professor or professors who supervised my thesis work or, in their absence, by the Head of the Department or the Dean of the College in which my thesis work was done. It is understood that any copying or publication or use of this thesis or parts thereof for financial gain shall not be allowed without my written permission. It is also understood that due recognition shall be given to me and to the University of Saskatchewan in any scholarly use which may be made of any material in my thesis.

Requests for permission to copy or to make other use of material in this thesis in whole or part should be addressed to:

Head of the Department Physics and Engineering Physics
162 Physics Building
116 Science Place
University of Saskatchewan
Saskatoon, Saskatchewan
Canada
S7N 5E2

Abstract

High Mass X-Ray Binary Stars (HMXBs) are stars that contain one early-type main sequence or giant star and one of a black hole, neutron star or white dwarf. HMXBs in the Large Magellanic Cloud (LMC) and the Small Magellanic Cloud (SMC) are instructive to study because both galaxies are metal poor in comparison to the Milky Way and they are fairly transparent to both optical and X-ray radiation. This allows a more complete study of the whole population, without the biasing effects of gas and dust that occur in our own Galaxy. The objective of this study was to find the periods of HMXBs in the LMC and SMC with known optical counterparts in the dataset acquired by the Robotic Optical Transient Search Experiment telescope. Two possible orbital periods were found for the objects XTE J0055-724 and RX J0101.3-7211 of 1724 days and 478 days, respectively. Continued observations are recommended to confirm the two periods.

Acknowledgements

I thank my supervisor, Gordon E. Sarty, as well as Stan Shadick for their advice and support of this research. Also, I thank Neil Johnson for his assistance in downloading the dataset.

This research made use of the SAO/NASA ADS Astrophysics Data System, and the SIMBAD database operated at CDS, Strasbourg, France.

I dedicate this thesis to my father and mother; Clarence and Audrey Briand.

Contents

List of Tables

List of Figures

List of Abbreviations

HMXBs	High Mass X-Ray Binary Stars
LOF	List of Figures
LOT	List of Tables
LMC	Large Magellanic Cloud
SMC	Small Magellanic Cloud
MCs	Magellanic Clouds
IRAF	Image Reduction Analysis Facility
RXTE	Rossi X-Ray Timing Explorer satellite
ROTSE	Robotic Optical Transient Search Experiment
OGLE II	Optical Gravitational Lensing Experiment phase II
MACHO	MAssive Compact Halo Object
LMXBs	Low Mass X-Ray Binaries
BeXs	Be X-ray Binaries
SGX	Supergiant X-ray Binaries
sgHMXBs	Supergiant High Mass X-ray Binaries
Quasar	QUAsi-StellAR object
2LPH	2005 Lui, Paradjis and Heuvel paper
AGN	Active Galactic Nucleus
QPO	Quasi-Periodic Oscillations
CCD	Charged Couple Device
ZAMS	Zero Age Main Sequence
PSF	Point Spread Function

Chapter 1

Introduction

Astronomical X-ray sources were first discovered from sounding rockets launched with Geiger counters as payload in 1962 by Giaccini *et al* [40]. Giaccini was able to localize an object called Scorpius XR-1 (now called Sco X-1) ([42] contains the paper by Giaccini in the appendix).

The theoretical models of High Mass X-ray Binary stars (HMXBs) have been proposed since the mid 1970's [42]. HMXBs are close binary systems where one companion has evolved into a neutron star or black hole and the other companion with a mass $> 10M \odot$ is still on either the Main Sequence or the Supergiant branch of the Hertzprung-Russell diagram. A list of HMXB sources has been compiled by Liu, van Paradijs, and van den Heuvel (hereafter 2LPH) [66], and forms the basis for target selection in this thesis.

1.1 The High Mass X-Ray Binaries

HMXBs provide a unique opportunity to study several areas of fundamental physics. First, the compact objects are excellent testing grounds for our knowledge of the effect of mass transfer on stellar evolution as well as testing theories of extreme physical processes that require high energy and intense gravitational fields. Some theories of mass transfer and stellar evolution make predictions about both the ranges and distribution of orbital periods in the HMXB population [24]. The objective of this thesis is to add to the list of known orbital periods. The opportunity also exists for serendipitous discoveries of other types of variations. Types of variability that can be detected are covered in Section 2.4 with more detail. Briefly, variability

like β-Cepheus pulsations, outbursts, ellipsoidal variation and other effects tell us a great deal about both the optical component and the circumstellar environment of HMXBs.

These systems are natural testing grounds for theories of extreme physical processes where there is high energy and intense gravitational fields. The first Black Hole candidate was found in a HMXB system – Cygnus X-1[6]. Black Holes do not emit any signal directly. Therefore, Black Holes can only be inferred by either the gravitational forces they exert on nearby bodies, or by radiation from accretion disks [68] and coronae [51] that form under certain circumstances in X-ray Binaries.

As well as testing extreme processes, these systems are a good test for how mass transfer affects stellar evolution in O and B type stars. The effects of mass transfer on stellar evolution can be dramatic and this is where optical observations are valuable [112]. They can steal mass from the less evolved partner and change the course of the system's evolution [114]. As van den Heuvel points out, mass transfer can even generate one White Dwarf where a neutron star would have evolved if the star were alone [114]. If the first partner to goes supernova and then spirals closer to the companion, it robs the less evolved star of mass and forces it to evolve into a White Dwarf. Any valid population models have to take this into account, so as to get the results that match known populations [25, 114]. Obtaining an orbital period for these systems can classify them as to which path they will evolve on, given the kick to the system by the first supernova. The supernova kick, if it does not disrupt the system entirely, will increase the orbital eccentricity [115]. Evidence that there are no kick supernovae comes from surveys that show two distinct HMXB populations, one with high orbital eccentricity, one with low eccentricity. (See section 2.3.5 for more details.) If we can survey the orbital periods of a complete population, we have a good check on the theory of evolution for interacting binaries by examining the distribution of orbital periods in that population.

1.2 HMXBs in the Magellanic Clouds

Inside our own Galaxy, the view of much of space is obscured by dust and gas within the galactic plane. As a result, we have a very biased sample of HMXBs [65]. If we consider only Galactic HMXBs we have a distorted picture of how often HMXBs form. If we look outside our Galaxy, we see a larger, less obscured sample of HMXBs. The metallicity of HMXBs in the LMC and SMC are not the same as in the Milky Way. This has an effect on the evolution of HMXBs [25]. Specifically, lower metallicity simulations produce more HMXBs, more Black Hole (BH) HMXBs, and a hint that low metallicity influences the population to have more no-kick supernovae. Interestingly enough, Dray's population models [25] fail for the SMC, possibly for the very reason of not predicting no-kick supernovae and that the SMC recently underwent a star formation burst. Some other important considerations of the Magellanic Clouds (MCs) over other associations of stars both in and out of our Galaxy are the following:

- The MCs are a tenth the distance of M31.
- The MCs are, on average, 4 kpc thick. Given that the distance to them is about 10 times the size of their thickness, this means that we can treat objects as being at the same distance.
- There is current star formation in the LMC and parts of the SMC. M31 has fewer massive stars than the MCs [73]. Hence the MCs are a better place to observe the whole population of HMXBs than M31.
- The SMC offers the highest-known density of HMXBs on the sky [65]. This is because the SMC underwent a recent and explosive episode of star formation from a close pass to the LMC.
- Star Formation Rate / Mass ratio is 150 times that of the Milky Way for the SMC and 100 times for the LMC [41].

- Being at high Galactic Latitude, the MC's HMXBs are less effected by the obscuring effects of dust than HMXBs within our own Galaxy.

For these reasons, the MCs make excellent choices for a place to conduct a study of as many HMXBs as possible.

1.3 The HMXBs in the ROTSE3a Data-set

Included are Tables 1.1 & 1.2: Lists of the sources of interest and maps of the SMC (Figure 1.1) and LMC (Figure 1.2) with HMXBs marked on them. There are 128 known HMXBs in both the LMC and SMC as of 2005. Of those, 76 have known optical counterparts and 51 out of the total have light curves in this thesis.

Table 1.1: A table of the HMXBs with optical counterparts located in the ROTSE3a's images of the SMC. Data is taken from 2LPH

No.	Name	RA	Dec	Vmag	SpType	Porb(d)
6	RXJ0047.3-7312	00 47 23.42	-73 12 27.3	16.19	B2e	48.8
7	AXJ0048.2-7309	00 48 14.90	-73 10 03.0	15.3	Be	
8	RXJ0048.5-7302	00 48 34.50	-73 02 30.0	14.6	Be	
9	AXJ0049-729	00 49 02.50	-72 50 52.0	16.92	Be	642
10	RXJ0049.2-7311	00 49 13.84	-73 11 36.7	16.51	Be	
14	RXJ0049.7-7323	00 49 42.00	-73 23 15.0	14.99	B1-3Ve	394
15	2S0050-727	00 52 07.70	-72 25 50.0	14	O9III-Ve	45.1
18	RXJ0050.7-7316	00 50 44.70	-73 16 05.0	15.44	B0III-Ve	1.42
21	RXJ0051.3-7216	00 50 55.80	-72 13 55.0	15.06	Be	88.4
27	RXJ0051.8-7231	00 51 53.00	-72 31 45.0	14.87	Be	28
28	RXJ0051.9-7311	00 51 52.29	-73 10 33.4	14.4	B[e]	67
31	2E0051.1-7304	00 52 52.40	-72 48 30.0	14.28	B0e	
32	XTEJ0052-723	00 52 06.60	-72 20 44.0	15.8	B0V-B1Ve	
33	XTEJ0052-725	00 52 09.10	-72 38 03.0	15.02		
34	RXJ0052.1-7319	00 52 13.90	-73 19 13.0	14.67	O9.5IIIe	
35	RXJ0052.9-7158	00 52 59.20	-71 57 58.0	15.46	Be	200
36	H0053-739	00 54 36.20	-73 40 35.0	16	B1.5Ve	
37	CXOUJ005323.8-722715	00 53 23.80	-72 27 15.0	16.19	Be	125
42	AXJ0054.8-7244	00 54 55.88	-72 45 10.5	14.78	O9Ve	261
43	XTEJ0055-724	00 54 56.17	-72 26 27.6	15.28	B0-1III-V	123
46	CXOUJ005527.9-721058	00 55 27.70	-72 10 59.0	16.8		
47	XMMUJ005605.2-722200	00 56 05.24	-72 22 00.9	16.51	Be	
48	XMMUJ005615.2-723754	00 56 15.20	-72 37 54.0	14.6	Be	
49	XMMUJ005724.0-722357	00 57 24.00	-72 23 57.0	14.7		

Continued on next page

No.	Name	RA	Dec	Vmag	SpType	Porb(d)
51	CXOUJ005736.2-721934	00 57 36.20	-72 19 34.0	15.97	Be	95.3
52	RXJ0057.8-7202	00 57 48.40	-72 02 42.0	15.65	Be	
53	CXOUJ005750.3-720756	00 57 50.30	-72 07 56.0	15.71		
54	RXJ0057.9-7156	00 57 57.00	-71 56 20.0	17.1	Be	
55	RXJ0058.2-7231	00 58 11.70	-72 30 50.0	14.9	B2-3Ve	59.72
57	RX J0059.2-7138	00 59 11.30	-71 38 45.0	14.1	B1IIIe	
58	1XMMUJ005921.0-722317	00 59 21.04	-72 23 16.7	15.02	B0	
62	CXOU J010036.9-721316	01 00 36.92	-72 13 16.3	16.73	B2V	
64	RXJ0101.0-7206	01 01 01.10	-72 06 57.0	15.81	B3-4Ve	
65	RXJ0101.3-7211	01 01 20.50	-72 11 18.0	15.49	Be	74.7
67	RX J0101.6-7204	01 01 37.56	-72 04 18.7	17.7	Be	
73	RXJ0103.6-7201	01 03 37.57	-72 01 33.2	14.65	O5Ve	
74	RXJ0104.1-7243	01 04 07.40	-72 43 59.0	14.1	Be	
75	RXJ0104.5-7221	01 04 35.60	-72 21 43.0	14.8	Be	
80	RXJ010619-720527	01 06 15.10	-72 05 25.0	16.7	B2-5III-Ve	
81	AX J0107.2-7234	01 07 10.90	-72 35 36.0	16.6	Be	
82	XTE J0111.2-7317	01 11 08.40	-73 16 46.0	15.32	B0.5-1Ve	
84	EXO 0114.6-7336	01 15 58.78	-73 21 25.0	11.89	B0I	
85	SMC X-1	01 17 05.50	-73 26 32.0	13.3	B0 Ib	3.890

Table 1.2: A table of the HMXBs in the LMC with identified optical companions that fit in the ROTSEIII data set. Data are taken from 2LPH.

No.	Name	RAJ2000	DEJ2000	Vmag	SpType	Porb(d)
99	RX J0516.0-6916	05 16 00.10	-69 16 09.0	15	B1V	
100	RX J0520.5-6932	05 20 30.30	-69 32 04.0	14.4	O9Ve	24.400
110	XMMU J053115.4-705350	05 31 15.40	-70 53 50.0	13.7		
121	3A 0540-697	05 39 39.50	-69 44 37.0	14.5	O8 III	4.220
123	RX J0541.4-6936	05 41 22.20	-69 36 29.0	12.01	B2SG	
122	XMMU J054134.7-682550	05 41 34.70	-68 25 50.0	13.7		
124	RX J0541.5-6833	05 41 37.10	-68 32 32.0	14.02	B0III	
127	1SAX J0544.1-7100	05 44 06.30	-71 00 50.0	15.33	B0Ve	286.000

1.4 Scope of Data

The data for this research are in the form of digital images, specifically .fit files produced by astronomical digital cameras. Information about the telescope which took the images is covered in detail in Chapter 3. A set of digital files that covers the same part of the sky is called a field. An individual digital photograph is called a plate, since before digital

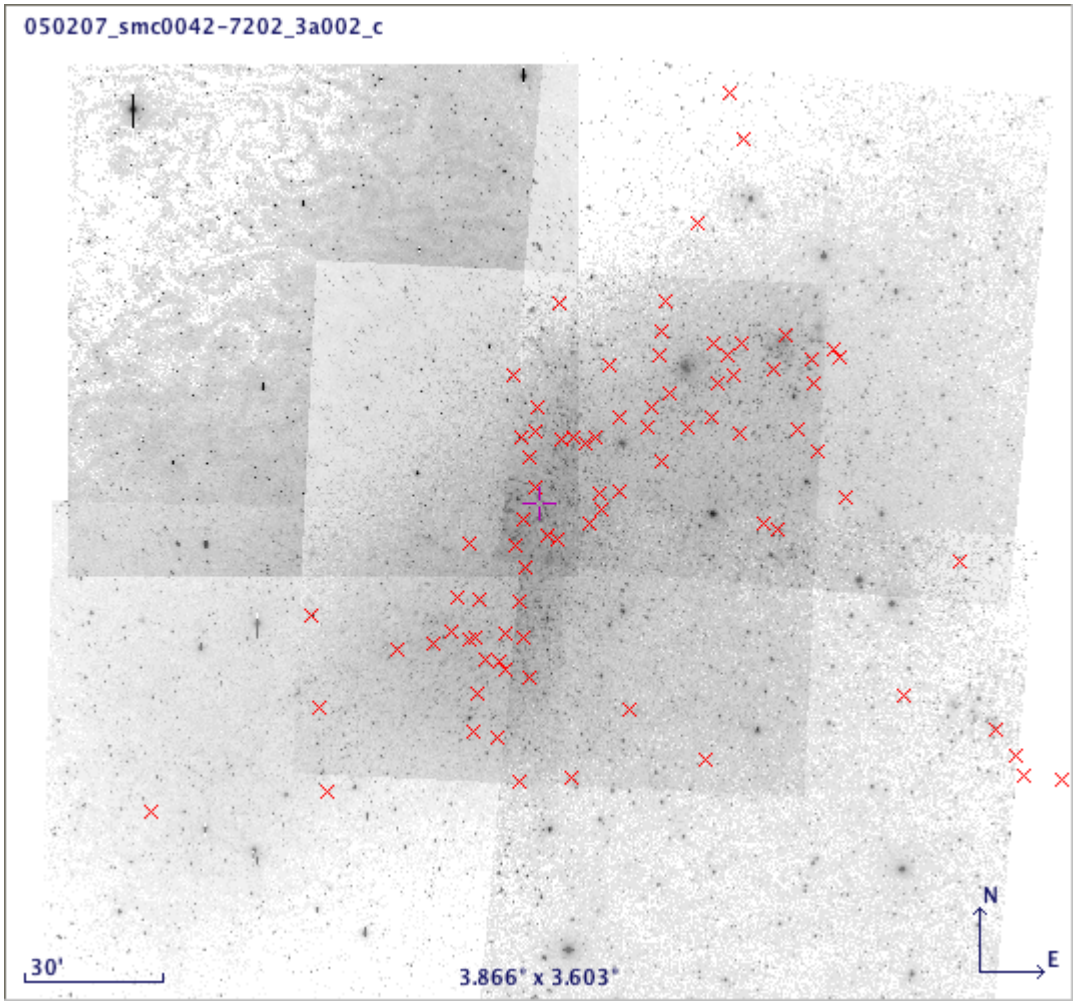

Figure 1.1: The Distribution of HMXBs with known optical counterparts in the SMC. Made from a mosaic of the fields in this study.

detectors all images were taken on glass photographic plates. The fields are coded by the galaxy (SMC or LMC) followed by the coordinates that mark the centre of the photograph. Thus SMC0103-7202 is a photograph of the SMC centered on 01^h03^m in Right Ascension (RA) and at $-72°02'$ Declination (Dec).

The data covers a period of 20 months. During this time atmospheric conditions limited the amount of data that was collected. Sometimes up to half the available images were no good (as in the case of the field SMC0103-7202), sometimes 95% of the images were available for processing (as with LMC0532-6953 in 2006). Most of the time only approximately 40% of the images were unusable.

The images covered 24'24" in Right Ascension (RA) 2°50' of sky in Declination (Dec). In a field this large, there were frequently several HMXBs. Therefore light curves for

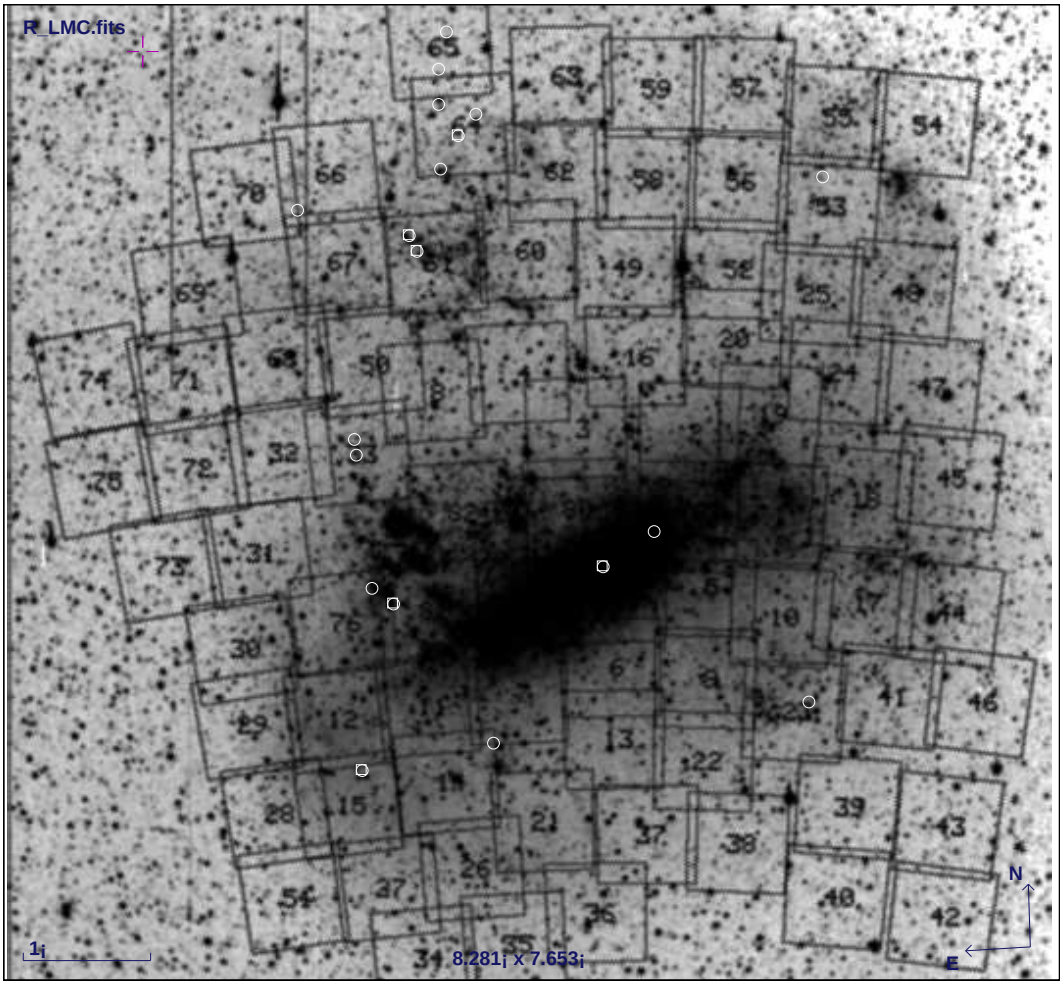

Figure 1.2: The Distribution of HMXBs with known optical counterparts in the LMC. Image by Greg Bothun, University of Oregon. Adapted by the MACHO collaboration.

multiple objects were generated for each field. Since the images overlap to some extent, multiple fields can contribute to the object's light curve, allowing triple the total data points than would otherwise be the case.

1.5 Outline

The main objective of this thesis is to search for additional orbital periods in the HMXB population of the MCs. The detection of other types of variation was also of interest.

This thesis is divided into 5 chapters. The second chapter covers the astrophysical properties of HMXBs and other X-ray sources. Also discussed in Chapter 2 are the types

of variability that these studies might detect. Chapter 3 introduces the reader to both the equipment that took the data and methods used to process the data. Chapter 4 contains the results in the form of light curves and Fourier transforms of these light curves and any significant detections. Lastly, Chapter 5 outlines what conclusions can be drawn from the results.

Chapter 2

Astrophysical Properties of HMXBs

2.1 Discovery of Astronomical X-Ray Sources

As noted in the introduction, astronomical X-ray sources were discovered by Giaccini and his research group in 1962. Much of the discussion here follows Gursky and Ruffini [42]. Giaccini also noted an X-ray background in addition to the one source he found near the Galactic centre on his detectors, (Scorpius is close to Sagittarius). At first, the only X-ray sources predicted were the Sun and the Moon. As technology improved, more extra-solar X-ray sources were found. Sounding rockets as well as balloon flights continued to be used, until December 1970, when UHURU (not an acronym, but Swahili for freedom) was launched. UHURU mapped the entire X-ray sky [42].

While the observational field was expanding, theoretical models were being developed to explain the measurements obtained from satellites, sounding rockets and balloons. The ideas that supernovæ could create neutron stars was already put forward in [3] and the nuclear processes occurring in a supernova to make a neutron star were outlined by A.G.W. Cameron in[9]. Cameron was working at Chalk River in Ontario at the time. The matching of Sco-X1 to its optical component in 1966 [91] further propelled the quest for an explanation of the nature of this source. Zel'dovich and Novikov, in the same year, described how X-rays could be generated by accretion onto a compact object [125].

Since the 1970s, other types of X-ray sources have been identified. With modern X-ray telescopes like *Chandra* and *Rossi X-ray Timing Experiment* (RXTE), more individual sources have been identified, classified and catalogued based on their behaviour.

2.2 Types of X-Ray Sources

Several types of objects in the sky emit X-rays. While there is a cosmic X-ray background, discrete sources can easily be seen in the output from telescopes now in orbit. The following is a list of objects whose X-ray emission is known:

The first (and brightest) astronomical object that emits X-rays is the sun. The solar corona is the source of the majority of X-rays, due to its high temperature and low density.

From this it follows that other stars emit X-rays in their coronae as well. However, at interstellar distances, coronal X-ray emission is part of the background [39].

Next are Active Galactic Nuclei (AGNs), a class that includes quasars. These are the nuclei of galaxies that are thought to have matter in-falling on the central supermassive black hole [68]. In many ways these are similar to micro-quasars (a special class of HMXB).

Supernovae and their remnants emit strong X-ray signals [52]. The Crab Nebula (M1) is the most well known example. As we know the date of the supernova explosion that created it (1054 C.E.), we have a very clear picture of the evolution of this object. Both the nebula and the associated pulsar in the centre are known X-ray sources.

Last are the X-ray Binaries. These are binary star systems that emit X-rays at a significant flux level. They can be transient, have long quiescent modes, or, can be X-ray pulsars. They come in several varieties based on the mass of the optical companion.

2.3 X-Ray Binaries

There are three broad categories of X-ray binaries: The Cataclysmic Variables (CVs), the Low- and High mass X-ray binaries. The following discussion on CV draws on [45], except where noted. For close binary stars, there are two concepts that are important to know: The Roche Lobe and the L1 point. The Roche Lobe is a theoretical equipotential surface generated by the balance of the both star's gravitational attraction. Fluid stellar matter will fill the enclosed volume as the radius of the star expands. The L1 point is the Lagrange point in the direct line between the centers of the two orbiting stars where gravitational forces cancel. If both stars fill their Roche Lobes, they touch at the L1 point.

2.3.1 Cataclysmic Variables

Cataclysmic Variables (CVs) are stars that contain a White Dwarf star in mutual orbit with a less-evolved star and where there is transfer of material from the younger star to the White Dwarf. White Dwarves are thought to be the final stage of stellar evolution for low and intermediate mass stars. Their degenerate cores (made of oxygen and carbon) were exposed by high stellar winds earlier on in their lives.

The primary optical characteristic of CVs is the cataclysmic outburst, an event where the brightness jumps several magnitudes and retains this peak level for up to a week before beginning a decline back to its normal state. CVs can vary in other ways that, on the surface, appear unpredictable; called flickering and Quasi-Periodic Oscillations (QPOs). Flickering is caused by turbulent flow in the accretion disk [88]. QPOs are thought to be caused by thermal instabilities in the accretion disk [104].

There are three broad classes of CV based on their variability: The Novae, an intense

thermonuclear runaway on the surface of the WD; The Dwarf Novae, a less intense explosion that reoccurs every few months and the polars, who are WD with strong magnetic fields.

CV accretion disks emit X-rays from their inner surfaces. However, a good portion of this X-ray illumination is reprocessed by the disk into visible and UV wavelengths. More still is absorbed by the interstellar medium. There are, however, X-ray light curves for many CVs but at far lower intensities than HMXBs and LMXBs. Both HMXBs and LMXBs contain many similar phenomena in their light curves as well.

Stars with neutron star or black hole compact companions fall into the other classifications of X-ray Binary: the Low- and High Mass X-ray Binaries.

2.3.2 LMXBs

Low Mass X-ray Binaries (LMXBs) are the other end of the mass spectrum from HMXBs and have a black hole or neutron star companion. These stars can be either K or M type stars on the main sequence. They exhibit many of the characteristics of polar class of CVs in their optical and X-ray light curves. The aforementioned Sco X-1 is an LMXB. The optical counterpart of an LMXB is a faint (if visible) star of mass $< 4M \odot$. Optical emission is dominated by the accretion disk if the NS's magnetic field does not stop one from forming. In most cases, accretion is wind-driven until the orbits shrink through mass loss and these systems end-up with very short periods and direct mass-transfer via the L1 point [104].

2.3.3 HMXBs

As noted in Chapter 1, High Mass X-Ray Binary stars (HMXBs) are constituted of a binary star system, where one companion has evolved and gone supernova. The collapsed stellar remnant is thought to be a neutron star or black hole.

HMXBs come in two major categories: BeX-ray Binaries (BeXs) and SuperGiant X-Ray Binaries (SGXs). The difference between the two is whether the optical star is on the Main Sequence or a Supergiant and is determined using the spectrum of the the optical star; Be stars having emission lines in their spectra and Supergiants having high luminosity.

Of the 128 sources in the 2LPH catalogue, only 4 are SGXs. The rest are BeXs. Also unusual is the fact that there are no BH HMXBs in the SMC, and only 2 in the LMC.

2.3.4 BeX

This is a sub-class of HMXB. BeXs tend to be divided into two groups based on orbital eccentricity, e. About half have circular orbits ($e < 0.25$) with low X-ray luminosity ($< 10^{34}$ ergs/s)[114]. In the circular orbit case, low eccentricity HMXBs are thought to

be formed via a kickless supernova; one which originated from a degenerate O-Ne-Mg core with electron capture. In the case of SMC X-1, this would imply mass transfer from a component that formed on the Zero Age Main Sequence (ZAMS) with a mass of 14 M ⊙and fell to about 8 M ⊙[116]. Others have high eccentricity and transient X-ray emissions that can reach 10^{38} ergs/s [116]. High eccentricity BeXs go into periodic outbursts when the compact object passes periastron and accretes mass from the optical component's circumstellar disk [83].

2.3.5 SGXs

Supergiant HMXBs, abbreviated SGXs (sometimes sgHMXBs), have excess emission in the infrared (taken as evidence of dust in the optical star) and a luminosity of $L_*/L_\odot \geq 4.0$, necessary for classification as a supergiant [56]. SGXs tend to have shorter periods than their BeX cousins [92]. The X-ray emissions are thought to be stellar wind fed as opposed Roche Lobe overflow fed if they are Supergiant Fast X-ray Transients (SFXT). The nature of SFXTs is not settled, however [117]. Walter and Heras define SFXT emission as fast transient X-ray emission in outbursts followed by low quiescent X-ray output. Otherwise, these are thought to be highly absorbed persistent systems because of the absorption of X-rays from the compact object by dust and the persistent nature of the X-ray emission [117]. SGXs also have their own section of the Corbet Diagram (see discussion below).

2.3.6 γ-Cas or Be/WD X-Ray Binaries

This is a newly proposed class of X-ray Binary [80]. The prototype for this class of binary is the star γ-Cas, an irregular variable star easily seen with the naked eye in the Northern Hemisphere. This classification is still under some debate because there is not the expected orbital variations in X-rays [89].

2.4 Types of Variability that can be Measured Photometrically

There are several regular signals that HMXBs can produce – signals that would be detectable in optical light curve data. The objective of this study is to find the orbital periods in MC HMXBs. If eclipses are visible, they will be preferentially seen in X-Ray data, as the compact object is eclipsed by the visual companion. Since the compact objects are small (as are the accretion disks), compared to the visual star they do not block much light from the visual companion. The effect of the compact object on the optical light curve is more subtle than it would be for an ordinary eclipsing binary, like Algol. At

times of X-Ray outburst, BeX stars may brighten by as much as a tenth of a magnitude for Galactic HMXBs [61]. Outburst occurs at or near periastron.

β - Cepheus pulsations are hypothesized to be in HMXBs, since these variations are found in single Be stars. Sarty *et al.* [92] found β - Cepheus pulsations for the Galactic HMXB RX J0146.9+6121. β - Cepheus pulsations are thought to be a mode of stellar pulsation. These pulsations are usually about a tenth of a magnitude in brightness and last about one third to one tenth of a day. They are only seen in O and B type stars. β - Cepheus pulsations are defined using both light curve variations and radial velocity curves; thus radial velocity curves are needed as confirmation any detection in light curves. This is a good check when looking for any orbital variation.

In SGXs, a variation of a tenth of a magnitude but at the orbital period of the star, is called ellipsoidal variation. Ellipsoidal variation is caused by the tidal forces induced by the compact object's gravity stretching the surface of the Supergiant star into an oval shape (see Figure 2.1). If the SGX is not close enough to deform the Supergiant (and thus not is likely disk accreter), it is likely a stellar wind accreter. However, stellar winds are not always uniform. (See section 2.4.1 for a discussion of wind accretion.) The mechanisms for the clumpy winds are not well understood. Clumpy winds are thought to be the cause of SFXT [114]. These wind clumps can create clumps in the accretion that lead to an X-ray outburst, visual outburst or both.

HMXBs, like Cataclysmic Variables, can exhibit irregular outbursts and long-term periods [101].

2.4.1 Effects of Accretion (and Decretion) Disks

Accretion

Accretion disks add to the complexity of HMXB systems. In HMXBs, the accretion disks can be temporary or permanent depending on the orbital characteristics of the system. In cases where the disks are temporary, the compact object passes close to the optical component and the gravity draws material from the Be star's circumstellar disk into its own orbit, thus forming the accretion disk, as long as there are no tidal resonances [83]. In cases where the periastron of the compact object is far from the circumstellar disk, accretion is wind-driven. In rare cases the disk is permanent, due to a close orbit of the compact object to the other star.

The interaction with the disk, or a lack of it, determines the type of eruptions that are detected in X-Rays. The luminosity of the outburst can be in the range of $L_x = 10^{(36-37)}$ ergs. (See below for the origin of Type II outbursts.)

The energy released by accretion comes entirely from gravitational potential energy:

$$L_{acc} = \frac{GM\dot{M}}{R_*} \tag{2.1}$$

Where L_{acc} is the luminosity of the accreting material, G is the universal gravitational constant, $\dot{M}$ is the mass infall rate and R_* is the radius of the neutron star/event horizon of the black hole. However, not all of this energy is radiated away, only about half is [47].

The minimum inner radius is called the Alfvén radius, or the radius where magnetic pressure is balanced by ram pressure. If the magnetic field lines are passing faster than the orbital material due to the rotation of the neutron star, material is ejected in streams that look like sprinklers. If it is moving slower, the material can follow magnetic field lines to the magnetic poles of the neutron star.

Decretion

Decretion (the reverse process of accretion – also referred to as mass loss) occurs in a belt around the equator of a Be star. This is thought to occur because of the high spin of these stars, in combination with non-radial pulsations. The exact nature of the formation process is not completely understood. It is here that the dust is formed and the infra-red excess is caused. Decretion disks can also disappear in Be stars.

Reig, Fabregat and Coe report that the Hα line widths are limited in a manner proportional to the orbital period of BeXs [87]. This provides evidence that in HMXBs the decretion disks are truncated by the presence of the compact object. Osaki, in 1996 showed that a disk that obeys a Shakura-Sunyaev viscosity characterization will be truncated to a 3:1 resonance with the orbit of the compact star [85]. Shakura-Sunyaev showed in 1973 that any accretion disk with turbulence (or, as is now believed magnetorotational instability) could shed angular momentum [85, 4].

If the compact star passes through the decretion disk while passing periastron, the result is a Type I eruption. The outbursts occur at the same frequency as the orbit. If the decretion disk of the primary has expanded to cover most of the orbit of the compact object, a Type II outburst may occur. The Type II outburst is a brightening that may last for months. In X-rays, this may be $L_x \geq 10^{37}$ ergs. In visible light, this may be up to a magnitude!

The Evolution of HMXBs

HMXBs are short-lived objects due to the nature of the O and B stars that are their constituents. Main Sequence lifetimes of O and B stars (over 8 M $\odot$) are thought to be on the order of 10^7 years [47]. Since these stars live fast and die young, the time between supernovæis between one and ten million years.

Figure 2.1 is a schematic of the possible evolution of a close binary system in the first column and a slightly wider system in the second column. In this figure it is the left star that evolves first, to become a Wolf-Rayet (WR) star (i.e. a star that has blows off it's outer hydrogen layer and is an exposed stellar core) [47].

This system is not an HMXB until the star on the left has gone supernova. In the first case it is a BeX (left), in the second it is an SGX (right). There are 3 points at which the system can unbind: at either supernova explosion or if mass loss from the second star is so extreme that it loses half its mass. Otherwise, these stars are bound to their fates [62].

The transfer of mass at all stages has an enormous effect on the transfer of angular momentum between stars. At various stages it will spin-up (or down) the neutron star. The 'recycled pulsar' is one such spin-up arrangement. The star spins down to an equilibrium state to allow accretion. With the demise of its partner, it will be spun-up again – thus 'recycled' [62].

One way to classify HMXBs and demonstrate their evolution is with the Corbet Diagram. [17] The Corbet Diagram is a diagram that plots the X-ray pulsar period versus orbital period. While there is much scatter in the diagram, it allows a fair amount of prediction for the orbital periods of systems for which that is unknown. It also allows a rough classification of the type of the system, even before the optical counterpart has been found! In the figure 2.2, from [72], squares are SGXs, diamonds are wind-fed systems and anomalous systems are + signs. X is the Galactic system EXO 1722-363 and the filled diamond is OAO 1657-415. The sources in this diagram are all within our own Galaxy.

The key reason the relation between pulse period and orbital period exists is that unless the neutron star can accrete matter, it is spun-down until its co-rotation radius falls below the Alfvén radius (or the radius where the ram pressure equals magnetic pressure). Following [36] the magnetic pressure is:

$$P_{mag} = \left[\frac{4\pi}{\mu_0}\right] \frac{B^2}{8\pi} \tag{2.2}$$

The magnetic field is treated like a dipole so $B = \mu/r^3$ where r is a radius from the surface of the neutron star and μ is the magnetic moment of the neutron star.

The ram pressure is:

$$|\rho v|\, v = \frac{(2GM)^{1/2}\dot{M}}{4\pi r_M^{5/2}} \tag{2.3}$$

Where v is the free-fall velocity, and $|\rho v|$ is the accretion rate. Equate these and solve for r, you get the Alfvén radius.

$$r_M = \left(\frac{2\mu^2\pi}{\mu_0\sqrt{2GM}\dot{M}}\right)^{\frac{2}{7}} \tag{2.4}$$

This equation can be rewritten using the accretion luminosity 2.1 and substituting numerical values for constants and defining $L_{37} = L_{acc}/10^{37}$ erg/s, $R_6 = R_*/10^6$ cm and $\mu_{30} = 10^{30}$G cm^3. (With a reasonable values of $B_* = 10^{12}$G and $R_* = 10^6$cm, for a neutron star, using the unit of μ_{30} makes sense.) [36]

$$r_M = \left[2.9 \times 10^8 M_1^{1/7} R_6^{-2/7} L_{37}^{-2/7} \mu_{30}^{4/7} \text{cm}\right] \tag{2.5}$$

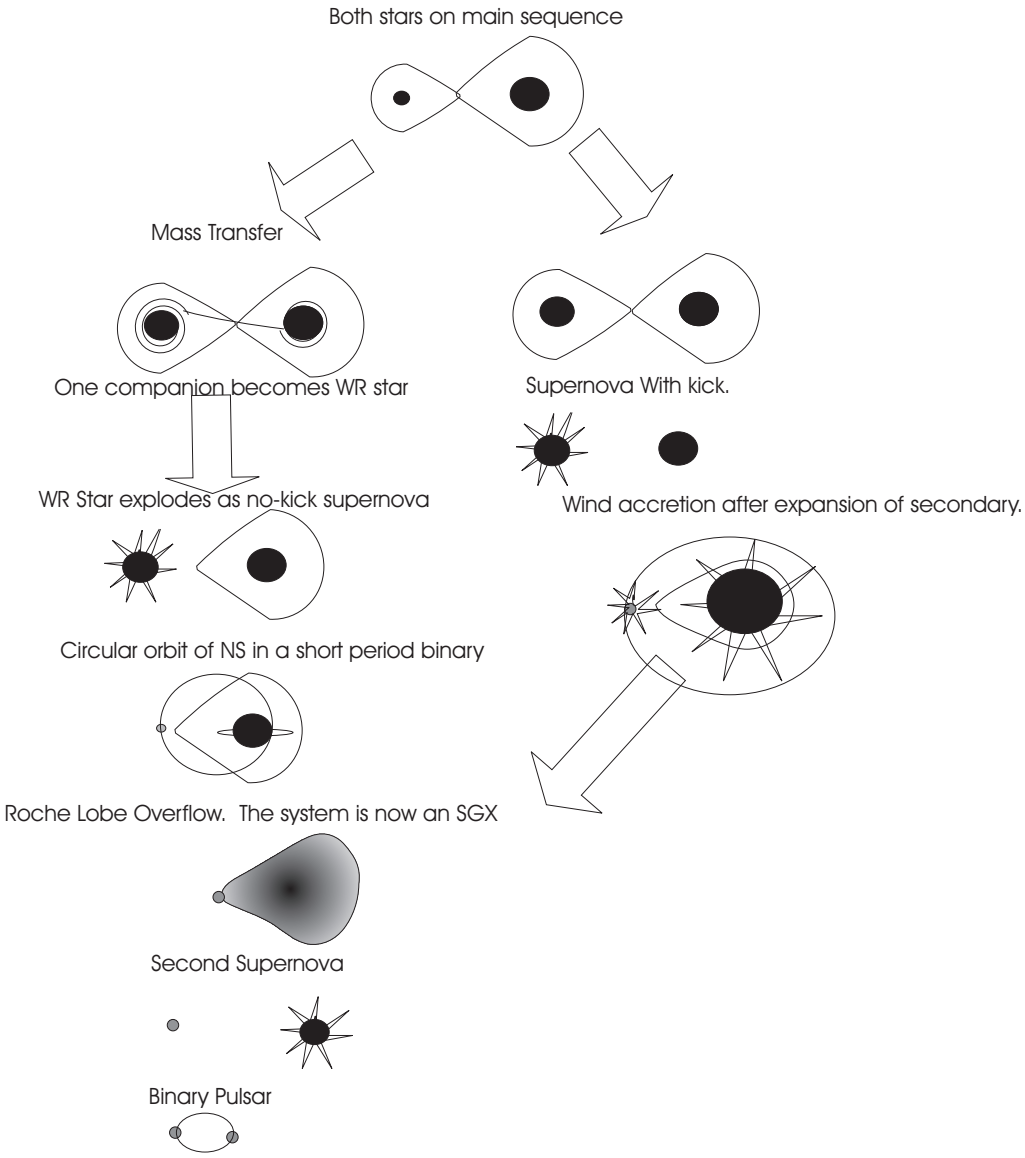

Figure 2.1: An evolutionary model of HMXBs. Adapted from [62]

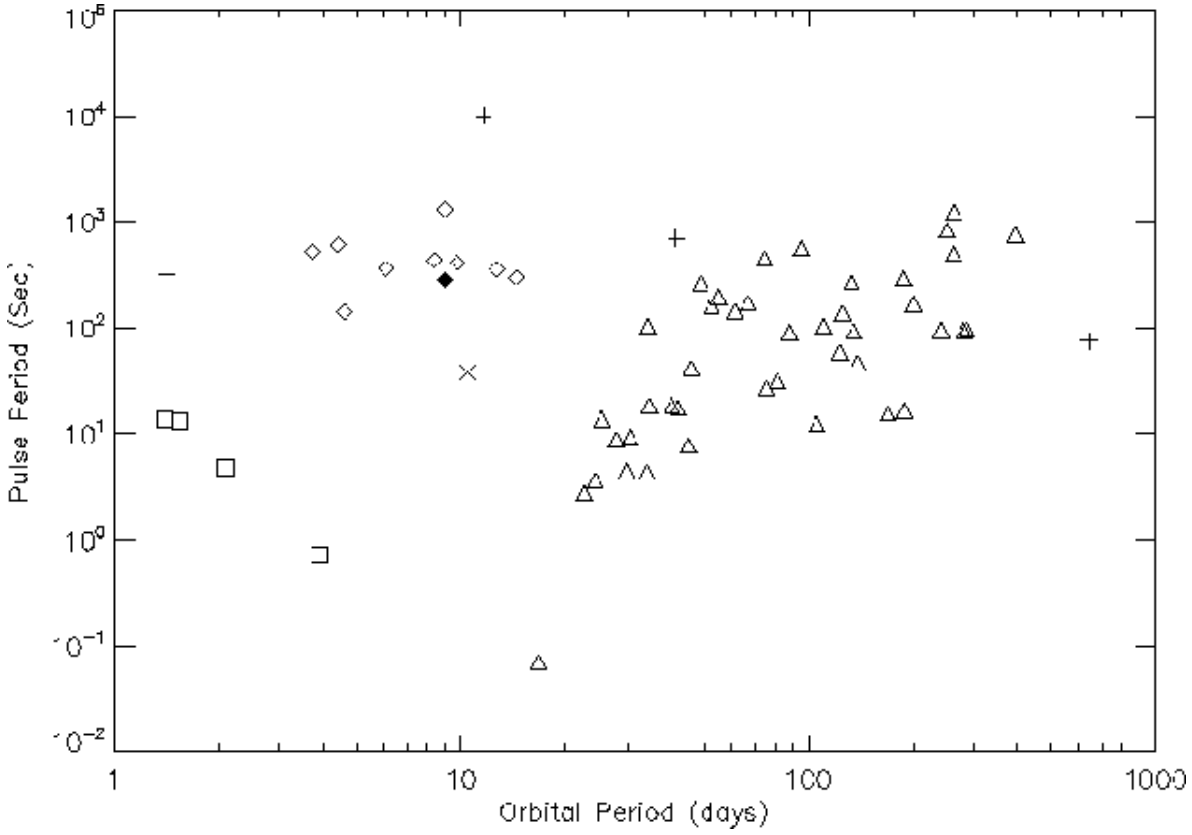

Figure 2.2: A Corbet Diagram from Mason [72].

Chapter 3

Photometric Data Acquisition and Analysis

This chapter will outline the process of photometric data reduction used for the ROTSEIII data and how the light curves were produced. In some circumstances, more detail is available in Appendix 2.

3.0.2 Other Photometric Datasets

There are several large public datasets that cover the directions of the LMC and SMC. Most notably, there are the Optical Gravitational Lensing Experiment (OGLE) II dataset, MAssive Compact Halo Object (MACHO) Project and Hubble Space Telescope archives.

Both the OGLE II and MACHO datasets have been analyzed primarily by Martin Coe. [37, 58, 11, 32, 12, 57, 27] In Chapter 4, references are provided for each star and many of these are the results of Coe's analyses of OGLE and MACHO data. These two datasets contain more than 10 years of data, enabling long-term study of HMXBs and other variable stars. A systematic error in the MACHO dataset causes a period of a half year to appear in that data[99].

For this project, the ROTSEIIIa dataset was selected. The ROTSEIII data program's data products are not made publicly available. With an application, the images are available on the internet via the Simple Image Access Service, via the University of New South Wales (UNSW) website. The data were made available by M. Ashley and G. Sarty. This dataset has not been analyzed for HMXBs before. The discussion on the ROTSEIIIa telescope follows [2].

3.1 The ROTSEIII Telescope

The data obtained for this thesis are obtained from the ROTSEIIIa located at the Siding Spring Observatory, near the town of Coonabarabran, New South Wales, Australia. The ROTSEIIIa camera was designed to look for transient optical sources, like the afterglow

from Gamma Ray Bursts. The ROTSEIIIa is an optical telescope, operating in the frequency range of 350 to 900 nm. See figure A.1 and Table A.1 for the spectral response of the camera. As part of a network of such telescopes, 4 around the world, it was meant to be easily and cheaply manufactured. The optical and mechanical design is slightly more complicated than other telescopes of the same size due to its need to slew quickly and have a wide field of view. The telescope's mount was modified from a standard fast-tracking mount design in order to maximize the rate a which the telescope could slew. The software that controls all aspects of the telescope's functioning was custom written by the design team to use an absolute minimum of bandwidth as these telescopes would be in remote locations around the world. Technical information about the ROTSEIIIa telescope is available in Appendix A.

The data are in the form of fit format images taken by the ROTSEIIIa telescope and are stored in a database called the Simple Image Access Service that is available via the internet. The images were taken between September, 2005 and April 2007. It should be noted that the lack of a filter on the ROTSEIIIa data, makes it difficult to transform to a standard magnitude system. Technical specifications follow in Appendix A. The ROTSEIII data acquisition is entirely automated from scheduling to camera to calibration.

The Marconi Applied Technologies CCD

The Marconi Applied Technologies CCD42-40-2-343 model Charge Couple Device (CCD) is the optical detector chip attached to the ROTSEIII telescope. The manufacturer's specification is available in [64]. The spectral response of the chip is given in Table A.1 in Appendix A. It responds best to the red portion of the visible spectrum. It was chosen to cool the CCD with propylene glycol for best results. The camera is cooled to about $-20°C$. This won't eliminate dark current, but it will reduce it.

One disadvantage to thinned CCDs is fringing [90]. The emission lines from the night sky reflect off the CCD backing and interfere with each other causing fringing patterns to appear. Fringing would be diminished by a filter, since they are narrow band in nature. However, because this telescope is un-filtered, the fringing interferes with the PSF (see section 3.5) and the magnitudes it produces. In order to correct for this a fringe map must be made from flats.

3.2 Calibration of Images

Before any work to obtain data from images is performed, the CCD images must be calibrated. This calibration is done using the additional images that were taken before observing begins: The dark, bias and flat frames. The following discussion follows Milone [78] and Budding and Demicran [8].

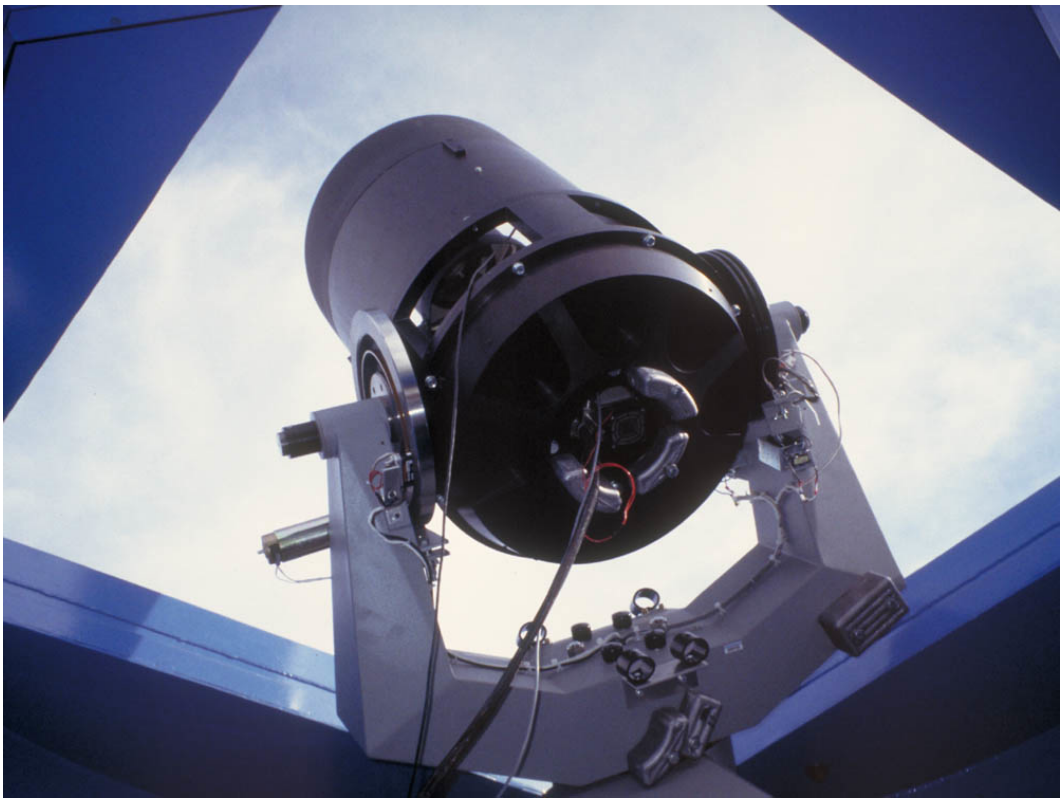

Figure 3.1: The ROTSEIIIa telescope. The photo is taken from the ROTSE collaboration website[a].

[a] `http://www.rotse.net/equipment`

3.2.1 Bias Frames

Even when not illuminated, CCDs have a base number of counts registered in each pixel due to bias voltage. To eliminate these base counts and to find and eliminate hot pixels (pixels that register too many counts when not exposed) this bias level must be subtracted. Several bias exposures are therefore taken to measure bias counts experimentally, and the median bias is subtracted. The result is a master bias frame which is then subtracted from all frames taken that night.

This bias subtraction was done automatically by the ROTSEIII software.

3.2.2 Dark Current Correction

Similar to bias frames, dark frames are taken to measure the current in the CCD generated by thermal activity without light falling on the chip. Several frames are taken for the expected length of the exposures taken that night and averaged. This is then subtracted from the actual plate after correction for exposure length.

This dark current subtraction was done automatically by the ROTSEIII software.

3.2.3 Flat Fielding

Flat fielding is done to eliminate the inter-pixel variation on the CCD as well as images of dust rings and imperfections in the optics of the telescope. A flat field is normally taken at dusk when sky illumination is fairly even. As noted in the CCD section 3.2.3, a further step is taken to make a map of the interference patterns created by the back-lit CCD. Flats need to be bias and dark subtracted before being applied to star fields.

This flat fielding was done automatically by the ROTSEIII software.

3.3 The Simple Image Access Service

The Simple Image Access Service is developed and maintained by the University of New South Wales in Sydney, Australia. The operation of the service is outlined in [113]. It contains data from the Automated Patrol Telescope (APT), the ROTSEIIIa telescope, as well as the APT webcam and the CONCAM all sky imager and several NOAA satellite images.

The astronomical data is not publicly available, but can be accessed with a registration to the site and contact with the owners of the data (i.e. one of the investigators on the ROTSEIII project). The data are catalogued according to coordinates in Right Ascension and Declination, date, telescope, object and airmass. A list of all images fitting the desired parameters is created and a thumbnail is generated, along with the header information from the file. When the images are selected, they are processed into a .tar file gziped in the downloads history page. Files are automatically removed from the downloads page after a week.

3.4 The Heliocentric Julian Date

The Julian Date is a system of time measurement that keeps track of each day as a simple number, without reference to months. Day 1 was January 1, 4713 BCE at noon in Greenwich. In order to eliminate light travel time errors, the reference frame of the Sun is used; thus Heliocentric Julian Date is the Julian Date minus or plus the light travel time to the Sun.

3.5 Extracting Photometric Data

The process of measuring the magnitudes of stars requires the use of computer routines. The computer must be programmed to differentiate between objects that are stars, background or other phenomena (e.g nebulas). Also, one must do a basic aperture photometry

to build the Point Spread Function (PSF) (treated in detail below). The absolute scale of the PSF is unimportant because differential photometry is used.

The data were downloaded from the internet database already calibrated using standard methods outlined in section 3.2 (e.g. bias correction, dark subtraction and flat-fielding). The process that was used to measure the magnitudes of stars in the data is called Point-Spread Function photometry, or PSF photometry. PSF photometry was used instead of sky-annulus photometry as other stars may contaminate the sky background in crowded fields like in the MCs. We follow Budding and Demicran [22] and [78] unless otherwise noted.

PSF photometry is used on CCD images since real telescopes are not ideal and do not focus all of the star's light into one point (or pixel) on the detector. Instead the light that makes up the image of the star is spread out over several pixels. Starlight is diffracted by the telescope aperture and spread out by turbulence in the atmosphere in a process astronomers call seeing. All stars regardless of magnitude are considered point sources. The PSF itself is analytically specified by the user for each plate when dealing with very large data sets like this one. (The analytic PSF is supplemented with a look-up table that is empirically derived.) Figure 3.2 shows a sample PSF; a Moffat Function to the power 2.5. This is called Moffat25. For PSF photometry in crowded fields, Moffat25 is usually better. Moffat25 is defined as [22]:

$$\text{Moffat25}(x, y) = \frac{A}{(1 + \frac{x^2}{p_1} + \frac{y^2}{p_2} + xyp_3)^{2.5}} \tag{3.1}$$

Where A is a normalization constant given by the aperture photometry step, x and y are plate coordinates, p_1, p_2, and p_3 are parameters that are fit by IRAF. Once the PSF is defined, the next step is to do differential photometry.

Differential photometry is a method of comparing light from a target star to a comparison star (comp) and a check star (chk). As opposed to all sky photometry where you flux calibrate your detector with standard stars in a catalogue to extract magnitudes directly, differential photometry allows you to pick a convenient star for comparison. In essence, differential photometry subtracts the variations in brightness of a non-variable star that is close by on the sky from the variable which provides a cancellation against atmospheric variations. The check stars are used to check if the comp star is variable. The magnitudes created in this technique are called differential magnitudes, to distinguish them from the standard magnitude system.

The definition of differential magnitude is:

$$\Delta m = -2.5 \log_{10} \left(\frac{F_o - F_s}{F_c - F_s} \right) \tag{3.2}$$

Where F_o, F_c, F_s are the fluxes of the object, comparison star and sky, respectively. However, this can be rewritten using the definitions of magnitude of your object (M_o) and comparison star (M_c):

$$M_o = -2.5 \log_{10} (F_o - F_s) \tag{3.3}$$

$$M_c = -2.5 \log_{10} (F_c - F_s) \tag{3.4}$$

Equation 3.2 becomes:

$$\Delta m = M_o - M_c \tag{3.5}$$

Since the stars are on the same image, no correction for atmospheric absorption is necessary.

Rather than write all of the software from scratch, the Image Reduction Analysis Facility (IRAF) was used to generate the PSF and measure the instrumental magnitudes of the target stars. Multiphot [1] was used to compile the light curves. Multiphot uses pattern matching between one reference plate and all the other plates to assign each star an ID number. The process behind Multiphot is outlined in [46]. A program called "dp", written by Gordon Sarty, was used to do the actual differential photometry. The details of these programs are available in Appendix B.

The end product of this process is a light curve: a graph of the brightness (in differential magnitudes) of a single star across different fields and plates versus time.

3.6 Finding Periods

After extracting the photometry from the images, the data were organized into light curves. Period04 is a standard program for use by the astronomical community for doing Fourier transforms of light curves. The user's manual appeared in [59], which is the source followed in this section. Period04 does a Discrete Fourier Transform on data. This makes it easy to find the period of the star, as the orbital period is usually the highest peak in the Fourier Transform of the light curve. Phase and a revised amplitude are calculated once a period is identified using a Least Squares fit. Data can be prewhitened to show additional periods in the light curve. Prewhitening is a process where the best fit amplitude and phase for a given frequency is subtracted from the data, leaving only the residuals of the fit. In summary:

1. Extract the first period from your light curve file by doing a Fourier Transform.

[1] Multiphot is distributed by Michael Richmond, at http://spiff.rit.edu/ensemble/

2. Find the phase, refine the amplitude and (most importantly) frequency with a least squares sinusoid fit.

3. Check the Signal to Noise (SNR).

4. Prewhiten your data if the SNR is > 4 (i.e. a significant detection). Using the SNR of 4 is a rule of thumb.

5. Find next frequency following steps 1 and 2.

6. Stop when your Signal to Noise Ratio (SNR) falls below 4.

Proceeding in this manner allows you to get as many signals from your data as possible. Each pass through the iteration above reduces the residuals from which your next signal is extracted. The objective is to minimize these residuals. The SNR is a measure of the significance of the peaks. A $S/N > 4$ is considered a potentially significant detection. In order for these results to make more sense, a periodogram is produced. A periodogram is a graph of amplitude versus frequency showing the peaks (and noise); in essence a Fourier spectrum.

The noise of the system is assumed to be white; that is constant across all frequencies. On the periodogram, the peak in the frequency spectrum is four or more times the amplitude of noise background for a significant detection. The false alarm probability roughly follows Z-statistics. A $S/N > 4$ means that the odds that your signal is in fact some form of noise have fallen well below 5%.

A graph where the data are re-plotted over the length of one cycle at the frequency determined by the Fourier transform is a folded light curve. These graphs allow for easier visual inspection of the results of period searching.

3.6.1 Fourier Transforms, Convolution and Identifying Periods

The following discussion follows [111]. The data that the Fourier transform work on are not continuous. They have gaps and appear like a signal has been convolved with a set of impulses separated in time by a varying distance t_n. Thus, it is important to select only cycles that are smaller than $\Delta\bar{t}$ the average of the varying distance t_n. The maximum frequency at which reliable data can be obtained is the Nyquist Frequency (in this case for $\Delta\bar{t}$ is the average separation):

$$\sigma_n = \frac{1}{2\Delta\bar{t}} \tag{3.6}$$

In addition to the Nyquist frequency, one must be aware of the Fourier transform's window function. For a Fourier transform of the data (using the Discrete Fourier transform)

$\hat{\text{d}}$:

$$\hat{d}(\omega) = \sum_{n=1}^{N} d\left(t_i\right) \exp 2\pi i \omega t_i \tag{3.7}$$

Where $d(t_i)$ is the the series that makes up your data and $\sum_{n=1}^{N} \exp\left(2\pi i \omega t_i\right)$ is the window function ($\hat{\text{w}}$). The data, when graphed as a light curve, is a multiplication of the unmeasurable continuous signal and the train of impulses at the time separation of the data (w): $d = f \cdot w$. Once the Fourier transform is done, the periodogram is the convolution of the signal with the window function $\hat{d} = \hat{f} * \hat{w}$ (The convolution theorem). A frequency peak – ideally an impulse – takes the shape of the Fourier transform of the window function.

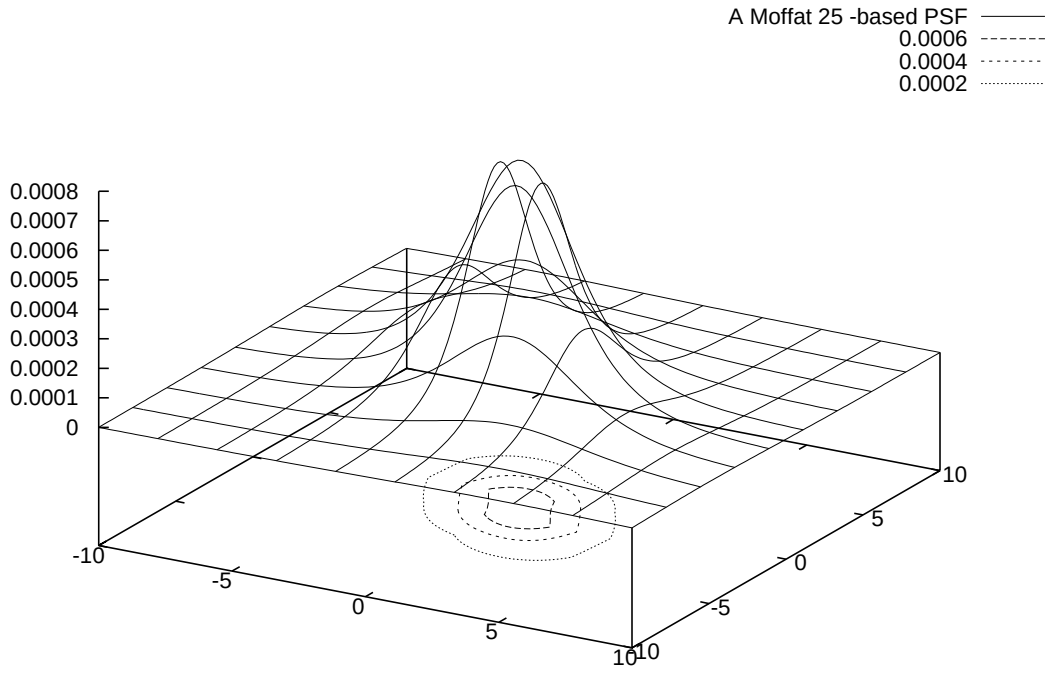

Figure 3.2: A Simple Moffat25 PSF. If the telescope were perfect and in vacuum, the star would be a point.

Chapter 4

Results

Of the 129 targets in the 2LPH catalogue, 51 that had known optical counterparts fell into the field of view of the ROTSEIII telescope. Light curves were obtained for these targets, where they were distinguishable from background or foreground objects. This chapter will draw attention to results obtained while looking for orbital periods. The following tables 4.1 and 4.3 relate the history of discovery for each star. Where appropriate, a brief history of discoveries related to each star will be related, so that this work is presented in context. Each star has a light curve (see Section 3.5), a periodogram (Section 3.6), a window function and a folded light curve (Section 3.6). The light curves, periodograms, window functions and folded light curves are the work done by the author. The window functions presented in the figures were normalized by dividing all frequencies by the highest peak in the window frequency spectrum. The y-axes of the light curves are in differential magnitudes, that is magnitudes generated by differential photometry, using Figure A.1 as the band. The period that was used to create each folded light curve is given in the figure caption.

4.1 SMC

Table 4.1: A list of the targets from the SMC and the references that give the history of each object.

No.	Name	X-ray discovery	Optical match	Period Found
006	RX J0047.3-7313	[48]	[44]	[23]
007	AX J0048.2-7309	[122]	[122]	
8	RX J0048.5-7302	[124]	[110]	[96]
9	AX J0049-729	[48]	[44]	[65]
10	RX J0049.2-7311	[48]	[34]	
14	RX J0049.7-7323	[123]	[27]	[19]
15	2S 0050-727	[63]	[63]	[28]
18	RX J0050.7-7316	[21]	[21]	[121]

Continued on next page

No.	Name	X-ray discovery	Optical match	Period Found
21	RX J0051.3-7216	[15]	[110]	[101]
27	RX J0051.8-7231	[7]	[44]	[99]
28	RX J0051.9-7311	[21]	[21]	[57]
31	2E 0051.1-7304	[7]	[44]	
32	XTE J0052-723	[16]	[57]	[12]
33	XTE J0052-725	[14]	[29]	[37]
34	XTE J0052-725	[55]	[19]	[37]
35	RX J0052.9-7158	[118]	[21]	[37]
36	RX J0054.5-7340	[63]	[86]	[104]
37	CXOU J005323.8-722715	[44]	[44]	[44]
42	AX J0054.8-7244	[54]	[44]	[32]
43	XTE J0055-724	[50]	[44]	[58]
46	CXOU J005527.9-721058	[31]	[31]	
47	XMMU J005605.2-722200	[49]	[122]	[99]
48	XMMU J005615.2-723754	[109]	[109]	
49	XMMU J005724.0-722357	[109]	[109]	
51	CXOU J005736.2-721934	[82]	[70]	[101]
52	RX J0057.8-7202	[118]	[44]	[82]
53	CXOU J005750.3-720756	[54]	[44]	[37]
54	RX J0057.9-7156	[55]	[44]	
55	RX J0058.2-7231	[54]	[44]	[77]
57	RX J0059.2-7138	[76]	[76]	[102]
58	XMMU J005921.0-722317	[71]	[71]	[37]
62	CXOU J010036.9-721316	[66]	[66]	
64	RX J0101.0-7206	[53]	[27]	[11]
65	RX J0101.3-7211	[54]	[73]	[101]
67	RX J0101.6-7204	[118]	[44]	
73	RX J0103.6-7201	[95]	[44]	[98]
74	RX J0104.1-7243	[54]	[44]	
75	RX J0104.5-7221	[95]	[44]	
80	RX J0106.2-7205	[49]	[75]	
81	AX J0107.2-7234	[7]	[44]	
82	XTE J0111.2-7317	[10]	[13]	[102]
84	EXO 0114.6-7336	[10]	[13]	[102]

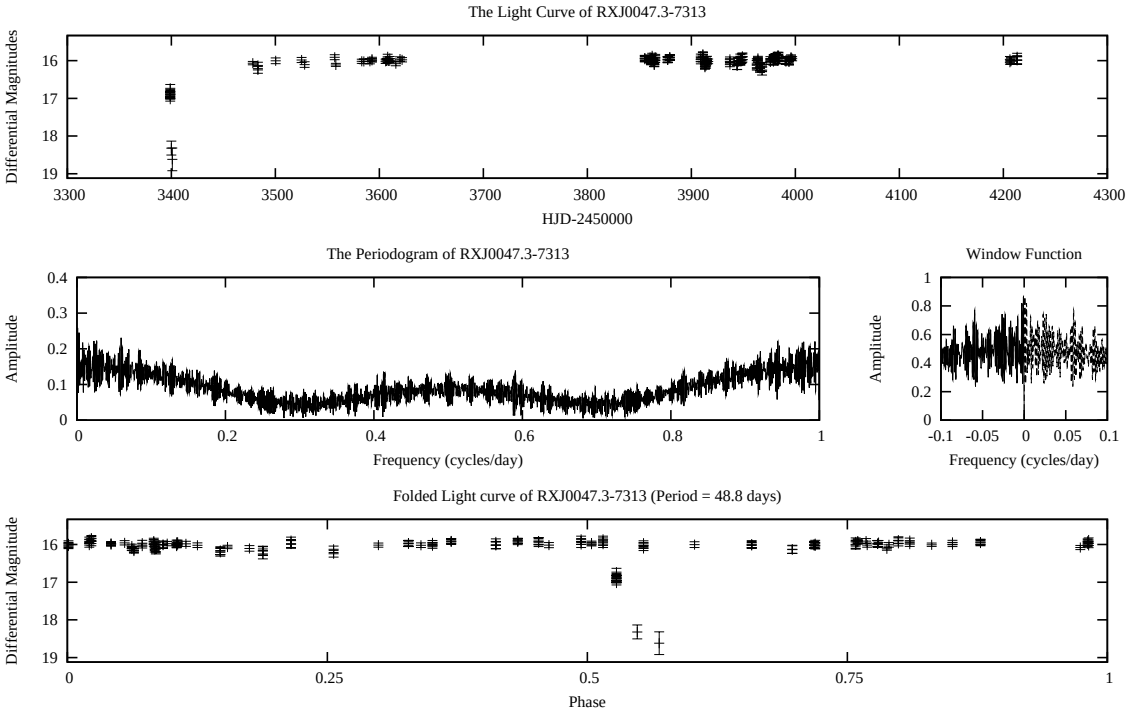

Figure 4.1: The Light Curve, Periodogram and Window Function of RX J0047.3-7313 This star has a listed period of 48.8 $\pm$ 0.6 days [30] or 49.1 $\pm$ 0.2 days [97] in two different papers. As the values overlap error regions, it can be argued the true period falls in this range. The folded light curve was made to the 48.8 day period, since the frequency that was found had a small SNR.

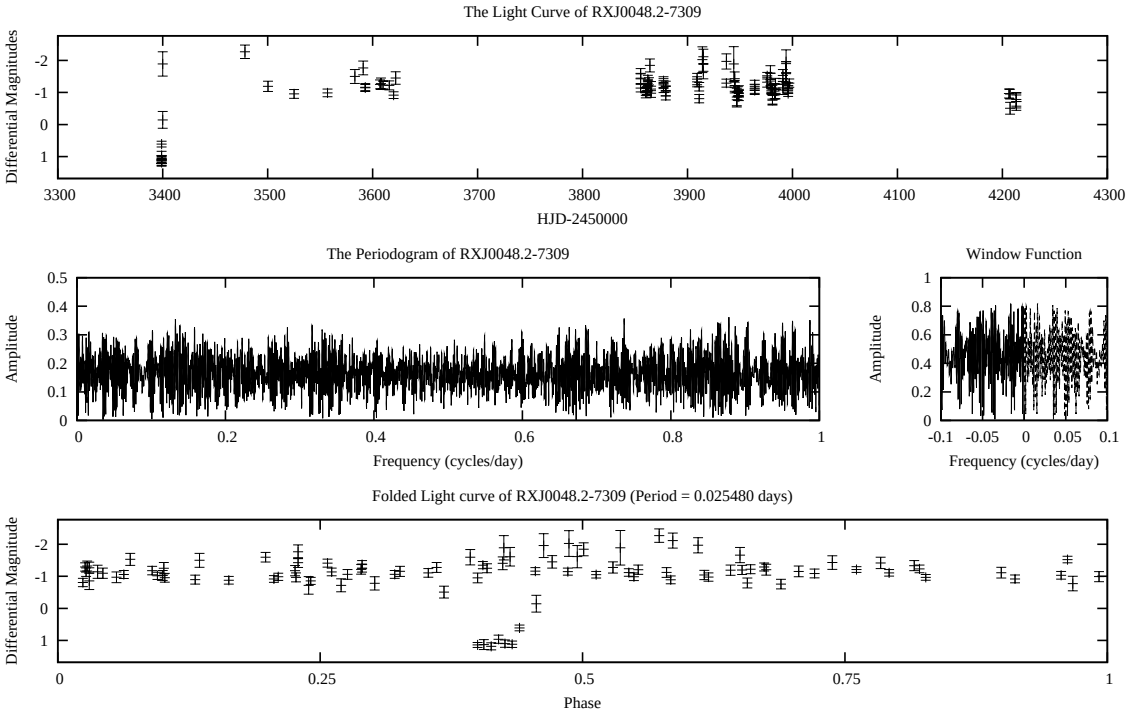

Figure 4.2: The Light Curve, Periodogram and Window Function of RX J0048.2-7309 There is no known period for this star. It was identified as an emission line star. The X-ray emission was identified from a method of matching hardness of spectrum to an unclassified source. The light curve was folded to the period found in the Fourier analysis, since no period was available.

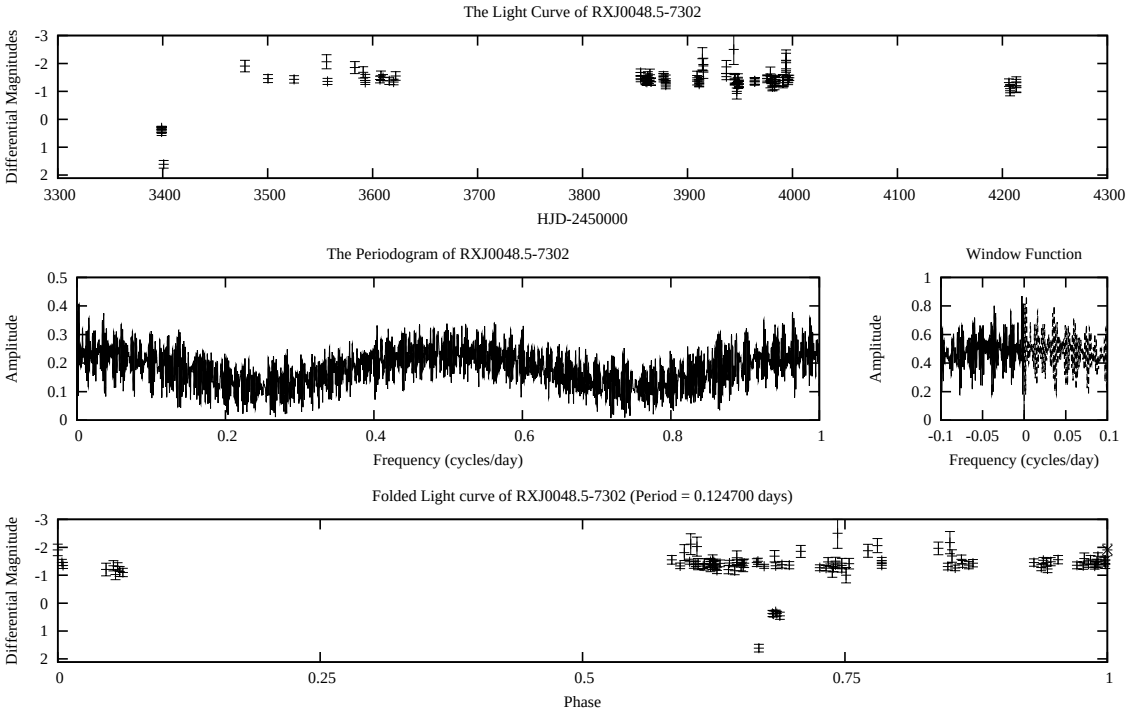

Figure 4.3: The Light Curve, Periodogram and Window Function of RX J0048.5-7302 The period for this star was first presented at an AAS conference using OGLEII data. Looking at the folded light curve, after having folded it to the frequency found in the data, half the light curve is missing. This is unlikely to be an orbital period because the frequency is too high. The folded light curve is folded to 0.1247 days.

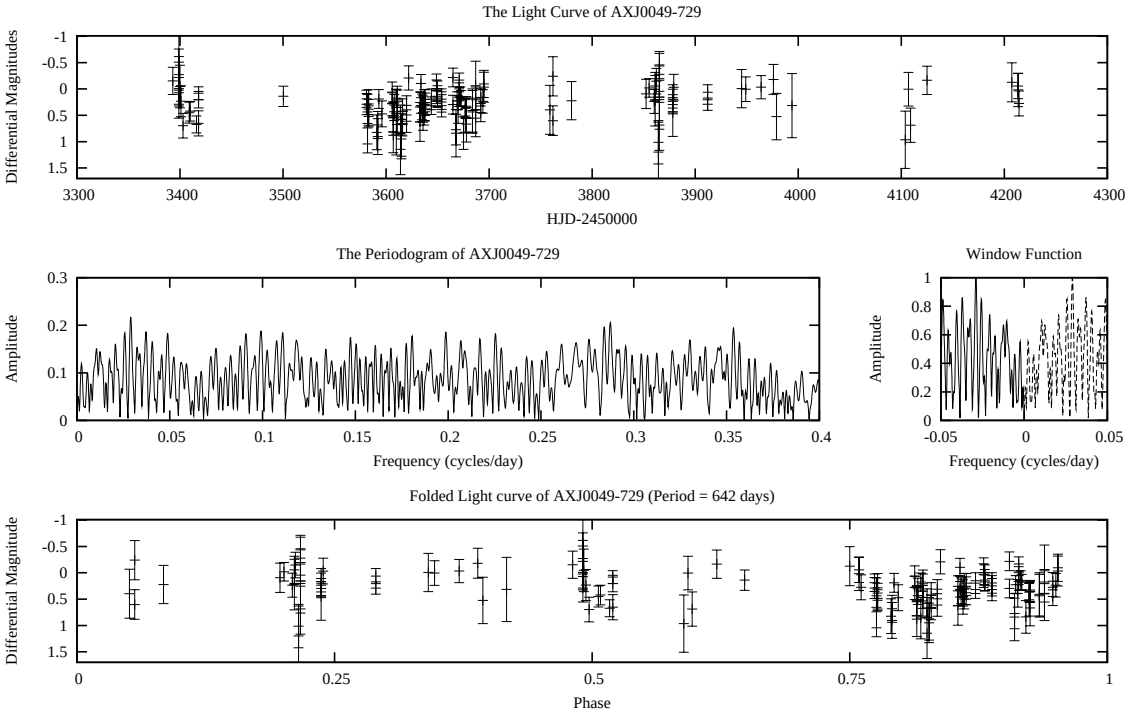

Figure 4.4: The Light Curve, Periodogram and Window Function of AX J0049-729 The folded light curve for AXJ0049-729 is folded to 642 days, the value for the period given in [66]. As can be seen, there was no significant signals in the periodogram. The Nyquist frequency for this star's data was 0.428 cycles per day.

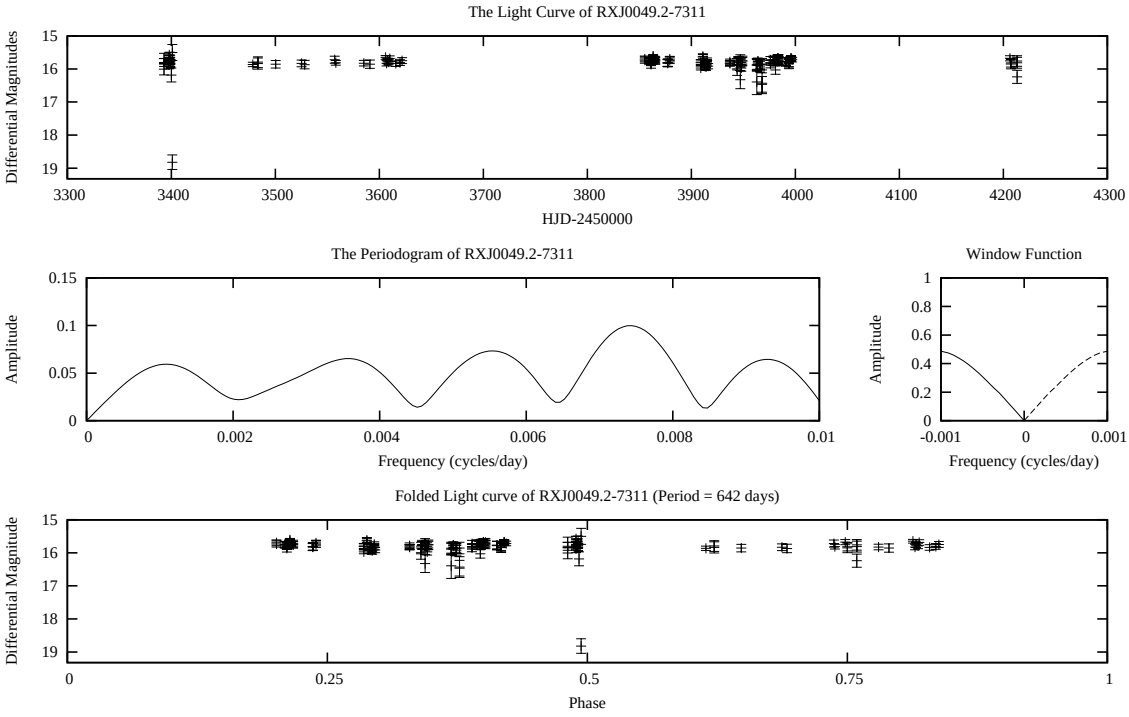

Figure 4.5: The Light Curve, Periodogram and Window Function of RX J0049.2-7311 The period for this star was not determined. The data for this star also has a low SNR. This can be treated as a non result. Since there was no available period, it was folded to 642 days as was AXJ0049-729.

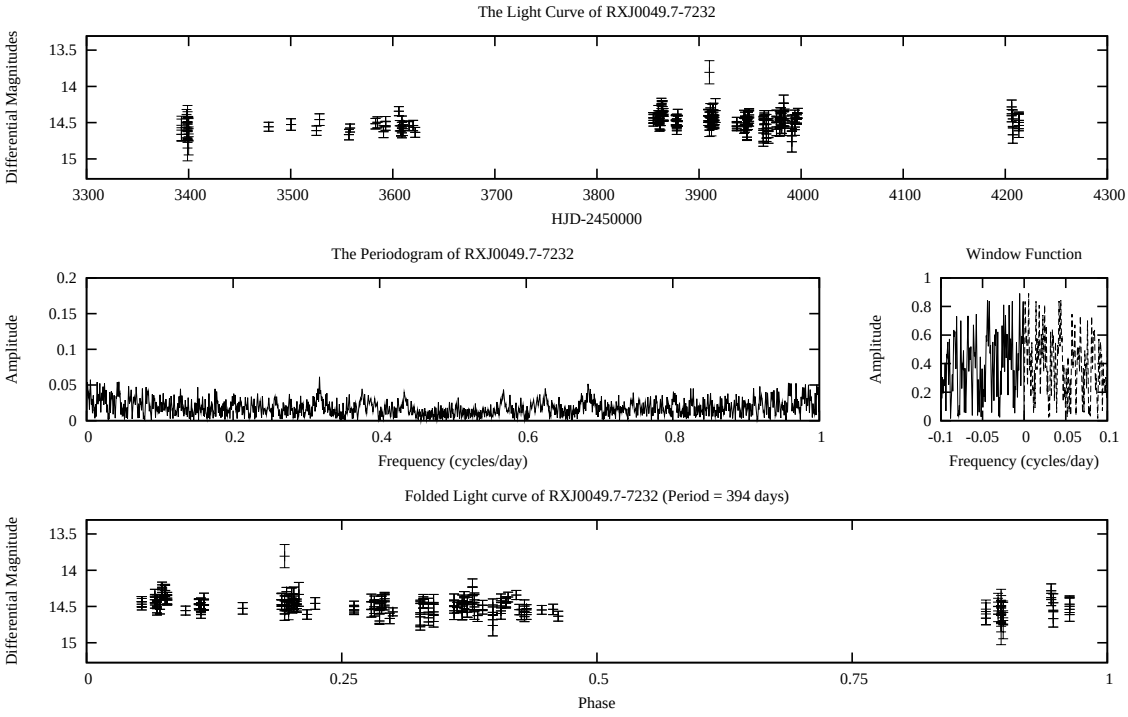

Figure 4.6: The Light Curve, Periodogram and Window Function of RX J0049.7-7323 This star can be treated as a non-result. There are no frequencies detected at a SNR > 4. It was folded to the 394 day period given in the literature.

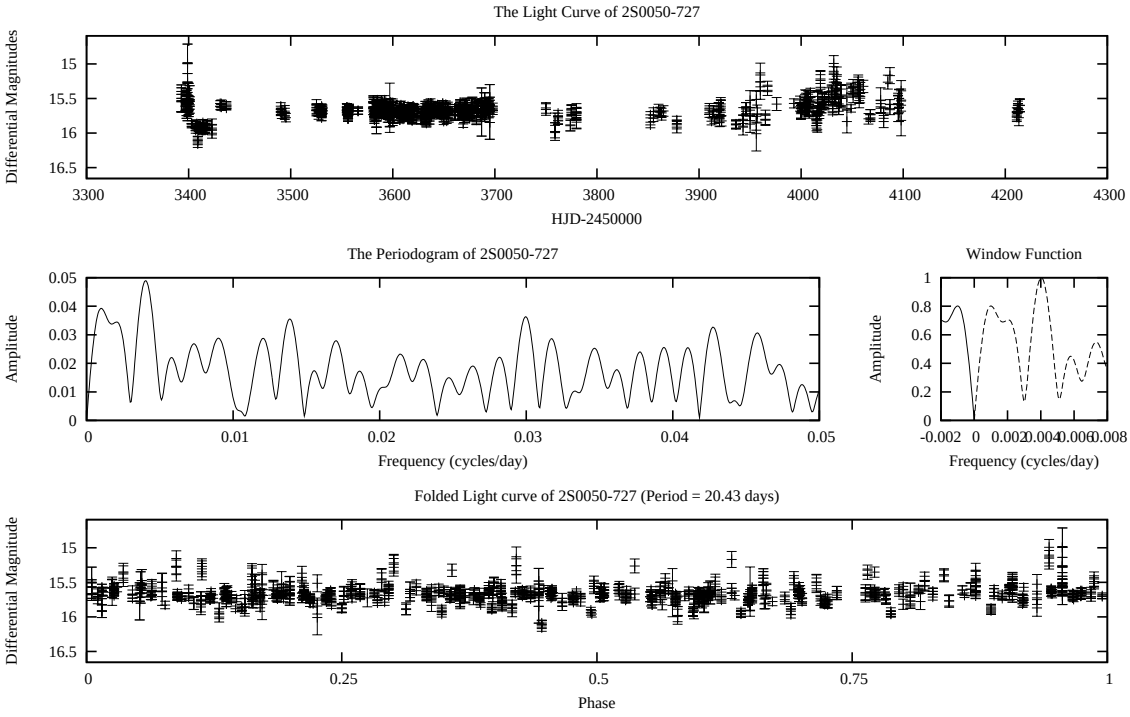

Figure 4.7: The Light Curve, Periodogram and Window Function of 2S 0050-727 This star gave several frequencies with an SNR > 4. One of them is a period of 209.5 days. There is a published orbital period of 45 days for this star [28]. The other periods that were found are located in Table 4.1. After trying a few of the frequencies, the period this is folded to is 243 days.

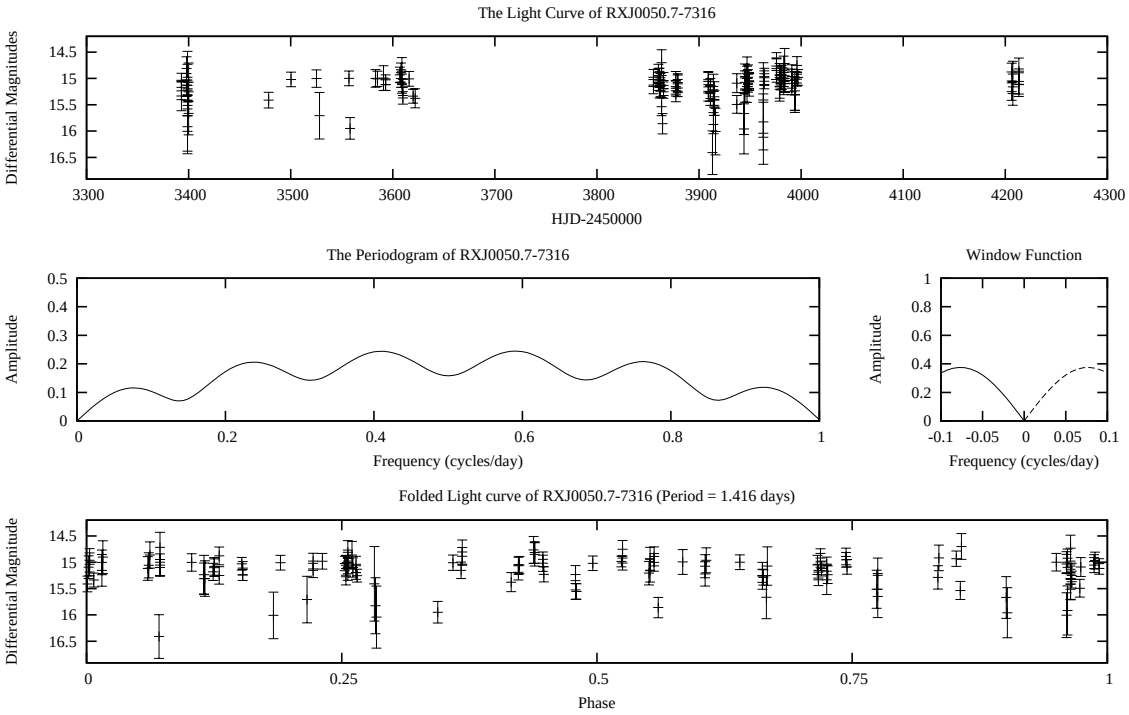

Figure 4.8: The Light Curve, Periodogram and Window Function of RX J0050.7-7316 This is a non-result. The SNR was 1.4; there is almost as much signal as noise.

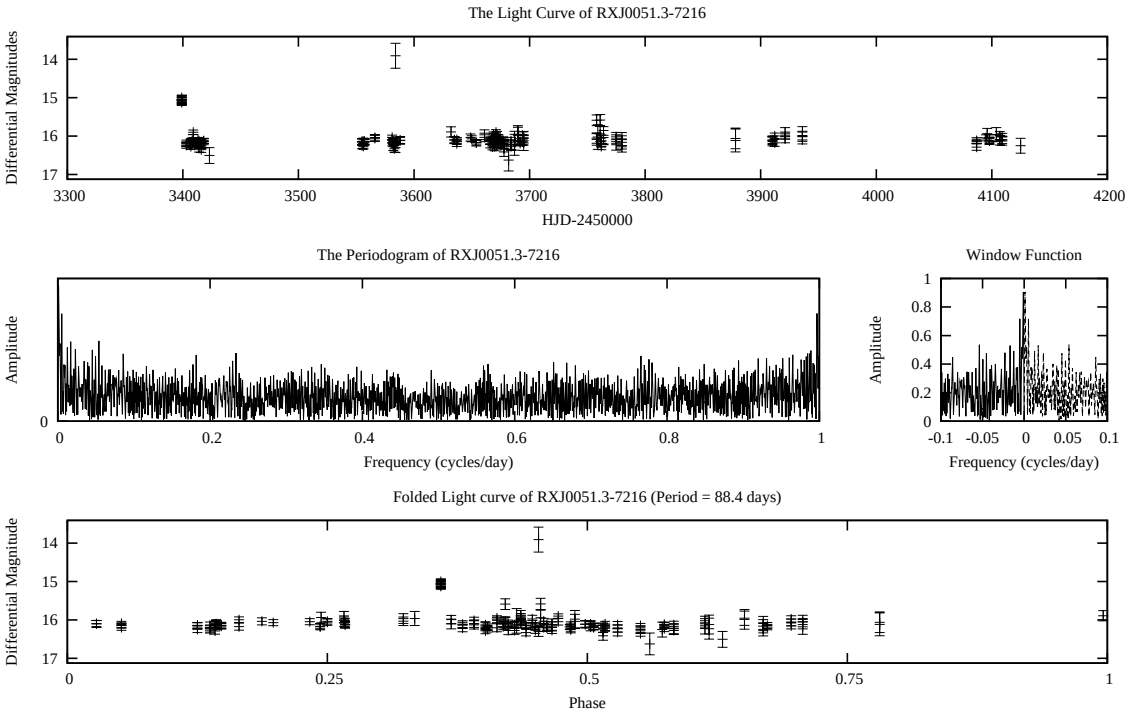

Figure 4.9: The Light Curve, Periodogram and Window Function of RX J0051.3-7216 Thanks to the aliasing, this is a non result.

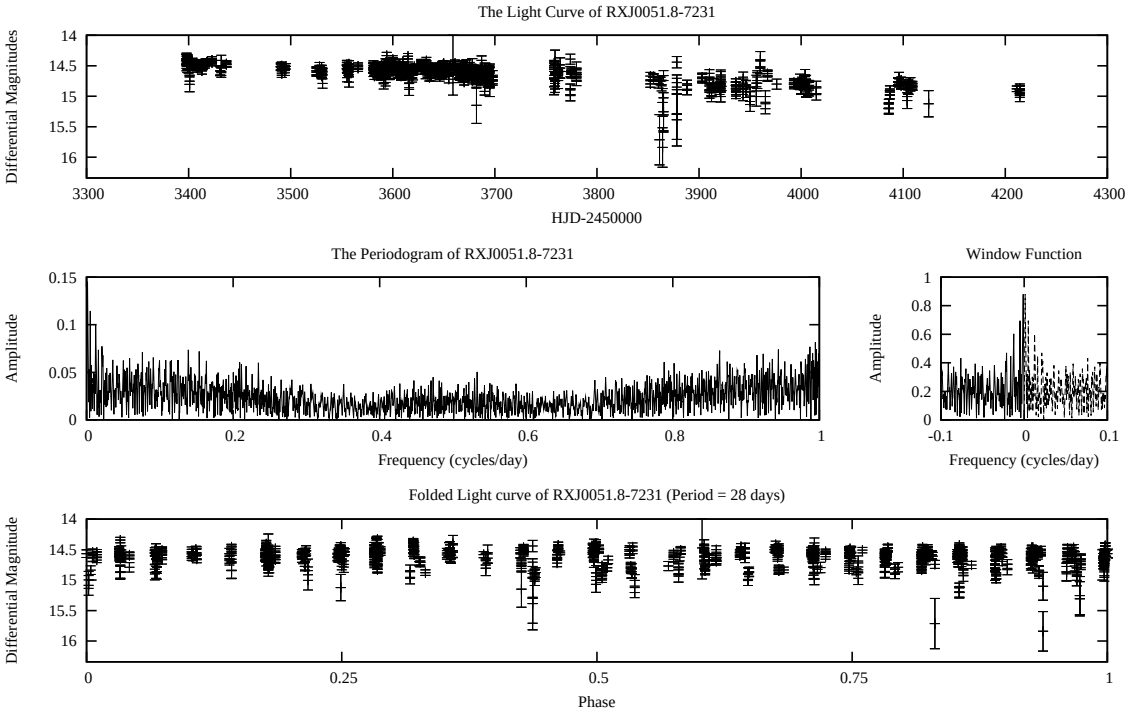

Figure 4.10: The Light Curve, Periodogram and Window Function of RX J0051.8-7231 There are actually two optical candidates for this source. However, IRAF could only distinguish one of the two sources. There are competing orbital periods for this X-Ray source. The folded light curve is folded to the 28 day period listed in [66],. Two periods were found in our data at 8.9997 and 8.9941 cycles per day. This is too fast for an orbital period. More than likely it was β-Cepheus pulsations that were detected.

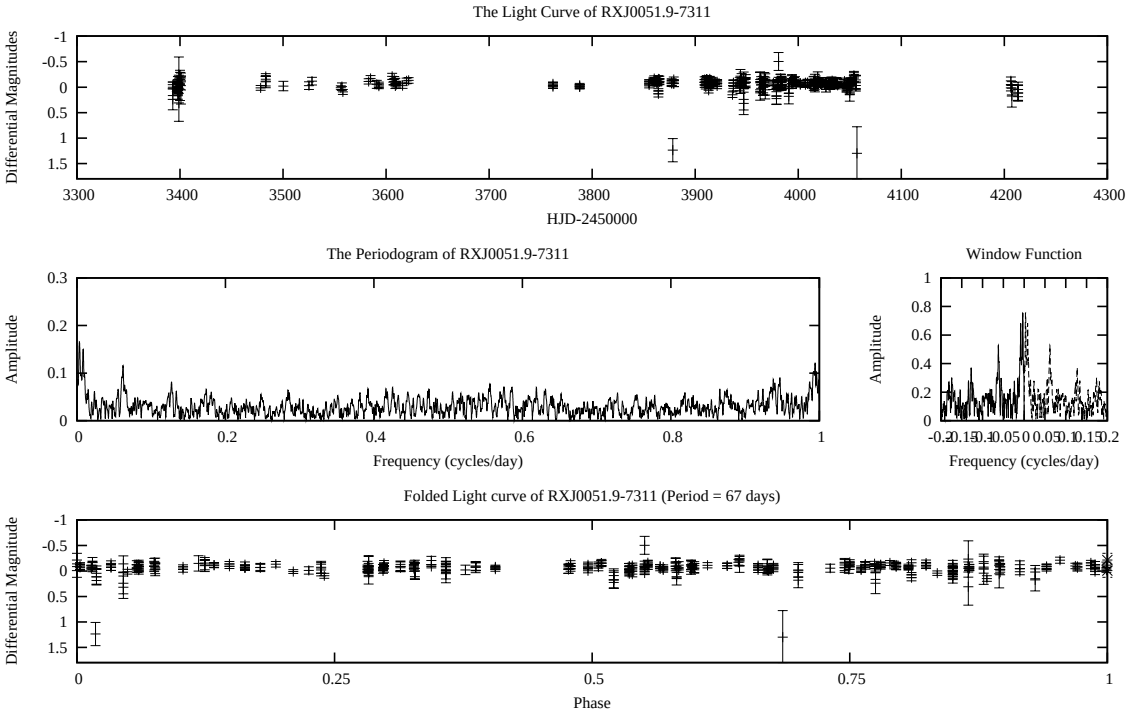

Figure 4.11: The Light Curve, Periodogram and Window Function of RX J0051.9-7311 Analysis of RXJ0051.9-7211's light curve didn't find an orbital period. It did find a 3 cycle/day periodicity, though. It is likely an alias. The light curve was folded to the 67 day period suggested by [57].

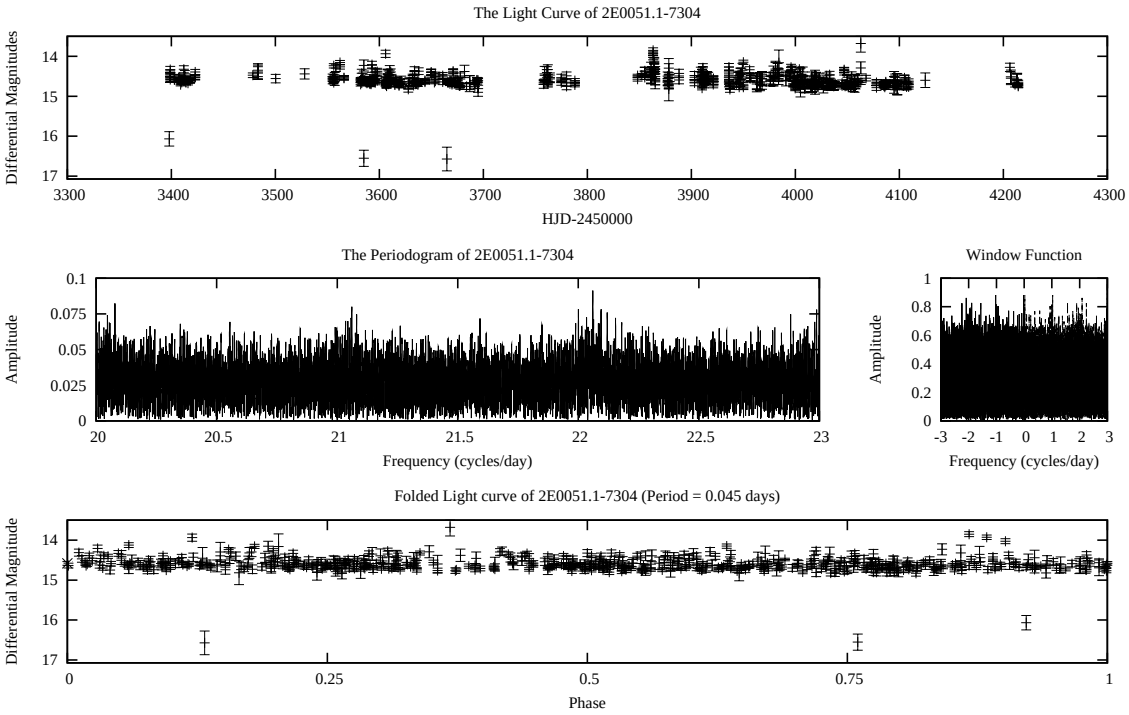

Figure 4.12: The Light Curve, Periodogram and Window Function of 2E 0051.1-7304 There is no known period for this object. Observations/papers on this object stopped in 2005. This was folded to 0.045 days.

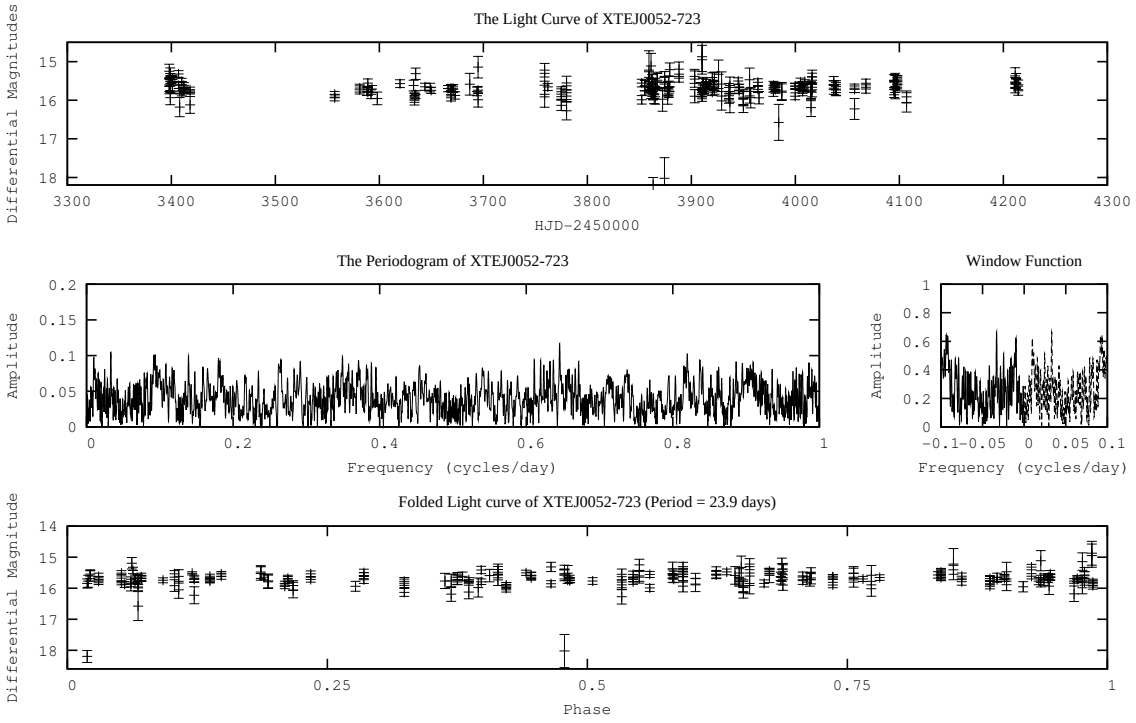

Figure 4.13: The Light Curve, Periodogram and Window Function of XTE J0052-723 The period given in [12] is 23.9 days; thus this light curve is folded to that period.

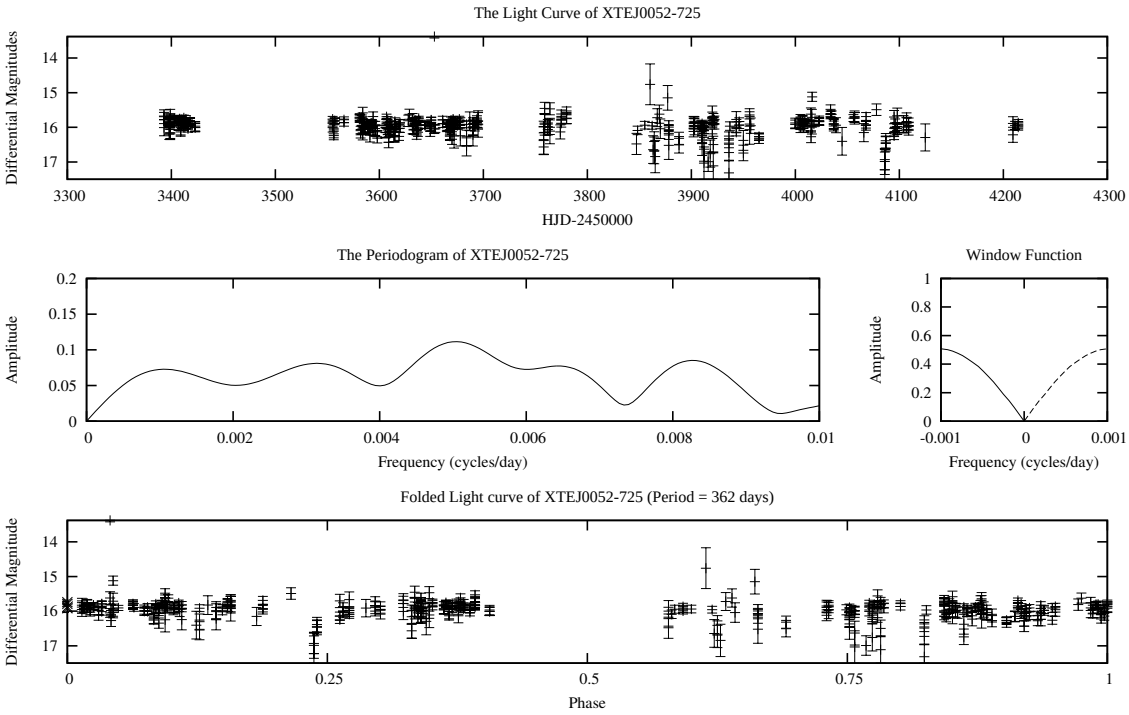

Figure 4.14: The Light Curve, Periodogram and Window Function of XTE J0052-725. Folded to the period given in Coe *et al* 2008; 362 days.

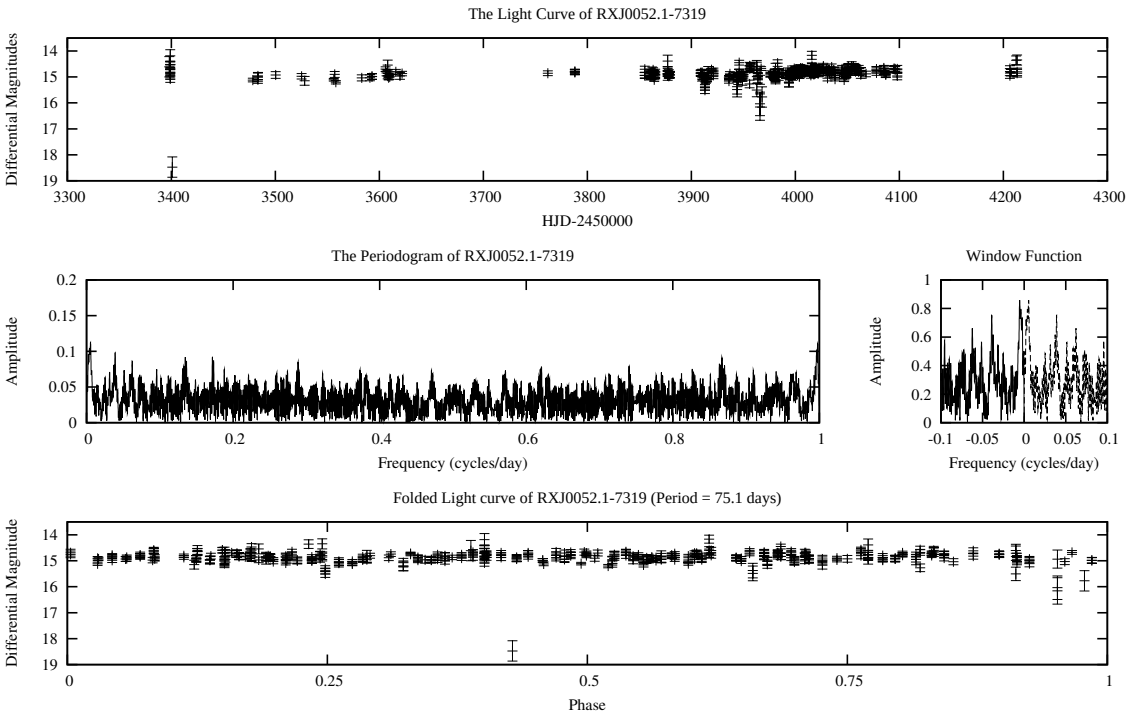

Figure 4.15: The Light Curve, Periodogram and Window Function of RX J0052.1-7319 Given as possibly 28 days from OGLE II data or 75 days from X-Ray data [37]. The period from X-Ray data was chosen for the plot, as X-Ray derived periods are usually considered more accurate.

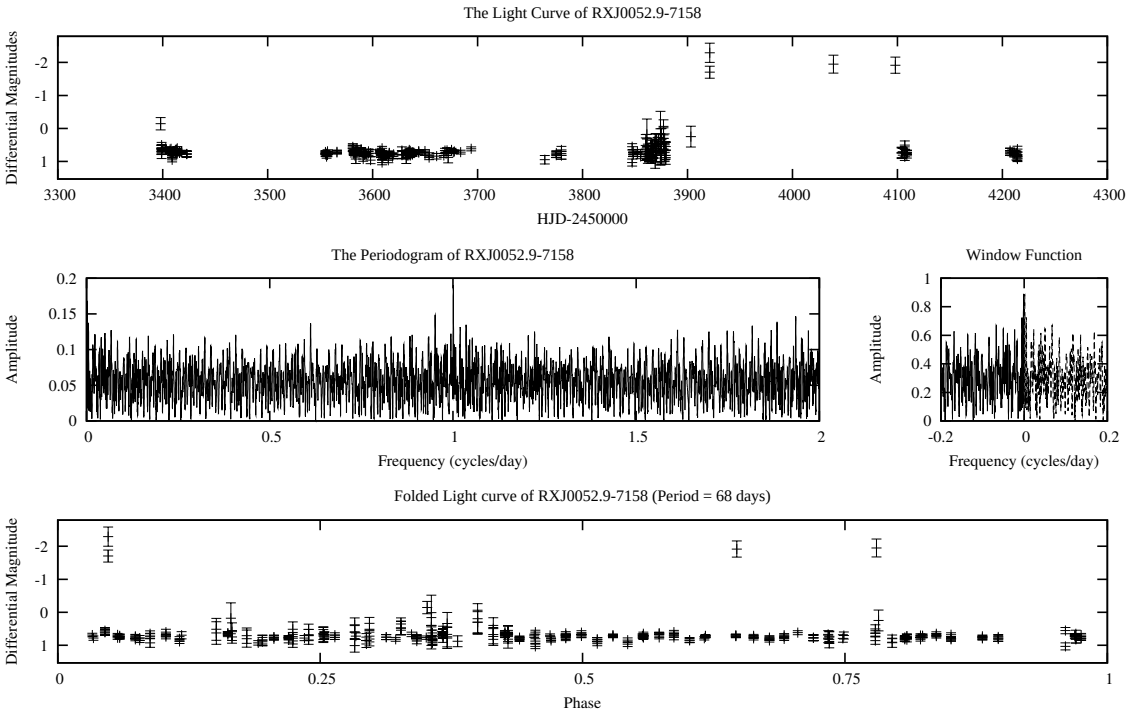

Figure 4.16: The Light Curve, Periodogram and Window Function of RX J0052.9-7158 Fourier analysis gives that peak at 1 cycle per day. This is likely an alias. The light curve is folded to 68 days

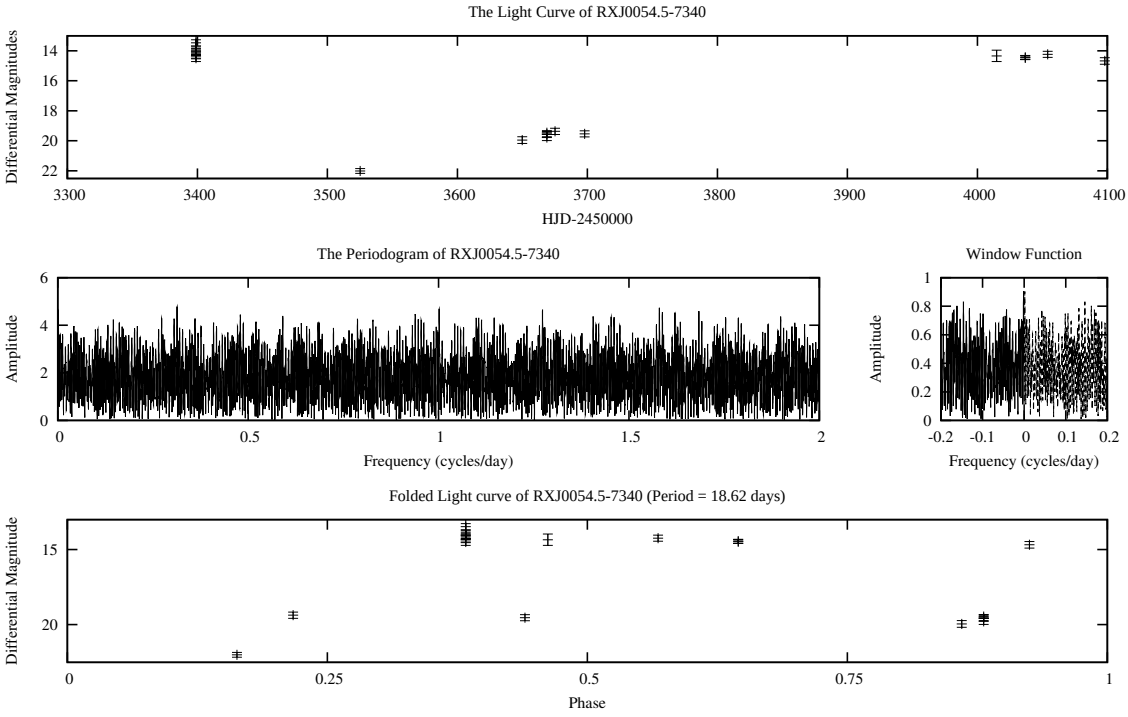

Figure 4.17: The Light Curve, Periodogram and Window Function of RX J0054.5-7340 The analysis of the light curve gives an SNR of 1.55. The data is sparse, probably due to being very close to another similar star and IRAF not being able to detect them separately. The light curve was folded to 18.62 days.

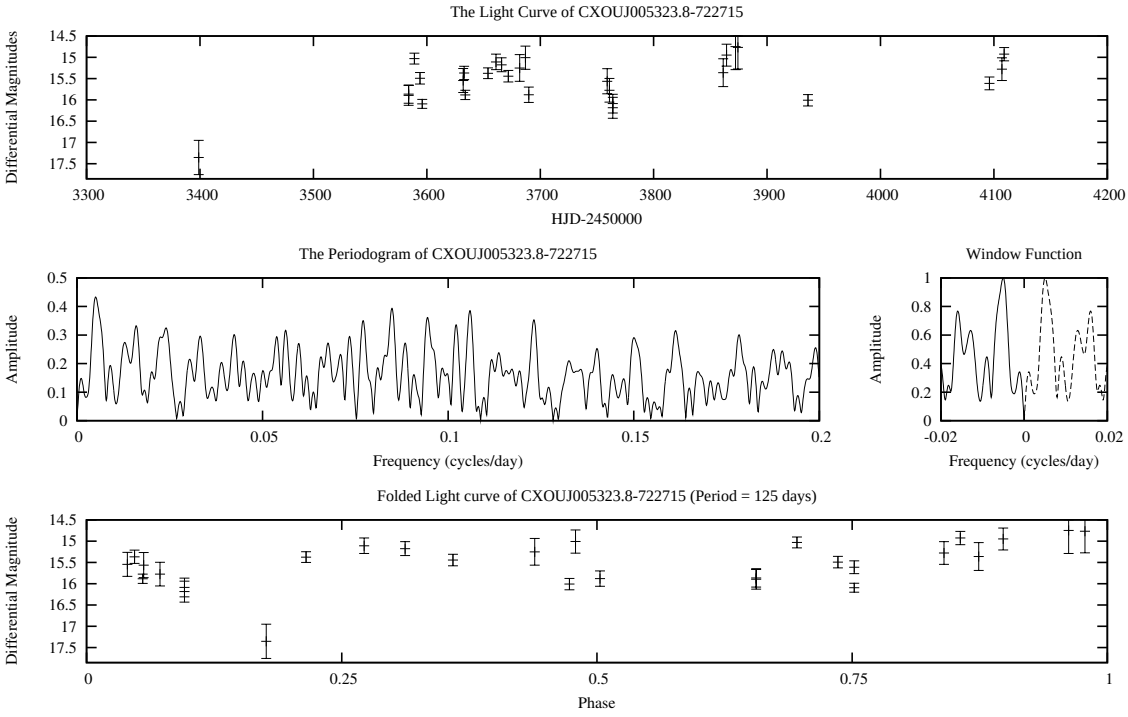

Figure 4.18: The Light Curve, Periodogram and Window Function of CXOU J005323.8-722715 This is non result with a SNR of 2.18. In fact, the Nyquist frequency is 0.208384 cycles per day. The period was folded to 125 days.

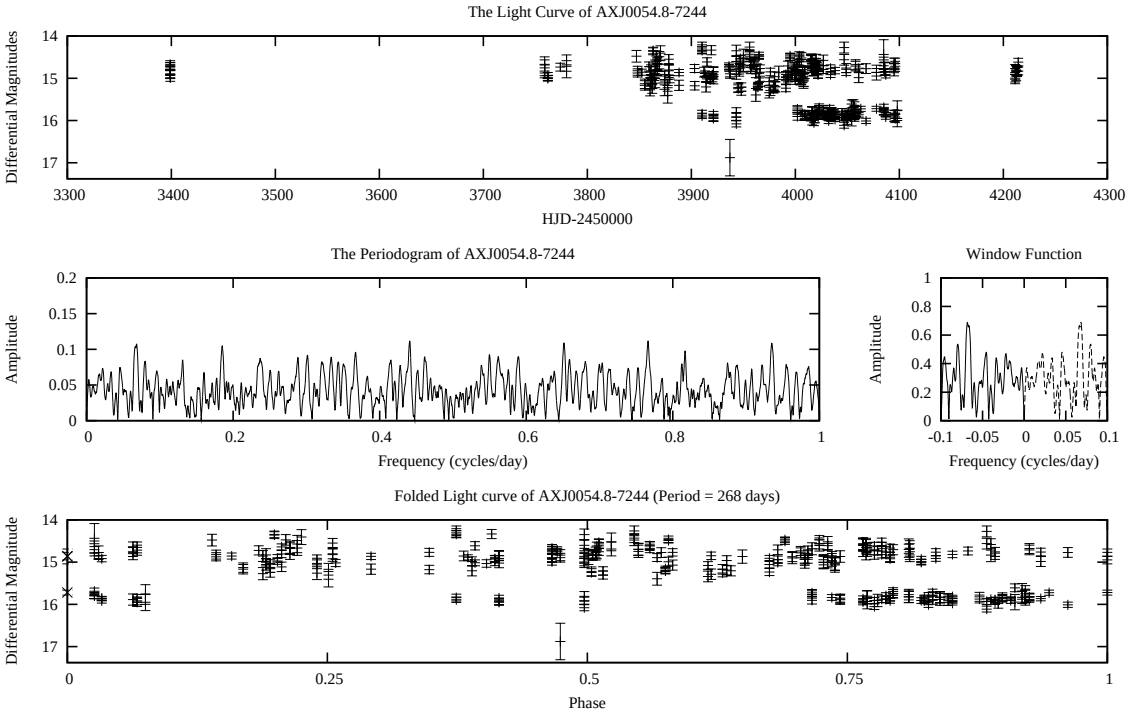

Figure 4.19: The Light Curve, Periodogram and Window Function of AX J0054.8-7244 This is one of those low SNR light curves. There is not enough information to extract a useful period. The light curve was folded to 268 days.

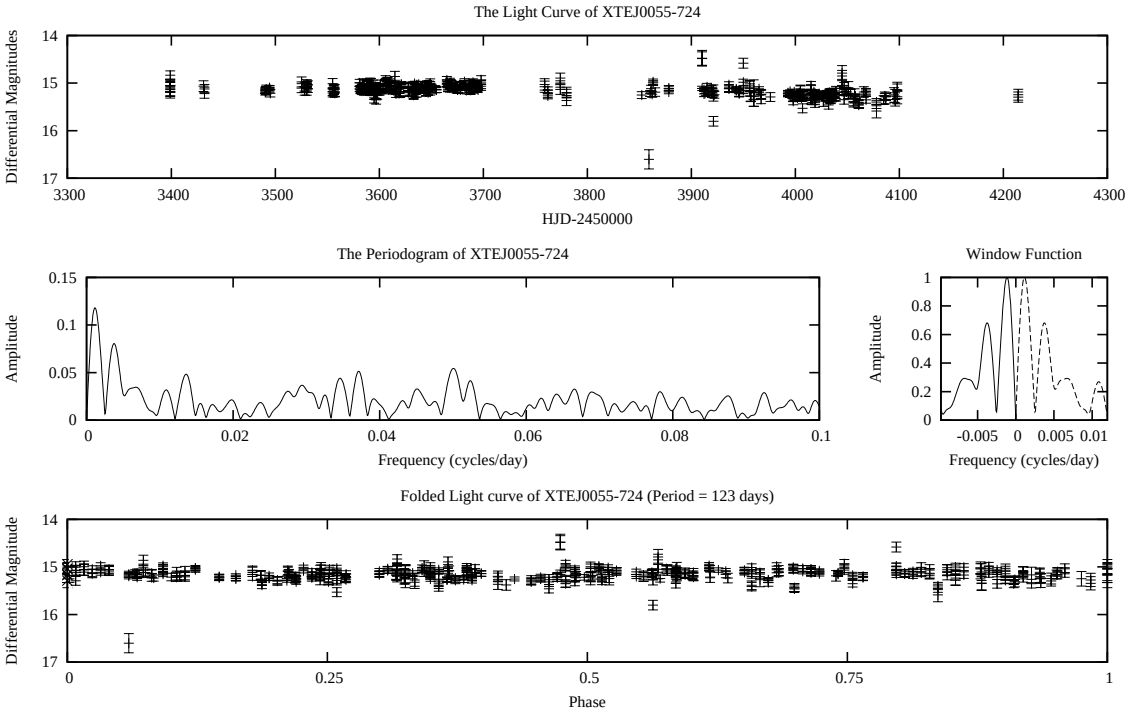

Figure 4.20: The Light Curve, Periodogram and Window Function of XTE J0055-724 This has a SNR of 9.72, and the peak at 0.00117 cycles per day works out to a period of 1729 days. The light curve was folded to 11729 days. However, this is outside the 600 day maximum allowed for by the length of our sample. It doesn't show very well with this scale, but there is a definite trend in the data. This could be a long-term brightening.

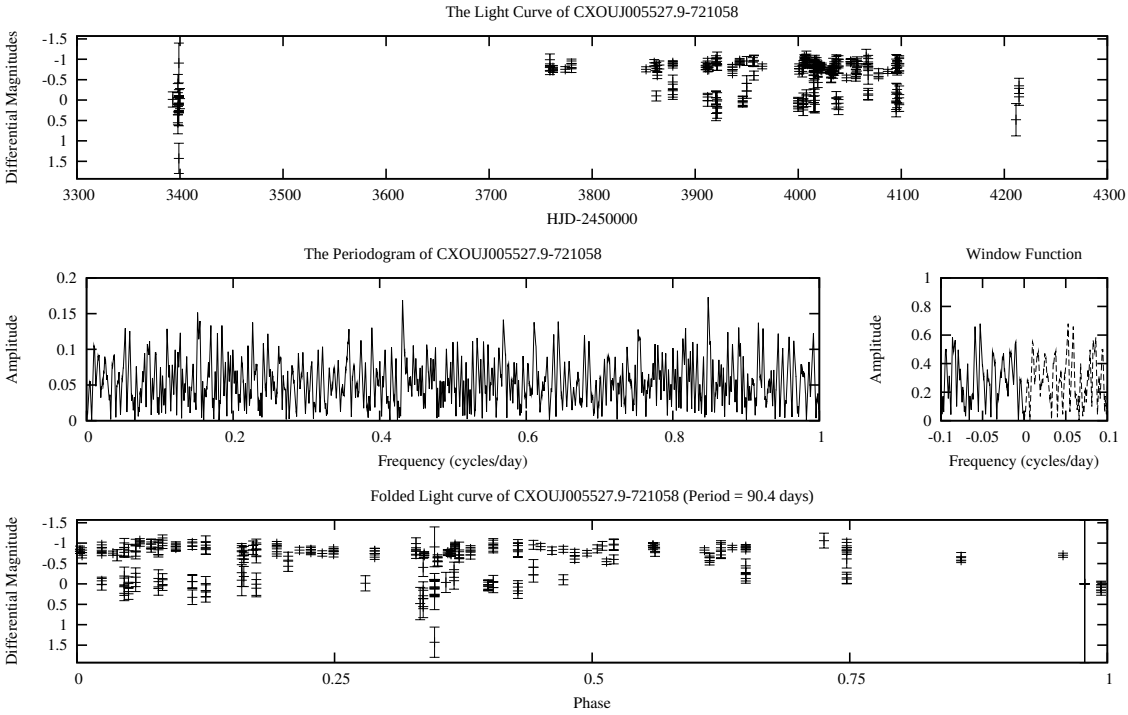

Figure 4.21: The Light Curve, Periodogram and Window Function of CXOU J005527.9-721058 There is no known period for this star. The SNR of this star is 2.81, thus the data here will not resolve the question. The light curve was folded to 90.4 days.

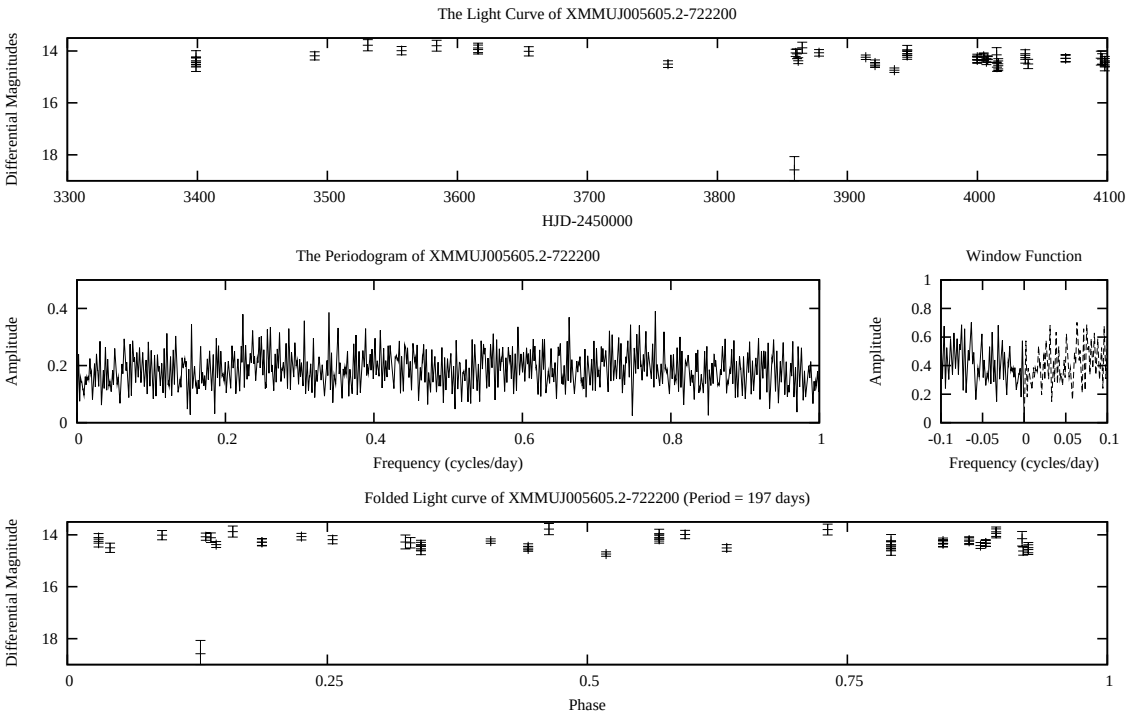

Figure 4.22: The Light Curve, Periodogram and Window Function of XMMU J005605.2-722200. It looks like there could be some ellipsoidal variation at the period suggested in [79]. However the data is pretty sparse and the SNR is too low for a confirmation.

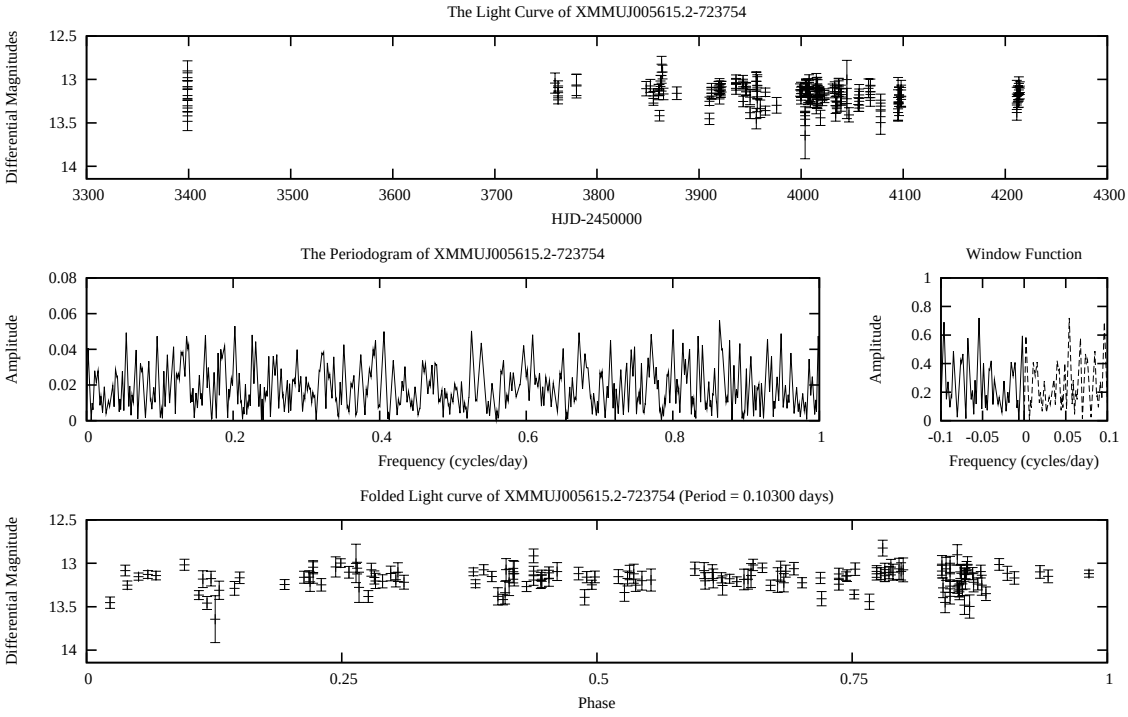

Figure 4.23: The Light Curve, Periodogram and Window Function of XMMU J005615.2-723754. This could be another example of β-Cephei pulsations; as the period and amplitude match, but the SNR is too low for a significant detection. The light curve was folded to 0.103 days.

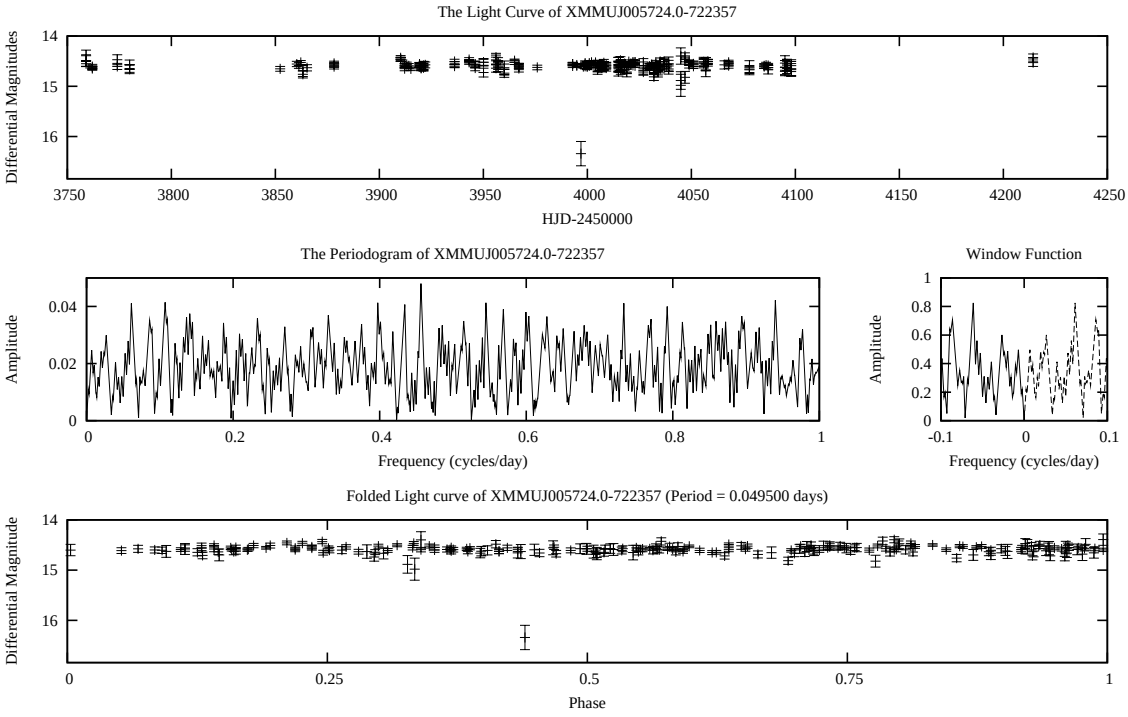

Figure 4.24: The Light Curve, Periodogram and Window Function of XMMU J005724.0-722357. This light curve is really nice and flat. There is no period on record, nor any signal worthy of note, so it was folded to 0.0495 days; the frequency that was found.

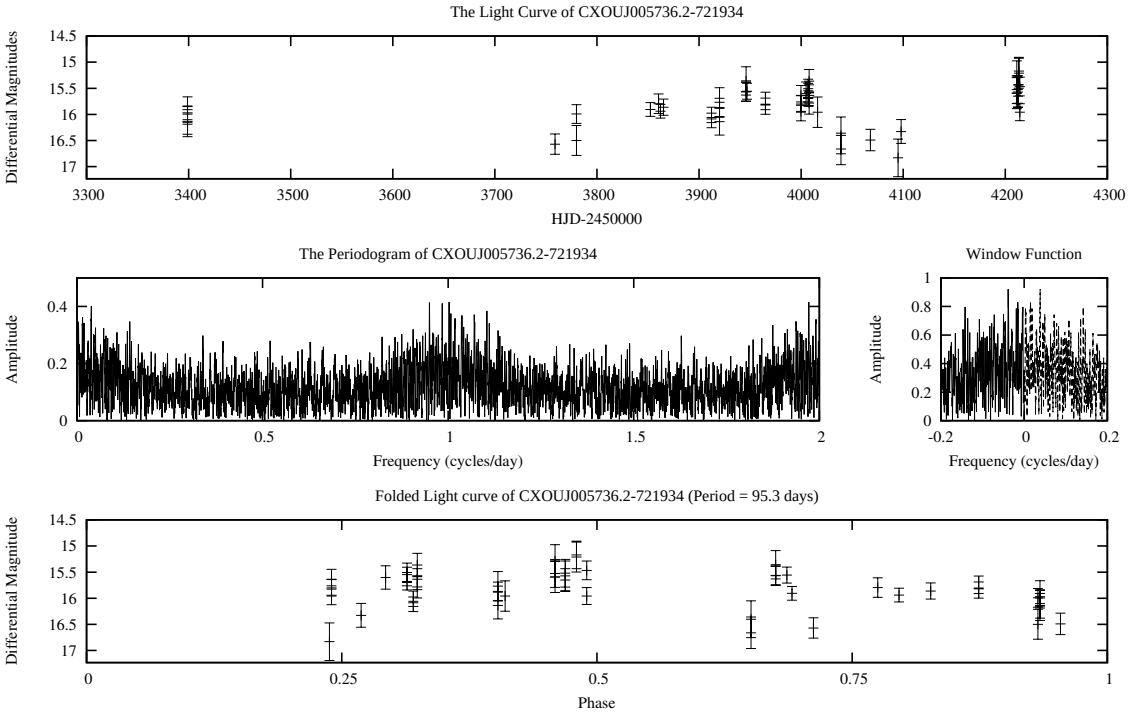

Figure 4.25: The Light Curve, Periodogram and Window Function of CXOU J005736.2-721934. This light curve was folded to 95.3 days after no significant detection was found. A quarter of the light curve at this frequency is missing. Notice the aliasing at one and two days in the periodogram.

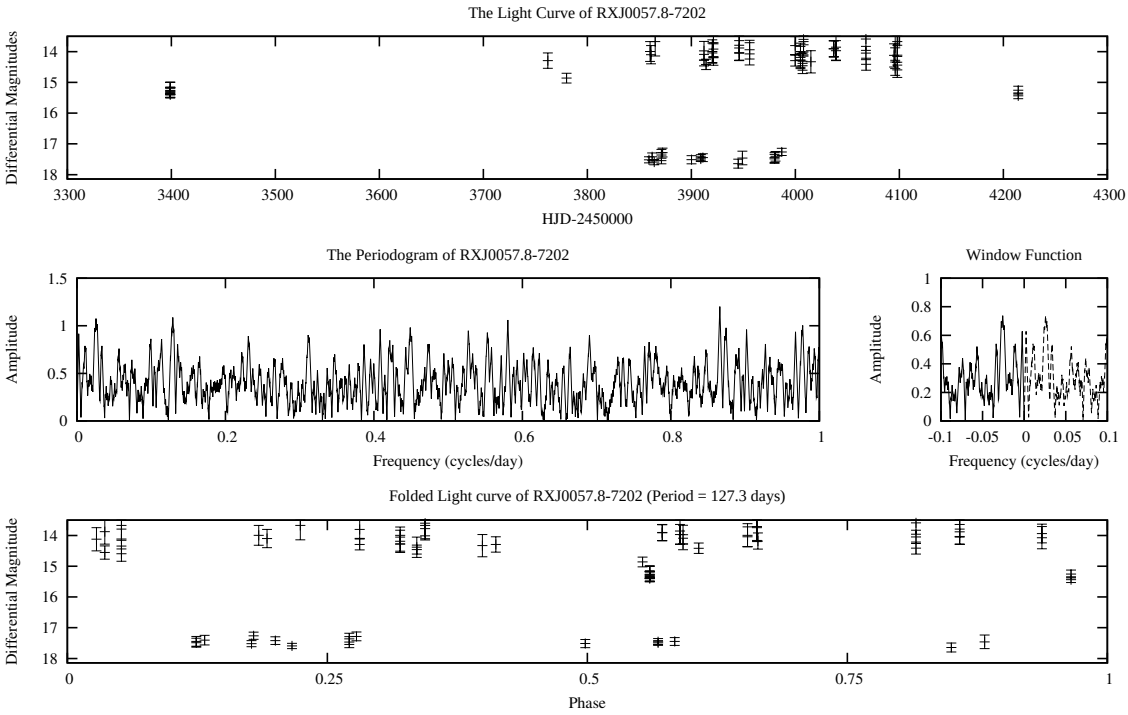

Figure 4.26: The Light Curve, Periodogram and Window Function of RX J0057.8-7202. This was folded to 127.3 days, the period suggested in [102].

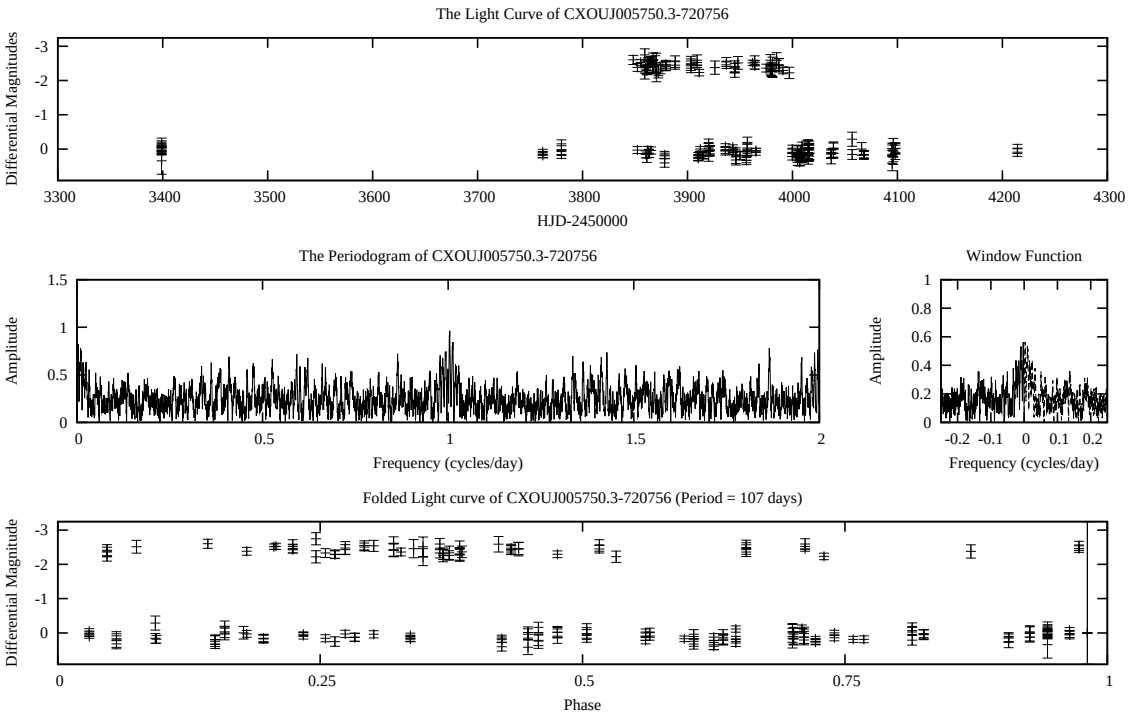

Figure 4.27: The Light Curve, Periodogram and Window Function of CXOU J005750.3-720756. There is a suggestion in [37] of a period at 107 days that fits the Corbet Diagram for this source. However, the power spectrum of the X-ray data in Galache *et a.l* is rather weak. The SNR on this source in our data was 4.49.

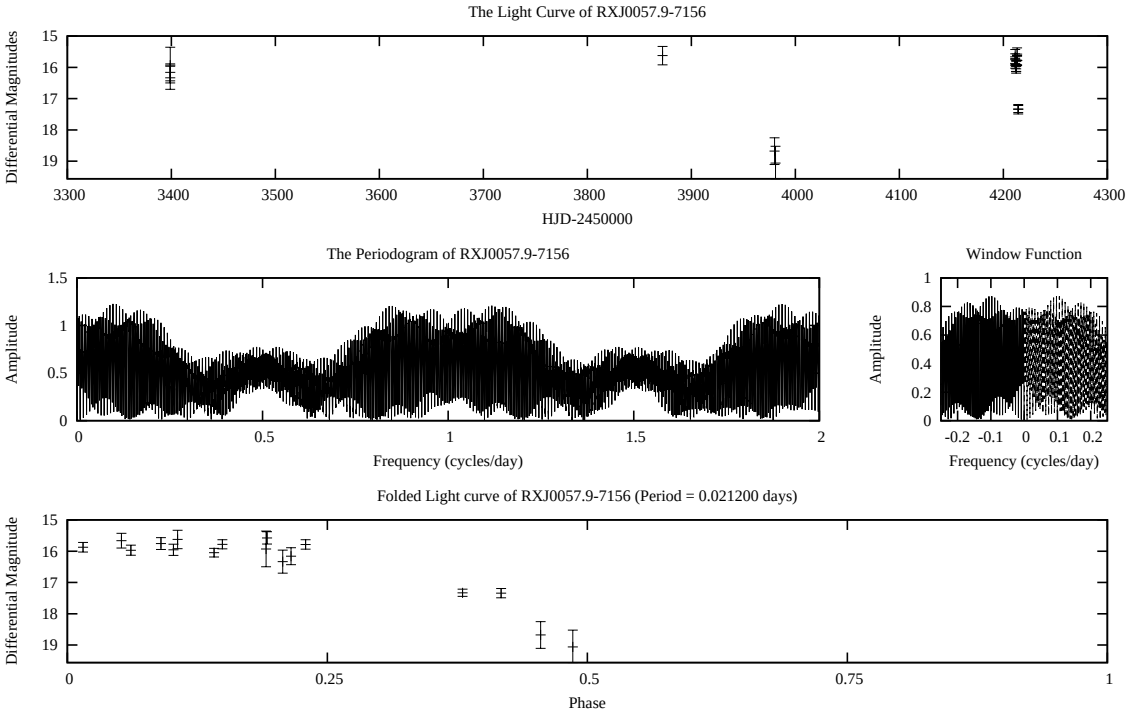

Figure 4.28: The Light Curve, Periodogram and Window Function of RX J0057.9-7156. Data on this star is very sparse. There is no period listed in the literature, so the light curve was folded to the period found in this study: 0.0212 days.

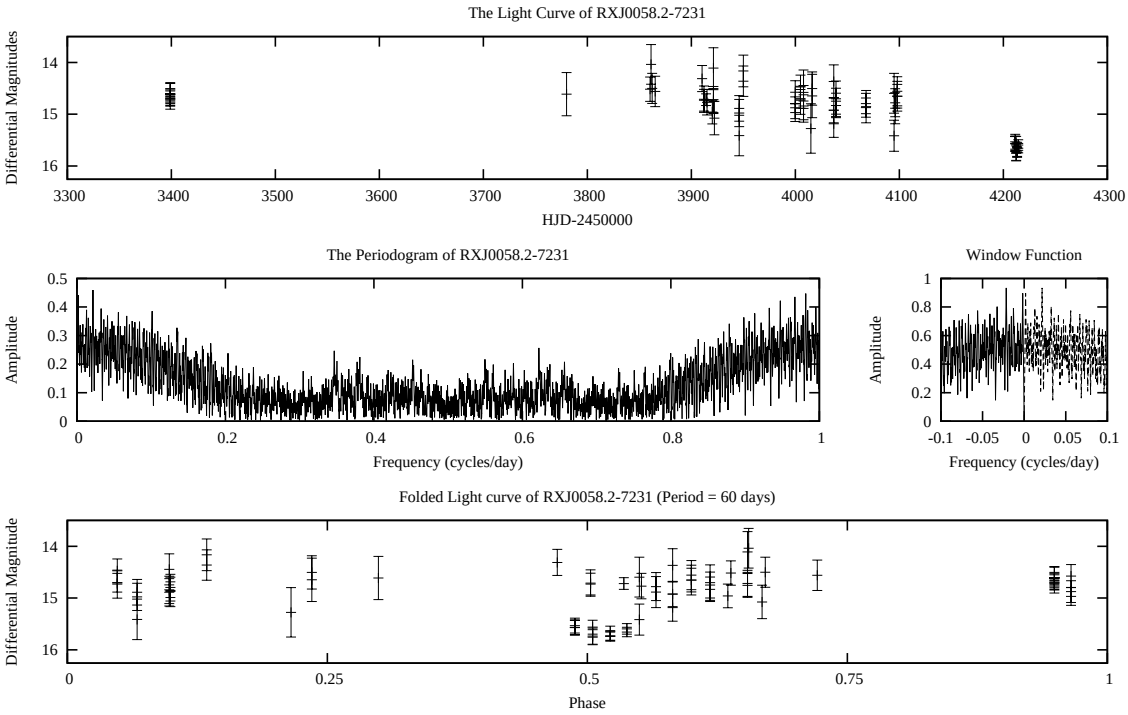

Figure 4.29: The Light Curve, Periodogram and Window Function of RX J0058.2-7231. The light curve was folded to 60 days.

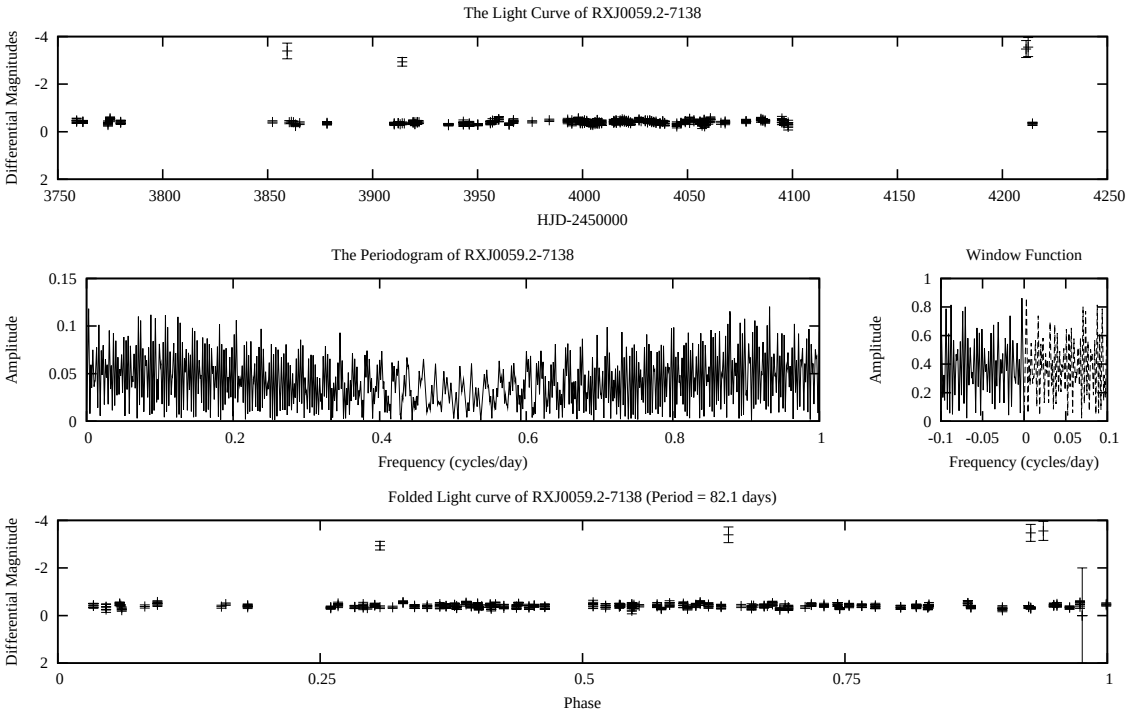

Figure 4.30: The Light Curve, Periodogram and Window Function of RX J0059.2-7138. This light curve was folded to 82.1 days.

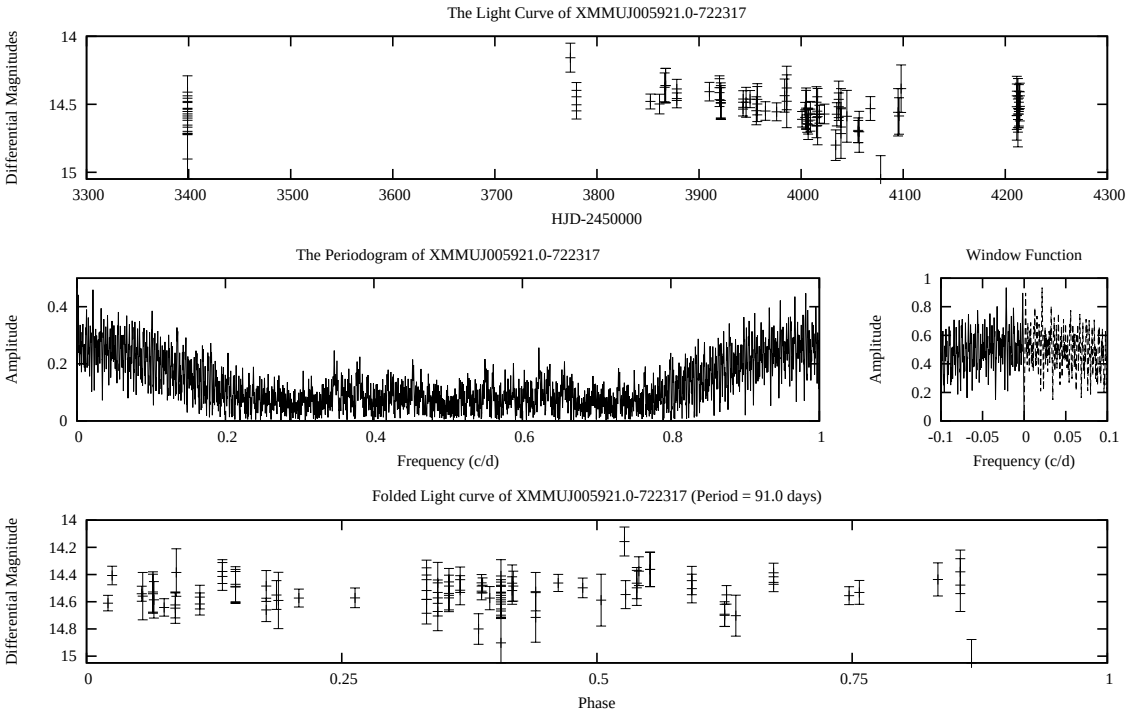

Figure 4.31: The Light Curve, Periodogram and Window Function of XMMU J005921.0-722317. The period was determined by outburst timing [37]. The light curve was folded to 91 days.

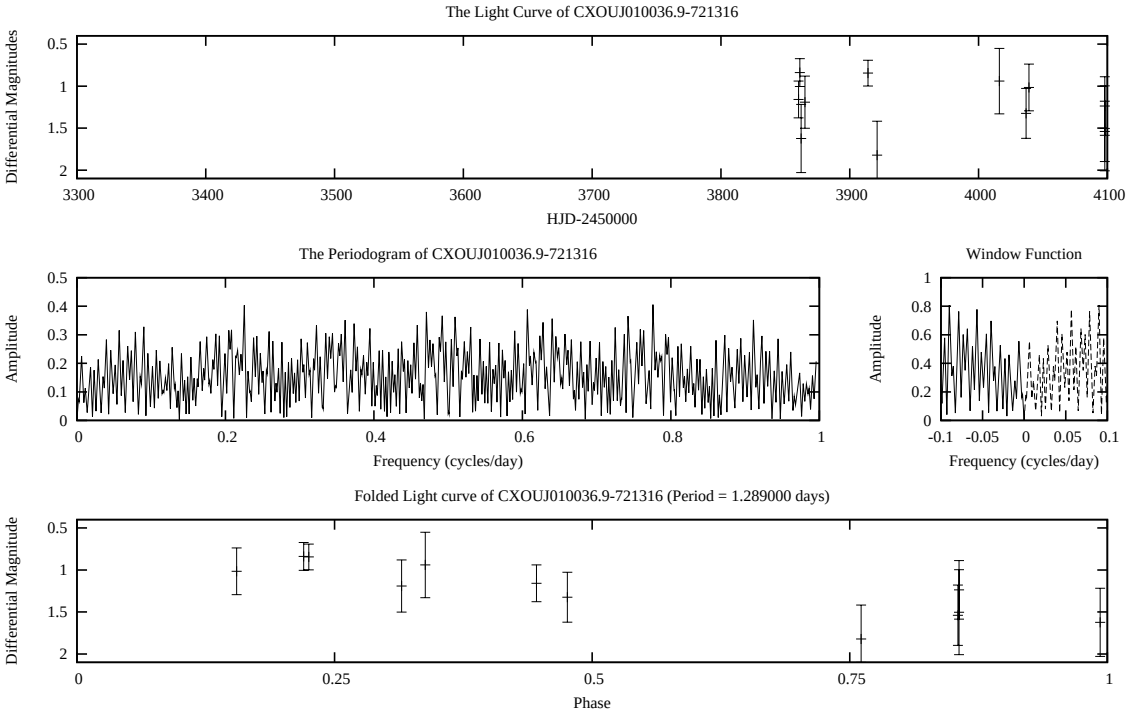

Figure 4.32: The Light Curve, Periodogram and Window Function of CXOU J010036.9-721316. The period was not determined. This object only appears in [66]. There were only a few data points, so the Nyquist frequency was 1 day. And the SNR was 2.01. However, the strongest peak was at 1.29 days, so that the period at which the light curve was folded.

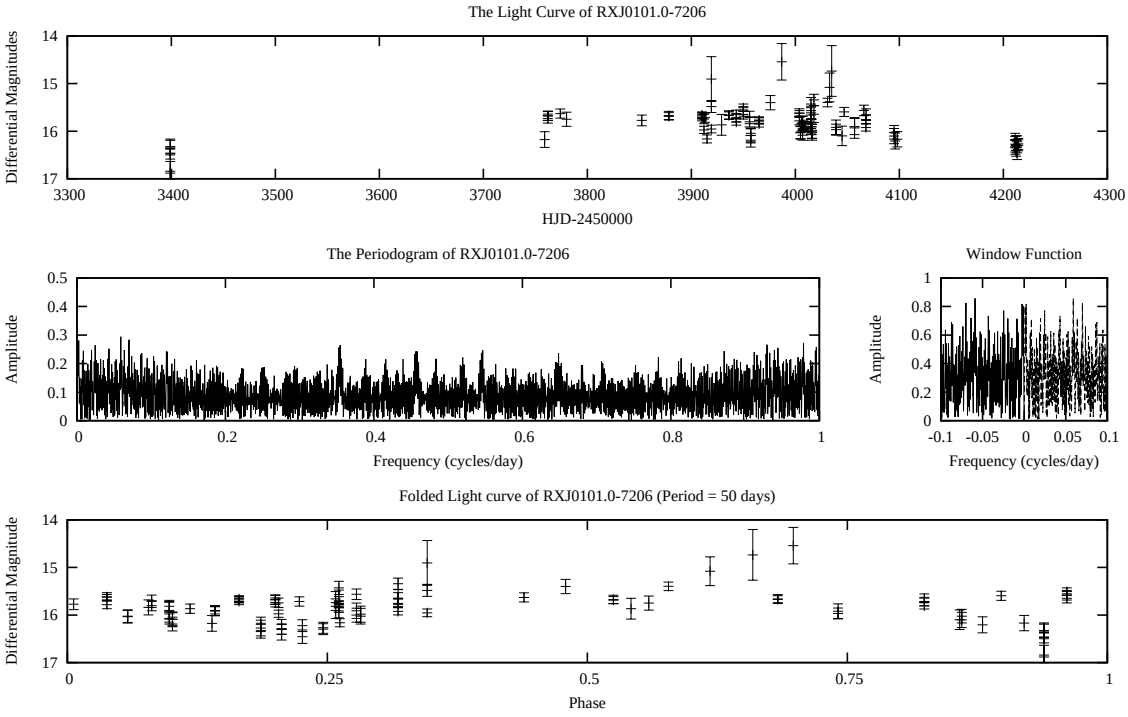

Figure 4.33: The Light Curve, Periodogram and Window Function of RX J0101.0-7206. When folding this to the period in [11], there appears to be some ellipsoidal variation. With a low signal to noise, its impossible to tell.

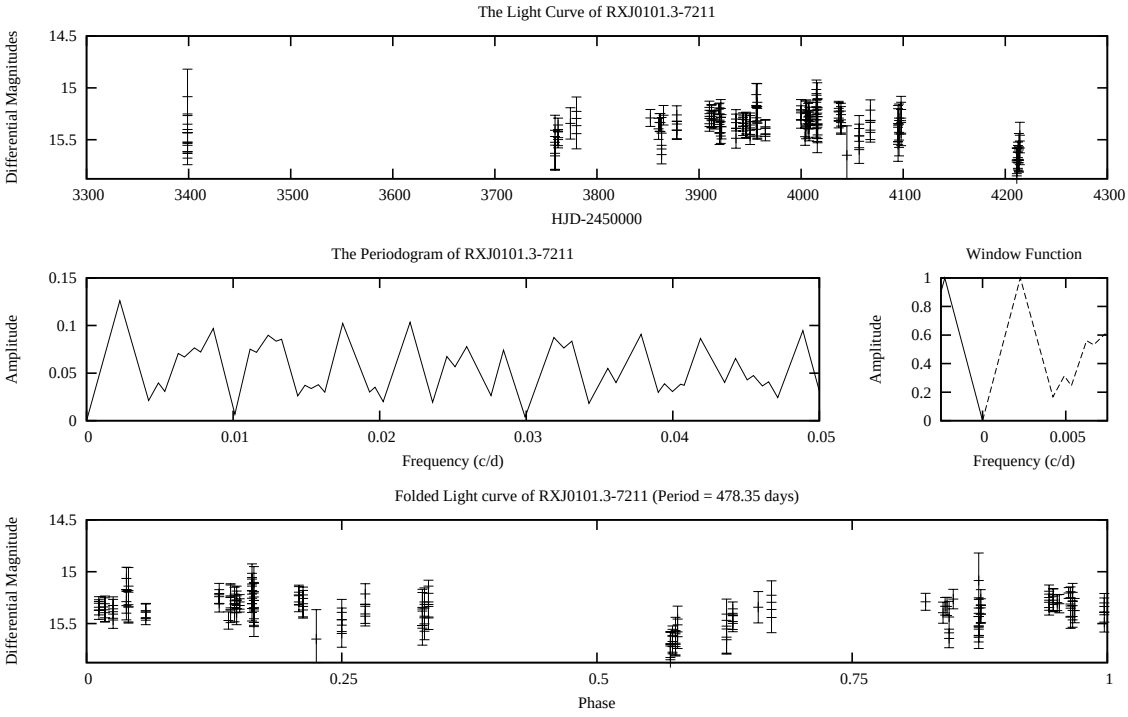

Figure 4.34: The Light Curve, Periodogram and Window Function of RX J0101.3-7211. This has an SNR of 4.09. This is one of 3 stars that showed activity consistent with an orbital period. The light curve was folded to 478 days.

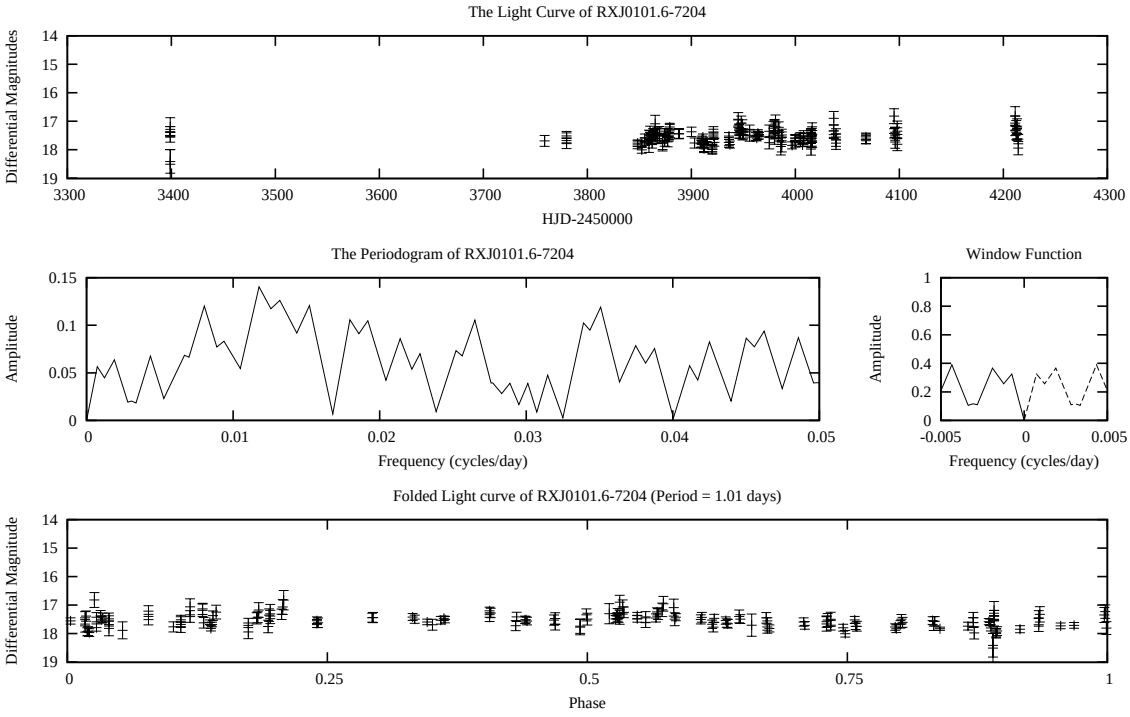

Figure 4.35: The Light Curve, Periodogram and Window Function of RX J0101.6-7204. Eger and Haberl (2008) are of the opinion that this source is a background AGN, not an HMXB [33]. The SNR of the period detected is 3.67. There is some variation at the 1 day period (which the light curve is folded to), but it could just as easily be aliasing.

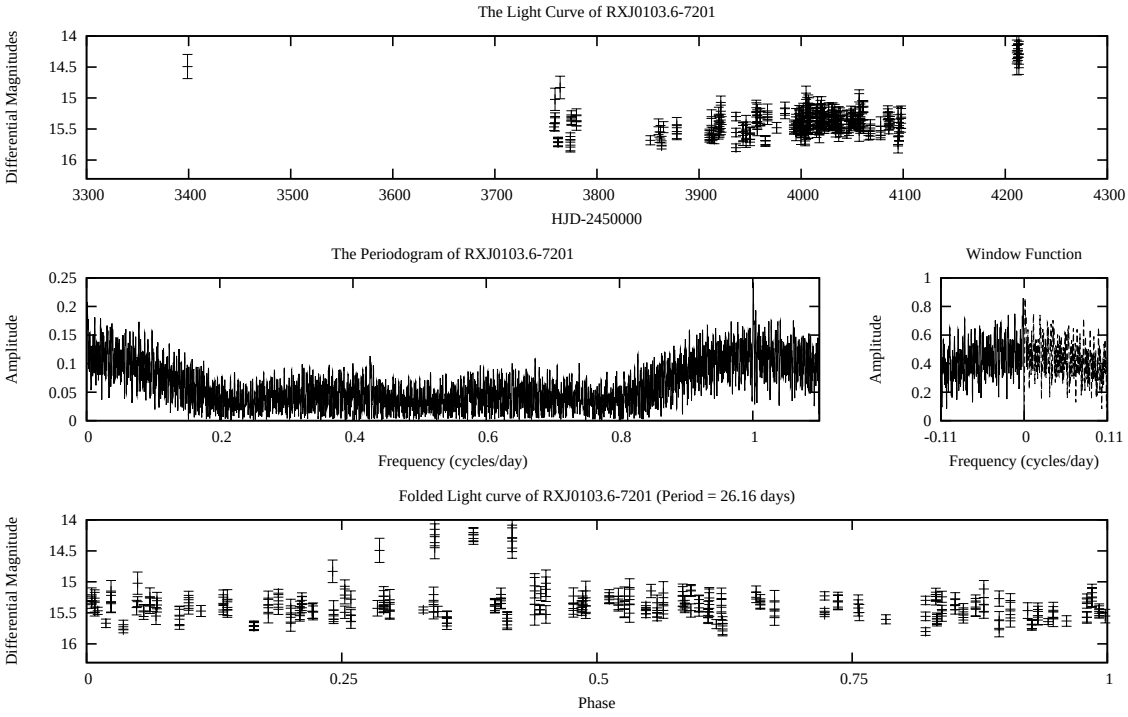

Figure 4.36: The Light Curve, Periodogram and Window Function of RX J0103.6-7201. There is no known period for this star. The SNR of the 1 day period is 10.46. However, it is most likely that this is an alias brought on by the sampling rate.

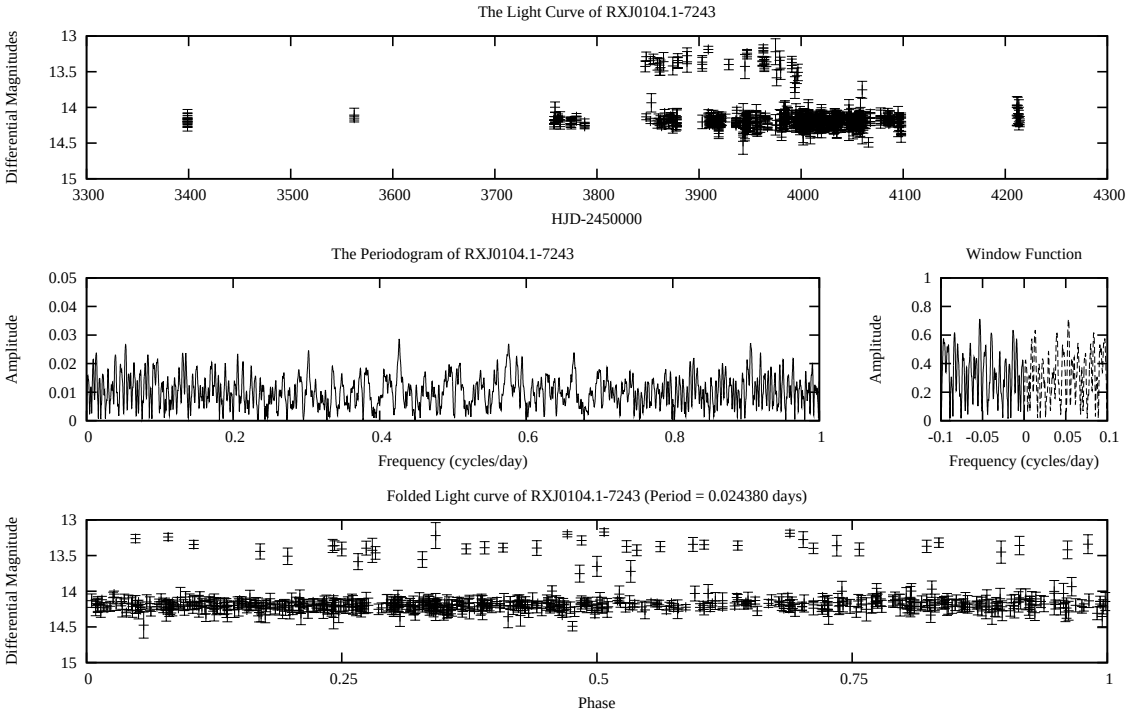

Figure 4.37: The Light Curve, Periodogram and Window Function of RX J0104.1-7243. There is no known period determined for this star. The light curve was folded to 0.02438 days, the result found by Period04. There is not a lot of variation.

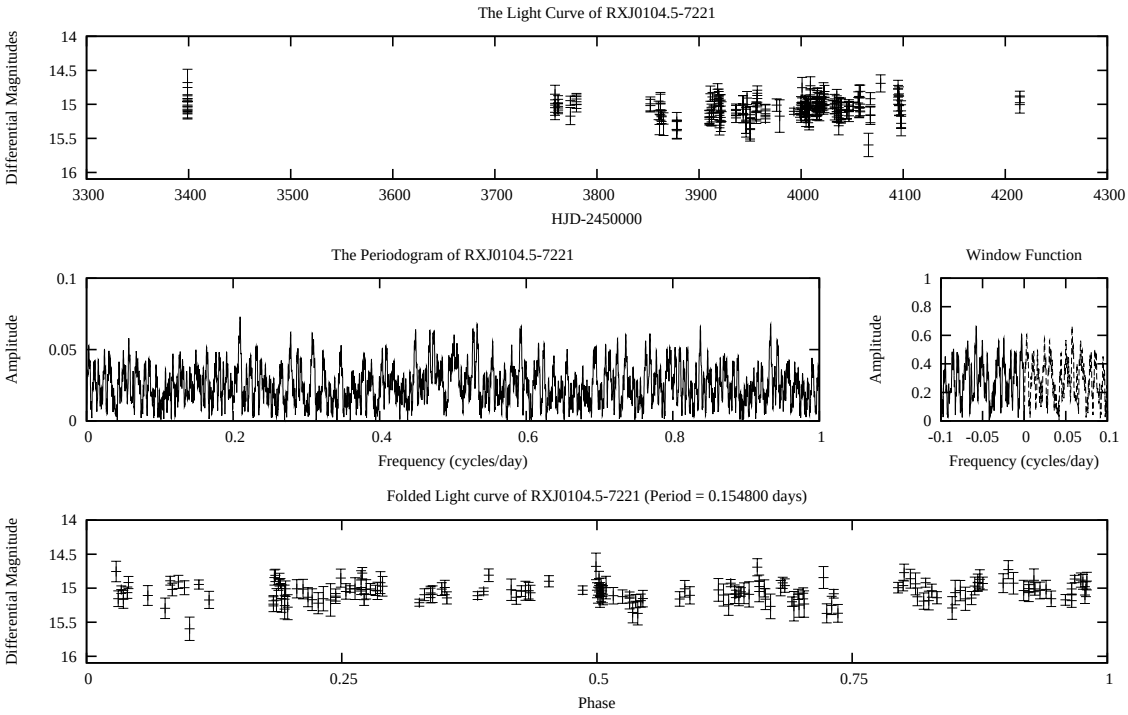

Figure 4.38: The Light Curve, Periodogram and Window Function of RX J0104.5-7221. This star has no known period. The light curve was folded to 0.1548 days, the result found by Period04.

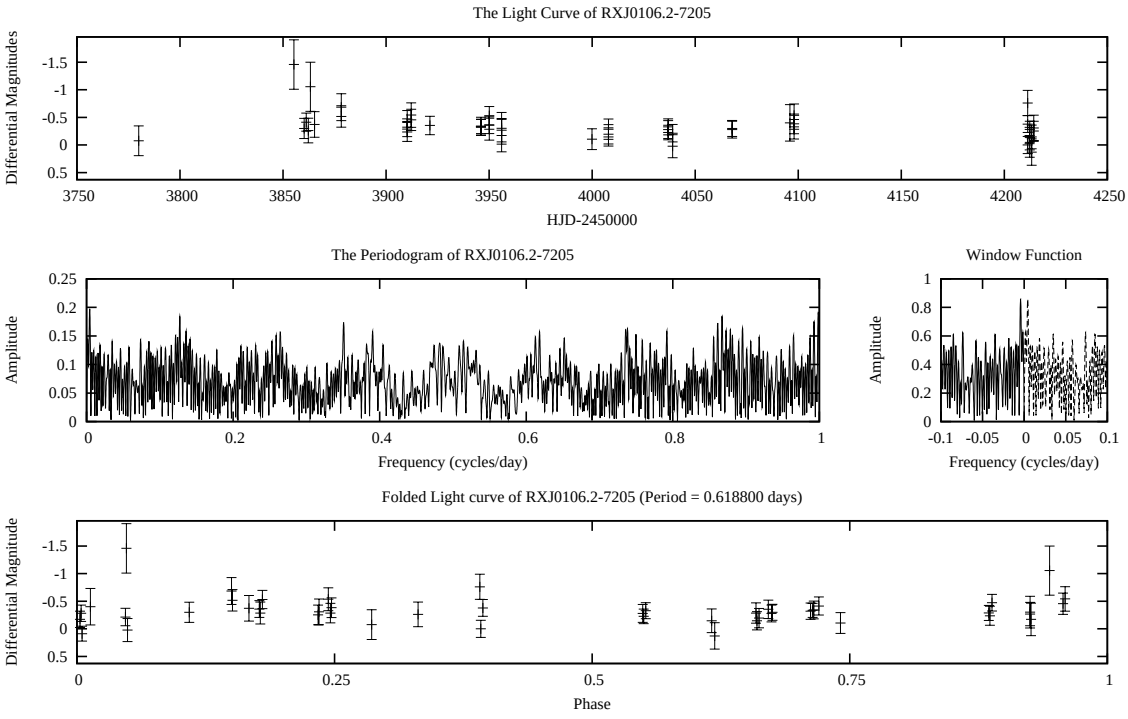

Figure 4.39: The Light Curve, Periodogram and Window Function of RX J0106.2-7205.

There is no known period for this star. The light curve was folded to the result of 0.6188 days.

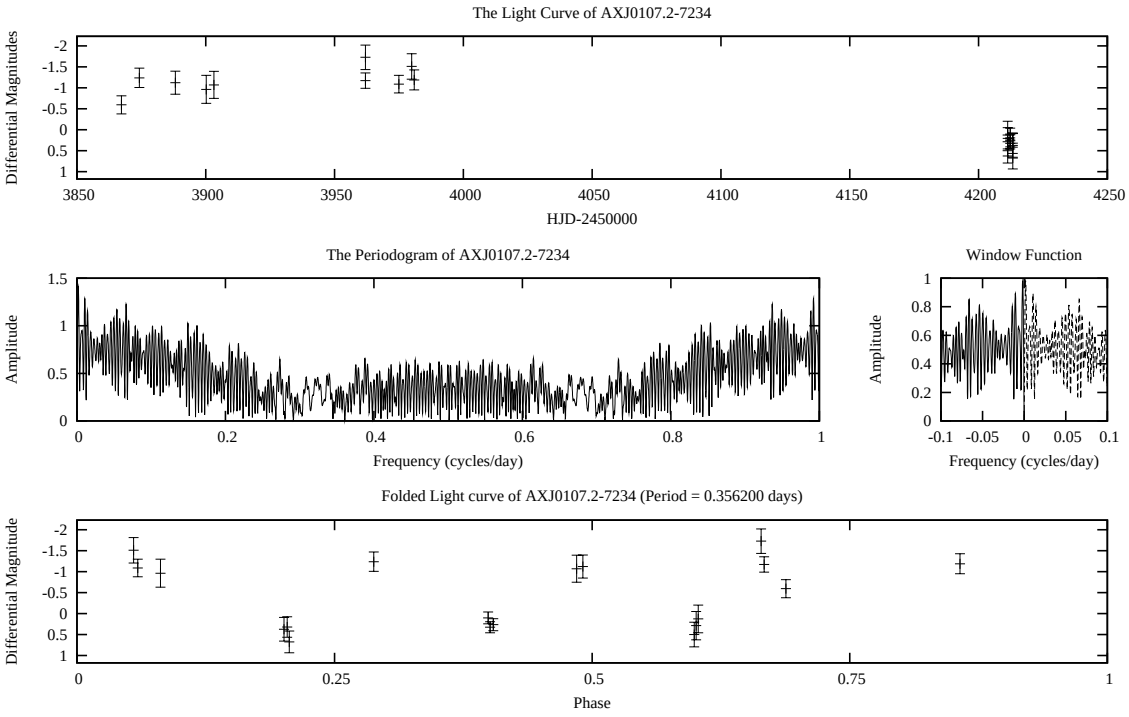

Figure 4.40: The Light Curve, Periodogram and Window Function of AX J0107.2-7234. Data is very sparse in this light curve. The light curve was folded to the Period04 result of 0.3562 days.

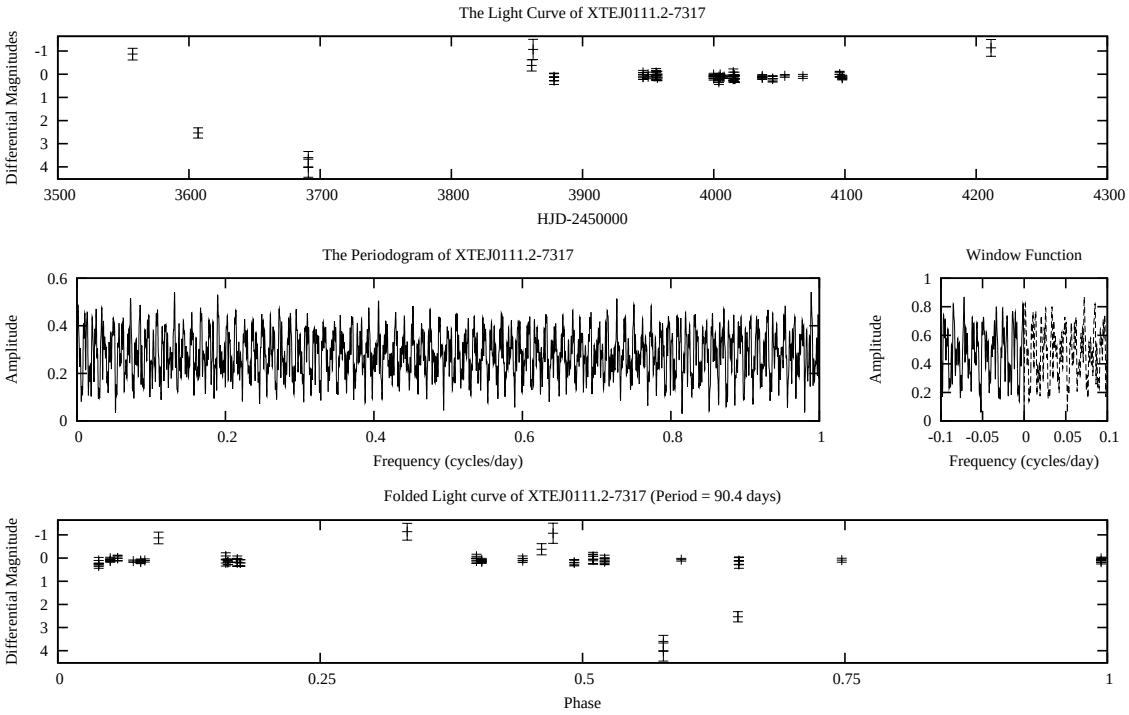

Figure 4.41: The Light Curve, Periodogram and Window Function of XTE J0111.2-7317. The data is very sparse. in this light curve. It was folded to 90.4 days.

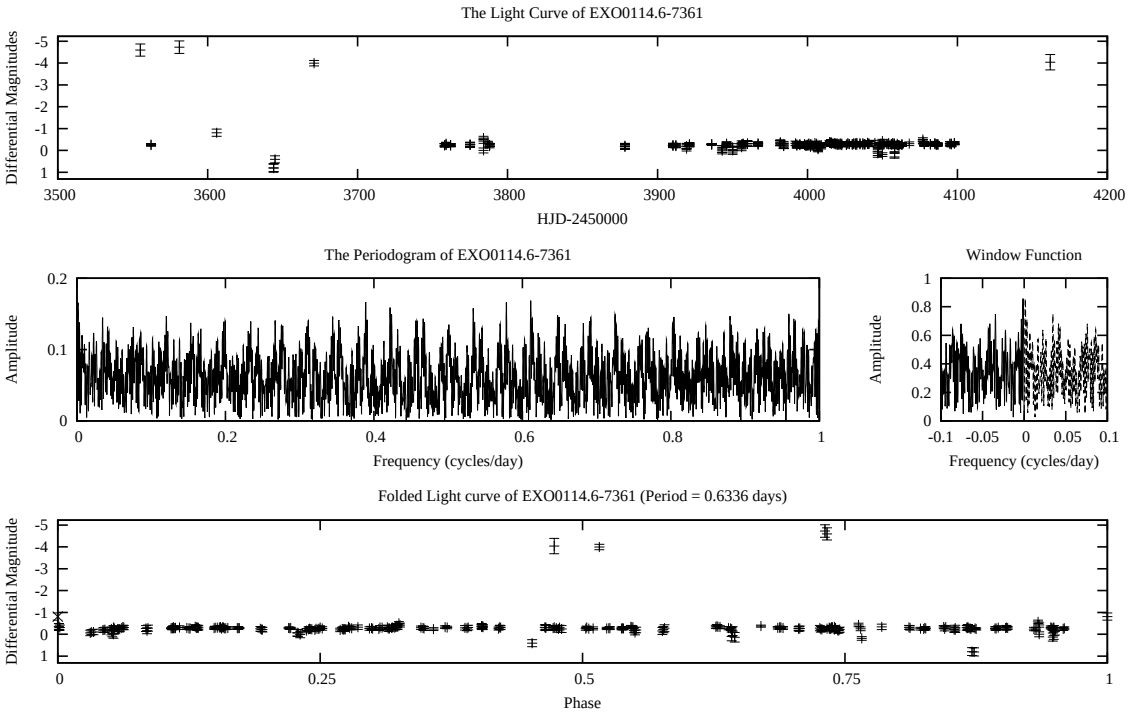

Figure 4.42: The Light Curve, Periodogram and Window Function of EXO 0114.6-7336. This light curve was folded to the 0.6336 day period found by Period04.

Table 4.2: A list of the frequencies and associated SNR for each significant detection.

2LPH No.	Name	Frequency (c/d)	SNR
006	RX J0047.3-7313	8.02185±0.000019	7.31
008	RX J0048.5-7302	8.02168±0.00002	5.75
015	2S 0050-727	0.00418±0.000061	5.39
		10.03±0.000038	5.81
		6.02±0.000053	6.19
		11.04±0.000065	5.10
027	RX J0051.8-7231	1.000091±0.00003	8.55
		8.99971±0.000059	5.60
		8.99407±0.000076	4.34
043	XTE J0055-724	0.00058±0.000035	9.56
053	CXOU J005750.3-720756	29.8008±0.000031	4.46
		48.1326±0.000036	14.68
		12.08817±0.000061	9.05
		33.47211±0.000086	6.31
		12.4984±0.000077	7.19
065	RX J0101.3-7211	0.002091±0.000046	4.73
		27.96796±0.000000011	9.01
		17.12192±0.00010	10.65
		14.30956±0.00017	6.34
		45.15532±0.00018	6.74
073	RX J0103.6-7201	1.00078±0.00001	10.46
		3.0012±0.000038	11.45
		44.20123±0.00011	3.97

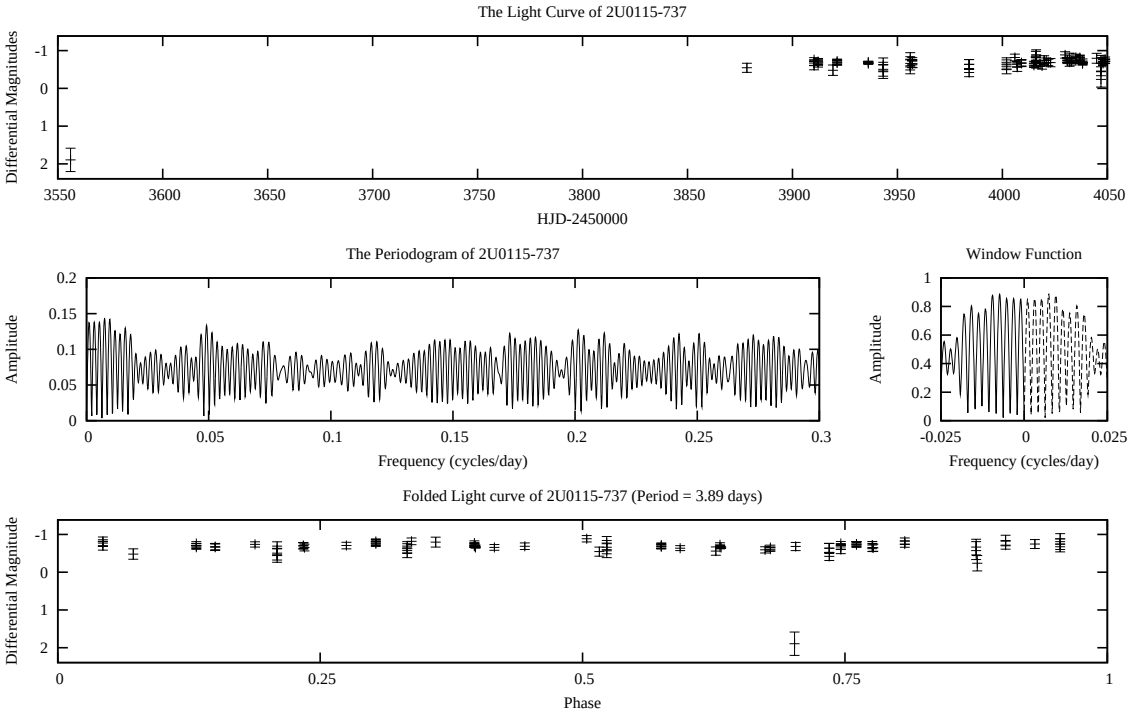

Figure 4.43: The Light Curve, Periodogram and Window Function of 2U 0115-737. First HMXB detected in SMC this object has 591 references and 48 identifiers! The SNR of the first frequency was 2.94, not good enough to be considered a detection. The graph was folded to 3.89 days.

Table 4.3: A list of the targets from the LMC and the references that give the history of each object.

No.	Name	X-ray Discovery	Optical Match	Period Found
099	RX J0516.0-6916	[21]	[21]	
100	RX J0520.5-6932	[100]	[100]	[100]
110	XMMU J053115.4-705350	[66]	[66]	
121	3A 0540-697	[49]	[60]	[84]
122	XMMU J054134.7-682550	[107]	[107]	
123	RX J0541.4-6936	[93]	[93]	
124	RX J0541.5-6833	[93]	[93]	
127	1SAX J0544.1-7100	[38]	[43]	

4.2 LMC HMXBs

Table 4.4: Statistically significant detections from LMC HMXBs.

No.	Name	Frequency (c/d)	SNR
100	RX J0520.5-6932	2.00402±0.000079	4.38
		1.99663±0.000086	6.02
110	XMMU J053115.4-70535	1.00183±0.000025	11.50
		1.00670±0.000025	11.86
		0.99780±0.000054	13.06
		17.01286±0.000049	5.51
		15.77175±0.00012	4.03
123	RX J0541.4-6936	1.00249±0.00013	4.44
124	RX J0541.5-6833	0.99062±0.000094	5.42

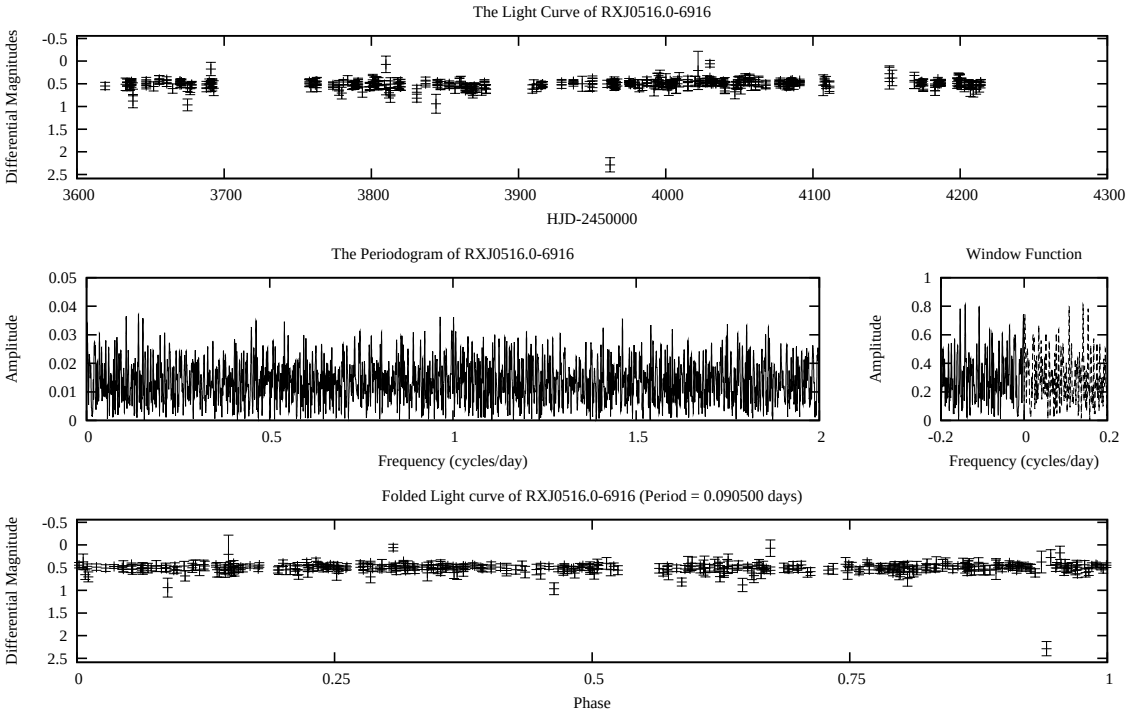

Figure 4.44: The Light Curve, Periodogram and Window Function of RX J0516.0-6916. There is no known period for this star. The frequency that was found (0.905 cycles per day) has an SNR of 2.79. However, seeing as there is no other published period for this star, this was the frequency to which the light curve was folded: 0.0905 days.

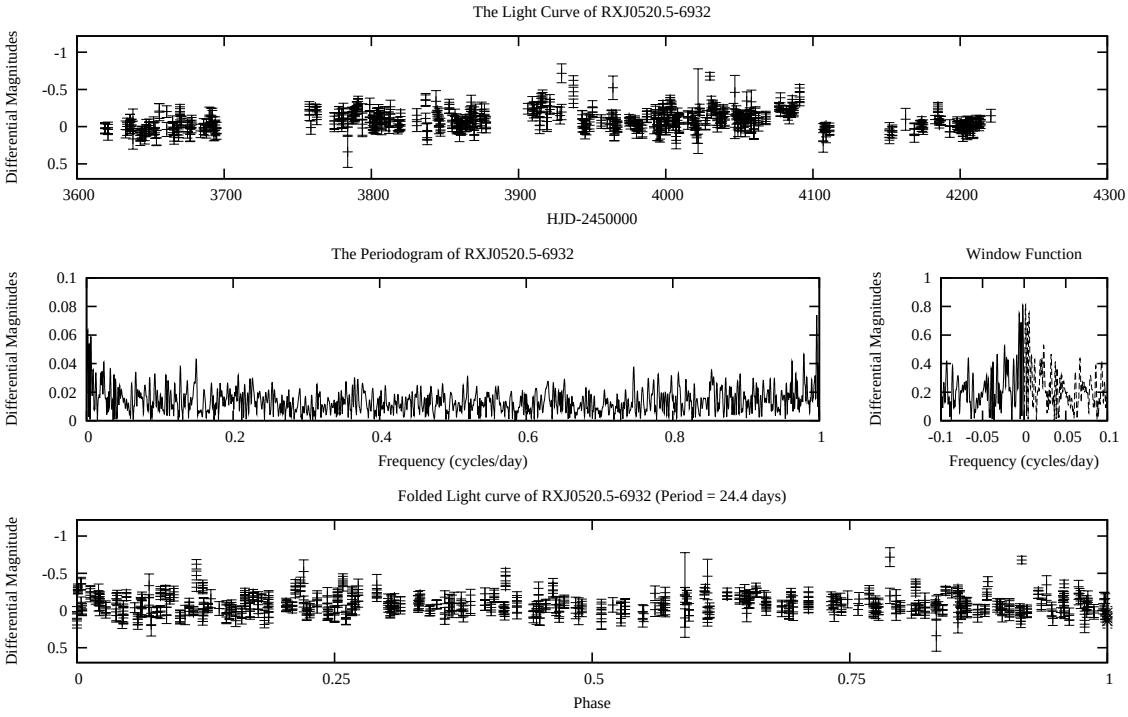

Figure 4.45: The Light Curve, Periodogram and Window Function of RX J0520.5-6932. There is no power at the frequency of the known period. The SNR of the 2 cycle/day period was 4.38. The light curve was folded to 24.4 days.

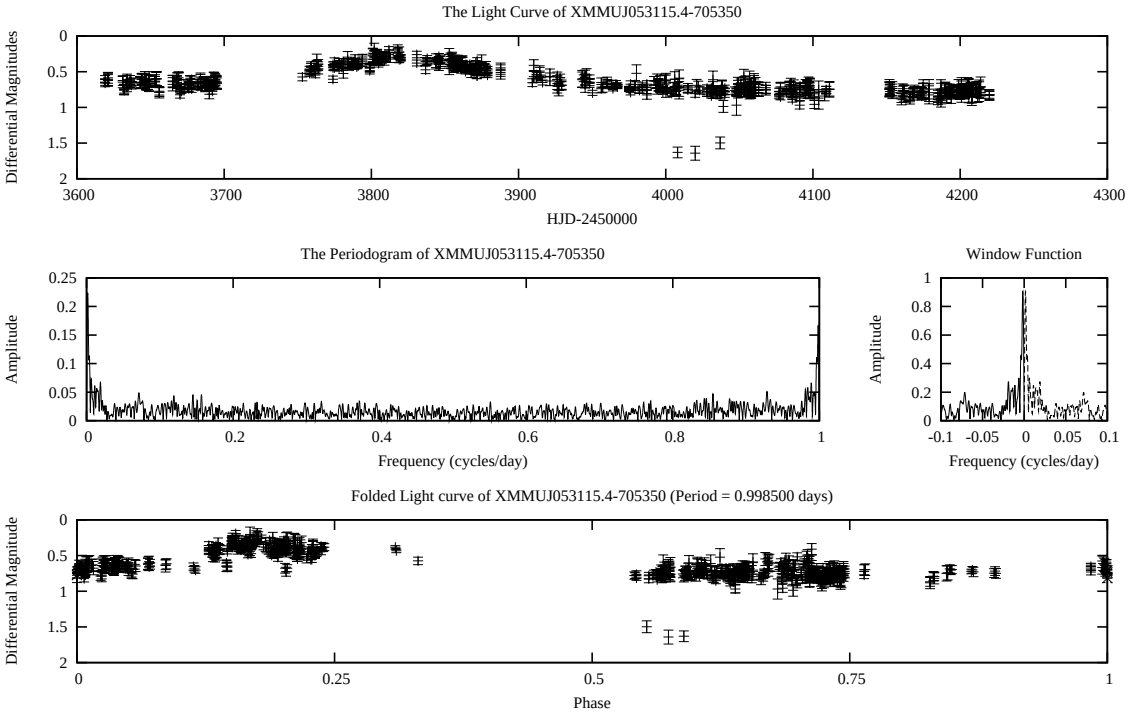

Figure 4.46: The Light Curve, Periodogram and Window Function of XMMU J053115.4-705350. There is no period known for this star. There is a very strong SNR at 1 cycle per day (11.50), the light curve was folded to this period. However, this is likely aliasing.

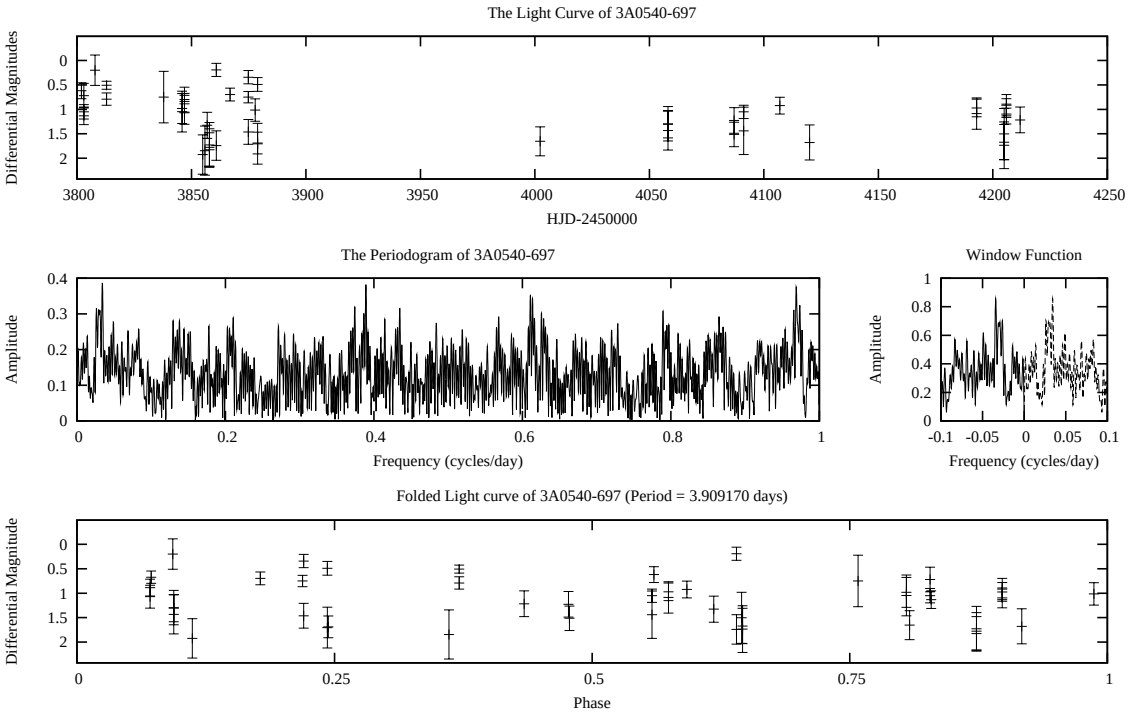

Figure 4.47: The Light Curve, Periodogram and Window Function of 3A 0540-697. The light curve was folded to the period given in [84], 3.909170 days.

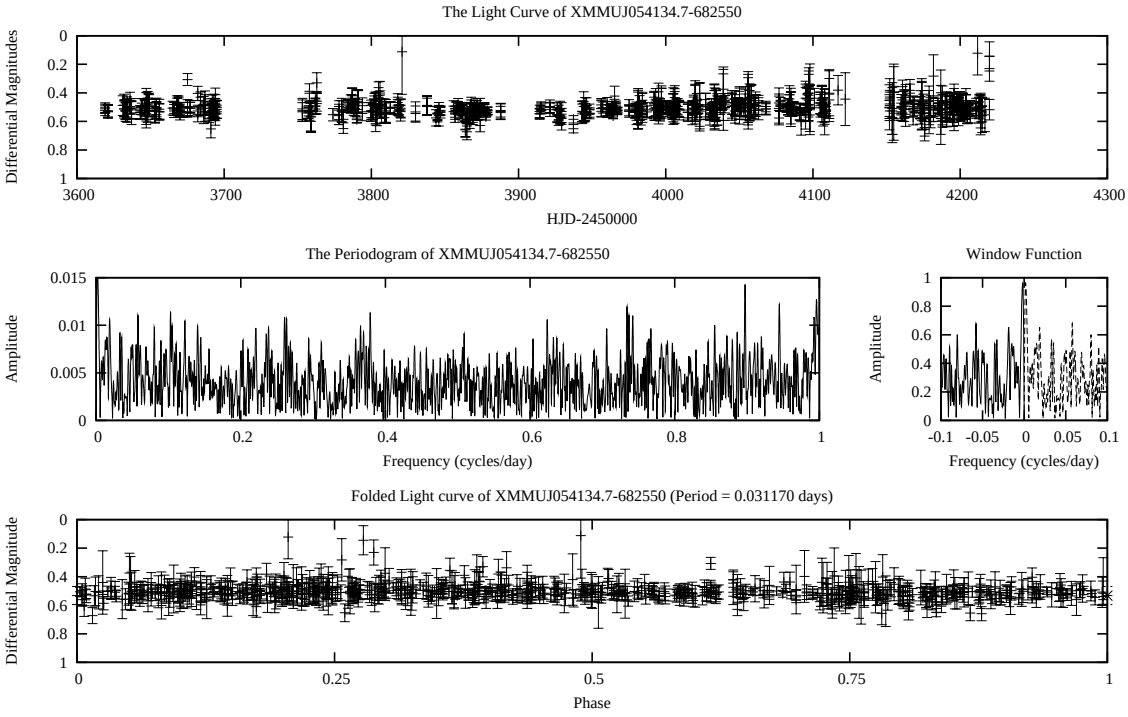

Figure 4.48: The Light Curve, Periodogram and Window Function of XMMU J054134.7-682550. There is no period determined for this star. The SNR for this first period was 3.87. The light curve was folded to this 0.03117 day period. There is a small variation in the light curves visible, but doesn't show up in the periodogram.

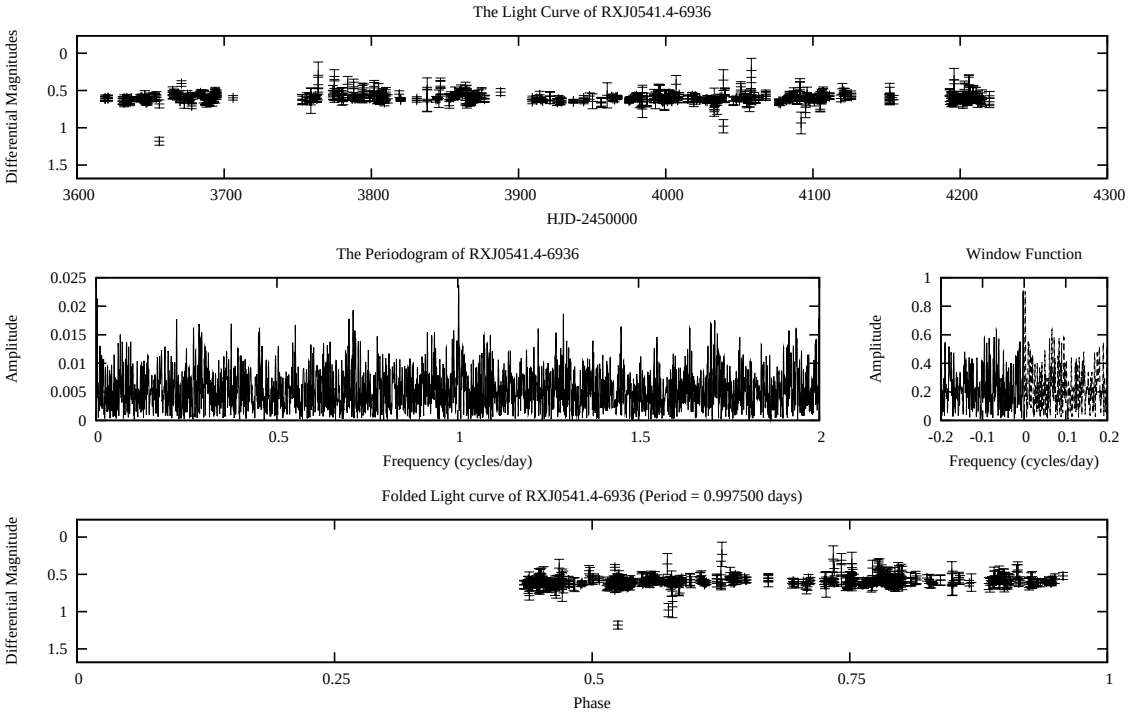

Figure 4.49: The Light Curve, Periodogram and Window Function of RX J0541.4-6936. The period of this star is also not determined. There is also aliasing at the one cycle/day rate. About half the folded light curve is missing when folded to this period. This leads one to believe this is not a true period.

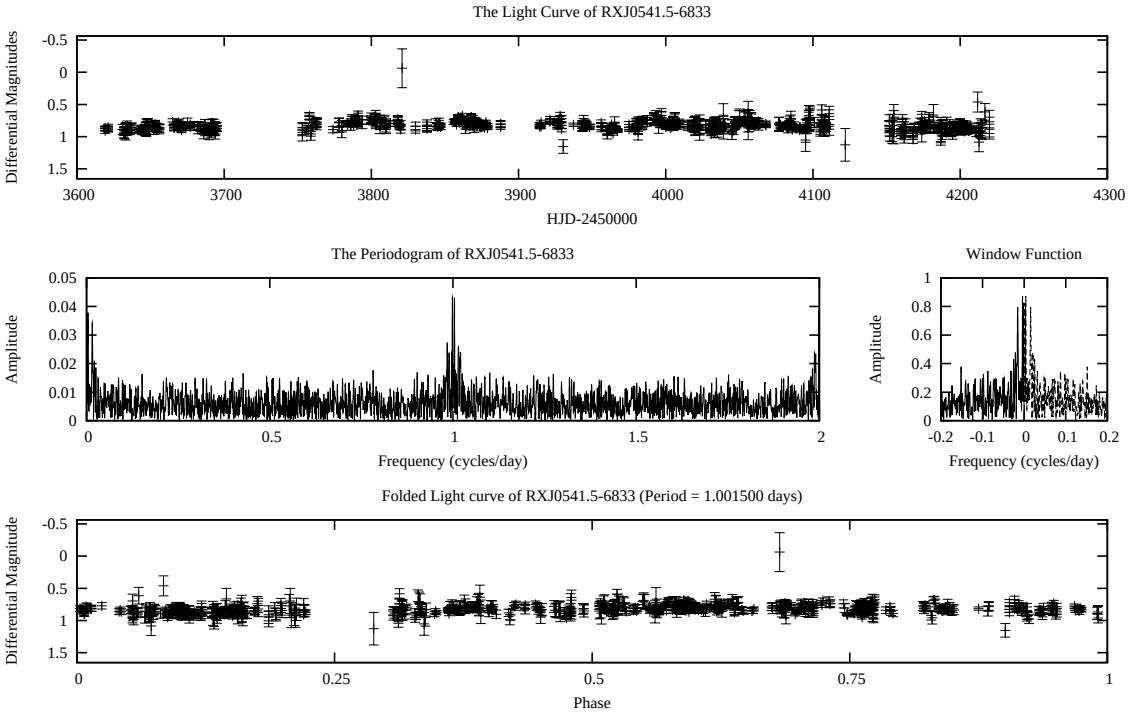

Figure 4.50: The Light Curve, Periodogram and Window Function of RX J0541.5-6833. Period not determined. The SNR of the 1 cycle/day period is 5.42, but seeing as it is so close to 1 cycle/day, this is likely just aliasing. However, the light curve was still folded to once day period.

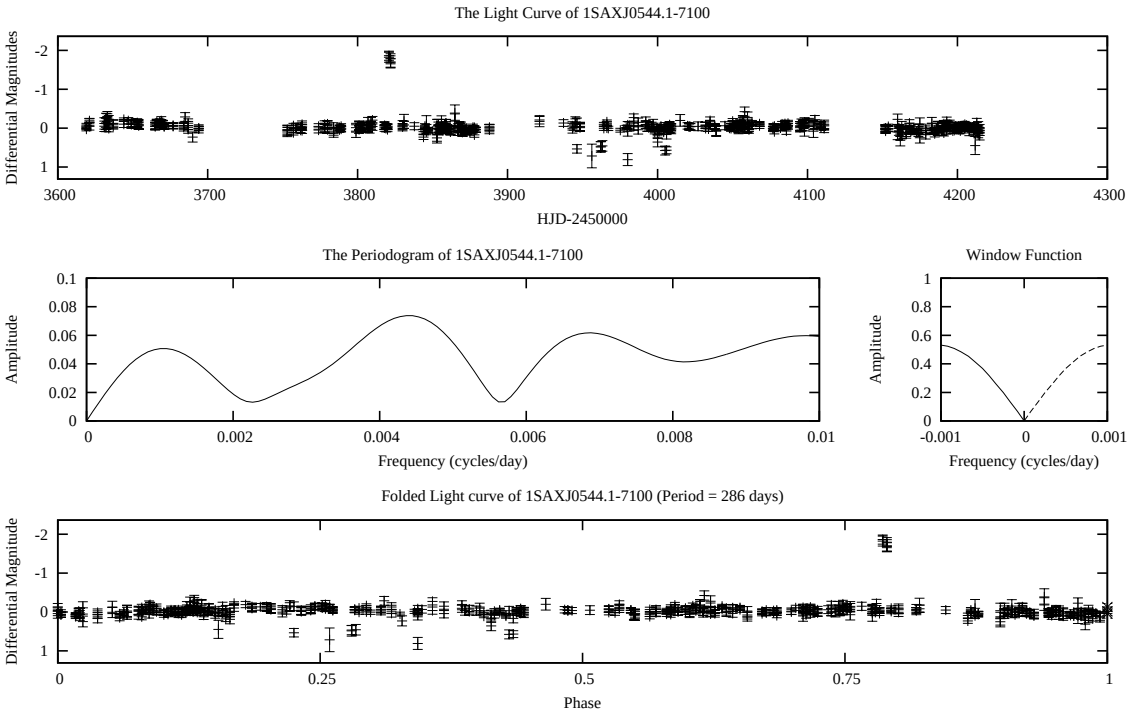

Figure 4.51: The Light Curve, Periodogram and Window Function of 1SAX J0544.1-7100. Period not determined. The SNR of the 4 cycle per day period is 3.06. The light curve was folded to 286 days.

Chapter 5

Conclusions

Fifty-one stars were examined from the available images from the ROTSEIIIa telescope. There are only three results that can be interpreted as possible orbital periods. That for 2S 0050-727 (catalogue number 15) XTE J0055-724 (catalogue number 43) and RX J0101.3-7211 (catalogue number 65).

The period of 2S 0050-727 given in [28] is 45.1 days. The ROTSEIIIa data shows a period of 243 days. (See Figure 4.7) There are multiple lines of evidence pointing to a 44 to 45 day period in multiple data sets. One probable interpretation of the 243 day period may be the product of a dust cloud that alternately reflects and then absorbs light as seen in [5]. Infra-red and spectroscopic investigation would confirm the existence of the cloud if its still there.

XTE J0055-724 (Figure 4.20; catalogue number 043) had displayed a period of 1724 days. Based on an overall shape of the raw light curve, this may not be an orbital period, instead a long term brightening that HMXBs do exhibit. A period of 1724 days is also far beyond the maximum reach of the dataset. For that reason, the finding for XTE J0055-724 is likely a true period.

For RX J0101.3-7211 (Figure 4.34, catalogue number 065), a period of 478 days was found. In the literature an orbital period of 74.4 days is reported [98]. The period of 74.4 days is not evident after folding the light curve to that period. 478 days is roughly half of my observation time, raising the possibility of a window function artefact.

It is clear that there are an insufficient number of periods determined in this study to comment on population models of HMXBs. All the periods that look likely conflict with established periods in the literature. This may be for three reasons:

1. There are no filters on the ROTSEIII telescopes. Recall that filters, among their many uses, would eliminate the fringing on the images taken by the ROTSEIII. The fringing pattern tends to change somewhat with time, necessitating new fringing maps be make on a regular basis. If an old map does not remove all the fringing, it may cause brightening where there isn't any real signal.

2. There are large gaps in the light curves. Important information may be missing during these periods where there is no data.

3. The images were taken at the same times every night, in the same order. This leads to very bad aliasing and may play a role in selecting what frequencies are allowed to be effectively analyzed.

5.1 Serendipitous findings

Given that several stars have a flat profile, this essentially means that there are no prejudicial systematic errors in the data set. Flat light curves like RXJ0051.3-7216 (Figure 4.14, catalogue number 021) and RX J0516.0-6916 (Figure 4.44, catalogue number 099) show that the sample is relatively free of systematic errors.

RXJ0047.3-7313 (Figure 4.1; catalogue number 006), RXJ0048.5-7302 (Figure 4.3; catalogue number 008), RXJ0051.3-7216 (Figure 4.9; catalogue number 027) displayed what look like β- Cephei pulsations. The period and amplitude of the fluctuations fall in the right range. A radial velocity study is needed to confirm this. There is apparently no β-Cephei variable catalogue for the SMC.

XMMU J053115.4-705350 (Figure 4.46, catalogue number 110) looks like it shows an optical outburst. X-ray data if they existed would confirm this finding.

RXJ0054.5-7340's (Figure 4.17, catalogue number 036) light curve has a very large change in magnitude. This could be argued to be contamination of its PSF from a nearby bright star, combined with fringing from the CCD along the edges of plates. In general, it was found that the closer to the centre of a field of stars was the target, the less variation there was in the light curve.

References

[1]

[2] C. W. Akerlof, R. L. Kehoe, T. A. McKay, E. S. Rykoff, D. A. Smith, D. E. Casperson, K. E. McGowan, W. T. Vestrand, P. R. Wozniak, J. A. Wren, M. C. B. Ashley, M. A. Phillips, S. L. Marshall, H. W. Epps, and J. A. Schier. The ROTSE-III Robotic Telescope System. *PASP*, 115:132, 2003.

[3] W. Baade and F. Zwicky. Remarks on Super-Novae and Cosmic Rays. *Physical Review*, 46:76–77, July 1934.

[4] S. A. Balbus. Enhanced Angular Momentum Transport in Accretion Disks. *ARAA*, 41:555–597, 2003.

[5] T. R. Bedding, A. A. Zijlstra, A. Jones, F. Marang, M. Matsuura, A. Retter, P. A. Whitelock, and I. Yamamura. The light curve of the semiregular variable L2 Puppis - I. A recent dimming event from dust. *Mon. Not. R. Astron. Soc.*, 337:79–86, November 2002.

[6] C. T. Bolton. Identification of Cygnus X-1 with HDE 226868. *Nature*, 235:271, 1972.

[7] F. C. Bruhweiler, D. A. Klinglesmith, III, T. R. Gull, and S. Sofia. Deep Einstein X-ray imagery of the Small Magellanic Cloud. *ApJ*, 317:152–162, June 1987.

[8] Edwin Budding and Osman Demicran. *Introduction to Astronomical Photometry*. Cambridge University Press, Cambridge UK, second edition, 2007.

[9] A. G. W. Cameron. Nuclear Reactions in Stars and Nucleogenesis. *PASP*, 69:201, June 1957.

[10] D. Chakrabarty, T. Takeshima, M. Ozaki, B. Paul, and J. Yokogawa. XTE J0111.2-7317. *IAU Circ.*, 7062:1, November 1998.

[11] M. J. Coe. An estimate of the supernova kick velocities for high-mass X-ray binaries in the Small Magellanic Cloud. *Mon. Not. R. Astron. Soc.*, 358:1379–1382, April 2005.

[12] M. J. Coe, W. R. T. Edge, J. L. Galache, and V. A. McBride. Optical properties of Small Magellanic Cloud X-ray binaries. *Mon. Not. R. Astron. Soc.*, 356:502–514, January 2005.

[13] M. J. Coe, N. J. Haigh, and P. Reig. The SMC X-ray transient XTE J0111.2-7317: a Be/X-ray binary in a supernova remnant? *Mon. Not. R. Astron. Soc.*, 314:290–294, May 2000.

[14] R. Corbet, C. B. Markwardt, F. E. Marshall, S. Laycock, and M. Coe. Transient X-Ray Pulsars. *IAU Circ.*, 7932:2, July 2002.

[15] R. Corbet, F. E. Marshall, J. C. Lochner, M. Ozaki, and Y. Ueda. XTE J0053-724 and AX J0051-722. *IAU Circ.*, 6803:1, January 1998.

[16] R. Corbet, F. E. Marshall, and C. B. Markwardt. XTE J0052-723. *IAU Circ.*, 7562:1, January 2001.

[17] R. H. D. Corbet. Be/neutron star binaries - A relationship between orbital period and neutron star spin period. *A & A*, 141:91–93, December 1984.

[18] A. P. Cowley and P. C. Schmidtke. Periodic Optical Outbursts from the Be-Neutron Star Binary AX J0049.4-7323. *AstronJ.*, 126:2949, 2003.

[19] A. P. Cowley and P. C. Schmidtke. Periodic Optical Outbursts from the Be-Neutron Star Binary AX J0049.4-7323. *AJ*, 126:2949–2953, December 2003.

[20] A. P. Cowley, P. C. Schmidtke, A. L. Anderson, and T. K. McGrath. Determination of the optical counterpart of LMC X-1. *PASP*, 107:145–147, February 1995.

[21] A. P. Cowley, P. C. Schmidtke, T. K. McGrath, A. L. Ponder, M. R. Fertig, J. B. Hutchings, and D. Crampton. Magellanic Cloud X-ray sources observed with ROSAT. *PASP*, 109:21–38, January 1997.

[22] Lindsey E. Davis. A reference guide to the iraf/daophot package. Technical report, National Optical Astronomical Observatories, Tucson, Arizona, 1994. Distributed via the IRAF website: http://www.iraf.net.

[23] J. F. Dolan and S. Tapia. The orbital inclination of Cygnus XR-1 measured polarimetrically. *ApJ*, 344:830, 1989.

[24] L. M. Dray. On the metallicity dependence of high-mass X-ray binaries. *Mon. Not. R. Astron. Soc.*, 370:2079–2090, August 2006.

[25] L. W. Dray. On the metallicity dependence of high-mass X-ray binaries. *Mon. Not. R. Astron. Soc.*, 370:2079, 2006.

[26] W. R. T. Edge. *Studies of Be X-ray Binaries in the Magellanic Clouds*. PhD thesis, University of Southampton, 2005.

[27] W. R. T. Edge and M. J. Coe. Optical counterparts to four X-ray sources in the Small Magellanic Cloud. *Mon. Not. R. Astron. Soc.*, 338:428–432, January 2003.

[28] W. R. T. Edge, M. J. Coe, R. H. D. Corbet, C. B. Markwardt, and S. Laycock. SMC X-3 Identified with RXTE 7.78s Pulsar from Archive Chandra Data. *The Astronomer's Telegram*, 225:1, January 2004.

[29] W. R. T. Edge, M. J. Coe, R. H. D. Corbet, C. B. Markwardt, S. Laycock, and F. E. Marshall. Position of RXTE 82.4s pulsar (XTE J0052-725) determined using archive Chandra Data. *The Astronomer's Telegram*, 215:1, December 2003.

[30] W. R. T. Edge, M. J. Coe, and J. L. Galache. Binary period in Optical counterpart to XMMU J004723.7-731226 (SXP 264). *The Astronomer's Telegram*, 405:1, February 2005.

[31] W. R. T. Edge, M. J. Coe, J. L. Galache, V. A. McBride, R. H. D. Corbet, C. B. Markwardt, and S. Laycock. Three new X-ray pulsars detected in the Small Magellanic Cloud and the positions of two other known pulsars determined. *Mon. Not. R. Astron. Soc.*, 353:1286–1292, October 2004.

[32] W. R. T. Edge, M. J. Coe, J. L. Galache, V. A. McBride, R. H. D. Corbet, C. B. Markwardt, S. Laycock, and F. E. Marshall. Binary period in Optical counterpart to CXOU J005455.6-724510 = RXJ0054.9-7245 = AX J0054.8-7244 = SXP504. *The Astronomer's Telegram*, 426:1, February 2005.

[33] P. Eger and F. Haberl. XMM-Newton observations of the Small Magellanic Cloud: Long term evolution of frequently observed Be/X-ray binaries. *A & A*, 491:841–849, December 2008.

[34] M. D. Filipović, W. Pietsch, and F. Haberl. A multi-frequency identification study of the SMC X-ray binary AX J0049-732. *A & A*, 361:823–826, September 2000.

[35] D. W. Fox and W. H. G. Lewin. MXB 1730-335. *IAU Circ.*, 7081:3, January 1999.

[36] Juhan Frank, Andrew King, and Derek Raine. *Accretion Power in Astrophysics*. Cambridge University Press, Cambridge UK, second edition, 1992.

[37] J. L. Galache, R. H. D. Corbet, M. J. Coe, S. Laycock, M. P. E. Schurch, C. Markwardt, F. E. Marshall, and J. Lochner. A Long Look at the Be/X-Ray Binaries of the Small Magellanic Cloud. *ApJS*, 177:189–215, July 2008.

[38] P. Garnavich, N. Suntzeff, M. Phillips, R. C. Smith, A. Clocchiatti, A. Diercks, P. Challis, B. Schmidt, A. V. Filippenko, A. G. Riess, D. C. Leonard, and E. C. Moran. Supernovae. *IAU Circ.*, 6861:1, April 1998.

[39] Riccardo Giacconi. Nobel lecture: The dawn of x-ray astronomy. *Rev. Mod. Phys.*, 75(3):995, Aug 2003.

[40] Riccardo Giacconi, Herbert Gursky, Frank R Paolini, and Bruno B. Rossi. Evidence for X-Rays from Outside the Solar System. *Phys Rev. Letters*, 9:439, 1962.

[41] H.-J. Grimm, M. Gilfanov, and R. Sunyaev. High-mass X-ray binaries as a star formation rate indicator in distant galaxies. *Mon. Not. R. Astron. Soc.*, 339:793–809, March 2003.

[42] Herbert Gursky and Remo Ruffini. *Neutron Stars, Black Holes and Binary X-Ray Sources*. Reidel Publishing Co, Dordtrecht , Holland, 1975.

[43] F. Haberl, W. Pietsch, and M. D. Filipovic. 1SAX J0544.1-710 = RX J0544.1-7100. *IAU Circ.*, 6867:1, April 1998.

[44] F. Haberl and M. Sasaki. Doubling the number of Be/X-ray binaries in the SMC. *A & A*, 359:573–585, July 2000.

[45] Coel Hellier. *Cataclysmic Variable Stars: How and Why they Vary.* Springer Praxis, Chichester, UK, 2001.

[46] R. K. Honeycutt. CCD ensemble photometry on an inhomogeneous set of exposures. *PASP*, 104:435–440, June 1992.

[47] R.Q. Huang and K.N. Yu. *Stellar Astrophysics*. Springer, Singapore, 1998.

[48] K. Imanishi, J. Yokogawa, and K. Koyama. AX J0049-732. *IAU Circ.*, 7040:2, October 1998.

[49] H. Inoue, K. Koyama, and Y. Tanaka. Soft X-ray observation of supernova remnants in the Small Magellanic Cloud. In J. Danziger & P. Gorenstein, editor, *Supernova Remnants and their X-ray Emission*, volume 101 of *IAU Symposium*, pages 535–540, 1983.

[50] G. L. Israel, L. Stella, S. Campana, S. Covino, D. Ricci, and T. Oosterbroek. 1SAX J0103.2-7209, AX J0051-722, and XTE J0055-724. *IAU Circ.*, 6999:1, August 1998.

[51] Agnieszka Janiuk and Božena Czerny. Time dependent accretion onto a black hole in a disk plus corona system. *Advances in Space Research*, 38:2903, 2006.

[52] Lyman Spitzer Jr. *Physical Processes in the Interstellar Medium*. Wiley - Interscience, New York, New York, 1978.

[53] P. Kahabka and W. Pietsch. X-ray binary systems in the Small Magellanic Cloud. *A & A*, 312:919–936, August 1996.

[54] P. Kahabka, W. Pietsch, M. D. Filipović , and F. Haberl. A ROSAT PSPC X-ray survey of the Small Magellanic Cloud. *AAS*, 136:81–94, April 1999.

[55] R. C. Lamb, T. A. Prince, D. J. Macomb, and M. H. Finger. RX J0052.1-7319. *IAU Circ.*, 7081:4, January 1999.

[56] H. J. G. L. M. Lamers, F. J. Zickgraf, de Winter D., Houziaux L., and Zorec J. An improved classification of B[e]-type stars. *A & A*, 340:117, 1998.

[57] S. Laycock, R. H. D. Corbet, M. J. Coe, F. E. Marshall, C. Markwardt, and W. Edge. X-Ray and optical observations of XTE J0052-723: a transient Be/X-ray pulsar in the Small Magellanic Cloud. *Mon. Not. R. Astron. Soc.*, 339:435–441, February 2003.

[58] S. Laycock, R. H. D. Corbet, M. J. Coe, F. E. Marshall, C. Markwardt, and J. Lochner. Long-Term Behavior of X-Ray Pulsars in the Small Magellanic Cloud. *ApJS*, 161:96–117, November 2005.

[59] P. Lenz and M. Breger. Period04 User Guide. *Communications in Asteroseismology*, 146:53–136, June 2005.

[60] C. Leong, E. Kellogg, H. Gursky, H. Tananbaum, and R. Giacconi. X-Ray Emission from the Magellanic Clouds Observed by UHURU. *ApJL*, 170:L67+, December 1971.

[61] Walter H.G. Lewin and Edward P.J. van den Heuvel, editors. *Accretion-driven Stellar X-ray Sources.* Cambridge University Press, Cambridge, UK., 1983.

[62] Walter H.G. Lewin and Michiel van der Klis. *Compact Stellar X-ray Sources.* Cambridge University Press, Cambridge, UK, 2006.

[63] F. Li, G. Jernigan, and G. Clark. SMC X-2 and SMC X-3. *IAU Circ.*, 3125:1, October 1977.

[64] Marconi Applied Technologies Limited. Marconi Applied Technologies CCD42-40 PGA Back Illuminated AIMO Large Area Sensor for Scientific Applications. Technical report, Marconi Applied Technologies Limited, Chelmsford, Essex, United Kingdom, October, 2001.

[65] Q. Z. Liu. HMXBs in the Galaxy and the MCs. In E. J. A. Meurs & G. Fabbiano, editor, *Populations of High Energy Sources in Galaxies*, volume 230 of *IAU Symposium*, pages 41–42, 2006.

[66] Q. Z. Liu, J. van Paradijs, and E. P. J. van den Heuvel. High-mass X-ray binaries in the Magellanic Clouds. *A & A*, 442:1135–1138, November 2005.

[67] QZ Liu, van Paradijs, and van den Heuvel. A catalogue of high-mass X-ray binaries. *Astron. Astrophys. Suppl. Ser.*, 147:25, 2000.

[68] Malcom S. Longhair. *High Energy Astrophysics*, volume 2. University of Cambridge Press, Cambridge U.K., second edition, 1994.

[69] R. Lopes de Oliveira, C. Motch, M. A. Smith, I. Negueruela, and J. M. Torrejón. On the X-ray and optical properties of the Be star HD 110432: a very hard-thermal X-ray emitter. *A & A*, 474:983–996, November 2007.

[70] D. J. Macomb, D. W. Fox, R. C. Lamb, and T. A. Prince. Three New Long-Period X-Ray Pulsars Discovered in the Small Magellanic Cloud. *ApJL*, 584:L79–L82, February 2003.

[71] W. A. Majid, R. C. Lamb, and D. J. Macomb. X-Ray Pulsars in the Small Magellanic Cloud. *ApJ*, 609:133–143, July 2004.

[72] A. B. Mason, J. S. Clark, A. J. Norton, I. Negueruela, and P. Roche. Spectral classification of the mass donors in the high-mass X-ray binaries EXO 1722-363 and OAO 1657-415. *A & A*, 505:281–286, October 2009.

[73] P. Massey. A UBVR CCD Survey of the Magellanic Clouds. *ApJS*, 141:81–122, July 2002.

[74] P. Massey, T. E. Armandroff, R. Pyke, K. Patel, and C. D. Wilson. Hot, Luminous Stars in Selected Regions of NGC 6822, M31, and M33. *AJ*, 110:2715M, 1995.

[75] D. S. Mathewson, V. L. Ford, M. A. Dopita, I. R. Tuohy, B. Y. Mills, and A. J. Turtle. Supernova remnants in the Magellanic Clouds. *ApJS*, 55:189–210, June 1984.

[76] T. K. McGrath, P. C. Schmidtke, A. P. Cowley, and A. L. Anderson. A New Be-star/X-ray Pulsar in the LMC. In *Bulletin of the American Astronomical Society*, volume 26 of *Bulletin of the American Astronomical Society*, page 1485, December 1994.

[77] R. E. Mennickent, L. Cidale, G. Pietrzyński, W. Gieren, and B. Sabogal. Blue and yellow long-period variables in the direction of the Small Magellanic Cloud. *A & A*, 457:949–961, October 2006.

[78] Eugene F. Milone. Asph 507: Senior astrophysics laboratory notes. Available from myself for inspection. Dr Milone makes a new set of notes every year to reflect changes in knowledge., 2003.

[79] I. F. Mirabel. Microquasars: Summary and Outlook. In T. Belloni, editor, *Lecture Notes in Physics, Berlin Springer Verlag*, volume 794 of *Lecture Notes in Physics, Berlin Springer Verlag*, page 1, March 2010.

[80] C. Motch, R. Lopes de Oliveira, I. Negueruela, F. Haberl, and E. Janot-Pacheco. X-ray and Optical Properties of New gcas-Like Objects Discovered in X-ray Surveys. In A. T. Okazaki, S. P. Owocki, & S. Stefl, editor, *Active OB-Stars: Laboratories for Stellare and Circumstellar Physics*, volume 361 of *Astronomical Society of the Pacific Conference Series*, page 117, March 2007.

[81] André Muller, editor. *The Magellanic Clouds*. Springer-Verlag, New York, 1971.

[82] Y. Nazé, J. M. Hartwell, I. R. Stevens, J. Manfroid, S. Marchenko, M. F. Corcoran, A. F. J. Moffat, and G. Skalkowski. An X-Ray Investigation of the NGC 346 Field in the Small Magellanic Cloud. II. The Field Population. *ApJ*, 586:983–995, April 2003.

[83] A. T. Okazaki and I. Negueruela. A natural explanation for periodic X-ray outbursts in Be/X-ray binaries. *A & A*, 377:161–174, October 2001.

[84] J. A. Orosz, D. Steeghs, J. E. McClintock, M. A. P. Torres, I. Bochkov, L. Gou, R. Narayan, M. Blaschak, A. M. Levine, R. A. Remillard, C. D. Bailyn, M. M. Dwyer, and M. Buxton. A New Dynamical Model for the Black Hole Binary LMC X-1. *ApJ*, 697:573–591, May 2009.

[85] Y. Osaki. Dwarf-Nova Outbursts. *PASP*, 108:39, January 1996.

[86] P. Pesch, N. Sanduleak, and A. G. D. Philip. SMC X-2 and SMC X-3. *IAU Circ.*, 3127:3, October 1977.

[87] P. Reig, J. Fabregat, and M. J. Coe. A new correlation for Be/X-ray binaries: the orbital period-Hα equivalent width diagram. *A & A*, 322:193–196, June 1997.

[88] M. T. Reynolds, P. J. Callanan, and A. V. Filippenko. Keck infrared observations of GRO J0422+32 in quiescence. *Mon. Not. R. Astron. Soc.*, 374:657–663, January 2007.

[89] R. D. Robinson, M. A. Smith, and G. W. Henry. X-Ray and Optical Variations in the Classical Be Star γ Cassiopeia: The Discovery of a Possible Magnetic Dynamo. , 575:435–448, August 2002.

[90] Eli Rykoff and Don Smith. Components and Operation of the ROTSE-III Telescope System. Technical report, University of Michigan, Ann Arbor, MI, USA, May 2003.

[91] A. Sandage, P. Osmer, R. Giacconi, P. Gorenstein, H. Gursky, J. Waters, H. Bradt, G. Garmire, B. V. Sreekantan, M. Oda, K. Osawa, and J. Jugaku. On the optical identification of SCO X-1. *ApJ*, 146:316, October 1966.

[92] G. Sarty, L. Kiss, R. Huziak, L. Catalan, D. Luciuk, T. Crawford, D. Lane, R. Pickard, T. Grzybowski, P. Closas, H. Johnston, D. Balam, and K. Wu. Periodicities in the high-mass X-ray binary system RXJ0146.9+6121/LSI+61deg 235. $Mon.Not.RAston.Soc.$, 392 : 1242, 2008.

[93] M. Sasaki, F. Haberl, S. Keller, and W. Pietsch. Discovery of pulsations from the Be/X-ray binary RXJ0101.3-7211in the SMC by XMM-Newton. *A & A*, 369:L29–L32, April 2001.

[94] M. Sasaki, F. Haberl, and W. Pietsch. ROSAT HRI catalogue of X-ray sources in the LMC region. *AAS*, 143:391–403, May 2000.

[95] M. Sasaki, F. Haberl, and W. Pietsch. ROSAT HRI catalogue of X-ray sources in the SMC region. *AAS*, 147:75–91, November 2000.

[96] P. C. Schmidtke and A. P. Cowley. Photometric Behavior of Be/X-ray Pulsars in the SMC. In *Bulletin of the American Astronomical Society*, volume 36 of *Bulletin of the American Astronomical Society*, page 1513, December 2004.

[97] P. C. Schmidtke and A. P. Cowley. Photometric Periodicities of Be/X-Ray Pulsars in the Small Magellanic Cloud. *AJ*, 130:2220–2229, November 2005.

[98] P. C. Schmidtke and A. P. Cowley. Multiple Photometric Periods in SXP1323 (RX J0103.6-7201). *The Astronomer's Telegram*, 716:1, January 2006.

[99] P. C. Schmidtke and A. P. Cowley. Photometric Variability of Be/X-Ray Pulsar Binaries in the Small Magellanic Cloud. *AJ*, 132:919–925, August 2006.

[100] P. C. Schmidtke, A. P. Cowley, L. M. Frattare, T. K. McGrath, J. B. Hutchings, and D. Crampton. LMC stellar X-ray sources observed with ROSAT. 1: X-ray data and search for optical counterparts. *PASP*, 106:843–857, August 1994.

[101] P. C. Schmidtke, A. P. Cowley, L. Levenson, and K. Sweet. Multiperiodic Variability in Magellanic Cloud Be/X-Ray Binaries. *AJ*, 127:3388–3393, June 2004.

[102] P. C. Schmidtke, A. P. Cowley, and A. Udalski. An Investigation of Be/X-Ray Pulsars with OGLE-III Data. *AJ*, 132:971–975, September 2006.

[103] E. Schreier, R. Giacconi, H. Gursky, E. Kellogg, and H. Tananbaum. Discovery of the Binary Nature of SMC X-1 from UHURU. *ApJL*, 178:L71+, December 1972.

[104] Matthew Peter Edward Schurch. *Optical and X-ray Studies of Be/X-ray Binaries in the Small Magellanic Cloud*. PhD thesis, University of Southampton, 2009.

[105] R. Seviour, M. Kosch, and F. Honary. Identification of clouds and aurorae in optical data images. *New J. Phys*, 5:6, 2003.

[106] P. R. Shapiro, M. L. Giroux, and A. Babul. Reionization in a cold dark matter universe: The feedback of galaxy formation on the intergalactic medium. *ApJ*, 427:25–50, May 1994.

[107] P. Shthkovskiy and M. Gilfanov. High mass X-ray binaries in the LMC: Dependence on the Stellar Population age and the "propeller" effect. *A & A*, 431:597, 2005.

[108] P. Shtykovskiy and M. Gilfanov. High mass X-ray binaries in the LMC: Dependence on the stellar population age and the "propeller" effect. *A & A*, 431:597–614, February 2005.

[109] P. Shtykovskiy and M. Gilfanov. High-mass X-ray binaries in the Small Magellanic Cloud: the luminosity function. *Mon. Not. R. Astron. Soc.*, 362:879–890, September 2005.

[110] J. B. Stevens, M. J. Coe, and D. A. H. Buckley. The optical counterparts to Be/X-ray binaries in the Magellanic Clouds. *Mon. Not. R. Astron. Soc.*, 309:421–429, October 1999.

[111] P.R. Swan. Discrete Fourier Transforms of Nonuniformly Spaced Data. *AJ*, 87:1608, 1982.

[112] Michelle Thaller. Colliding Winds in Massive Binary Systems. *PASP*, 110:636, 1998.

[113] Martin Thompson and David Woods. UNSW V.O. Archive for the APT and ROTSE-IIIa Telescopes. Technical report, University of New South Whales, Sydney, Australia, March 2007.

[114] E. P. J. van den Heuvel. Double Neutron Stars: Evidence For Two Different Neutron-Star Formation Mechanisms. *AIPC*, 924:598V, 2007.

[115] E. P. J. van den Heuvel, S. F. Portegies Zwart, D. Bhattacharya, and L. Kaper. On the origin of the difference between the runaway velocities of the OB-supergiant X-ray binaries and the Be/X-ray binaries. *A & A*, 364:563–572, December 2000.

[116] A. van der Meer, L. Kaper, M. H. van Kerkwijk, M. H. M. Heemskerk, and E. P. J. van den Heuvel. Determination of the mass of the neutron star in SMC X-1, LMC X-4, and Cen X-3 with VLT/UVES. *A & A*, 473:523–538, October 2007.

[117] R. Walter and J. Zurita Heras. Probing clumpy stellar winds with a neutron star. *A & A*, 476:355, 2007.

[118] Q. Wang and X. Wu. A comprehensive X-ray study of the Small Magellanic Cloud. *ApJS*, 78:391–401, February 1992.

[119] B. L. Webster, W. L. Martin, M. W. Feast, and P. J. Andrews. SMC X-1-Optical candidate. *Nature*, 240:183, December 1972.

[120] R. Wright and P. Hodge. *The Large Magellanic Cloud*. Smithsonian Press, Washington, D.C., 1967.

[121] L. Wyrzykowski, A. Udalski, M. Kubiak, M. K. Szymanski, K. Zebrun, I. Soszynski, P. R. Wozniak, G. Pietrzynski, and O. Szewczyk. The Optical Gravitational Lensing Experiment. Eclipsing Binary Stars in the Small Magellanic Cloud. *Acta Astronomica*, 54:1, March 2004.

[122] J. Yokogawa, K. Imanishi, M. Tsujimoto, K. Koyama, and M. Nishiuchi. Review of Discrete X-Ray Sources in the Small Magellanic Cloud: Summary of the ASCA Results and Implication on the Recent Star-Forming Activity. *PASJ*, 55:161–189, February 2003.

[123] J. Yokogawa, K. Imanishi, M. Ueno, and K. Koyama. Discovery of the Slowest X-Ray Pulsar in the SMC, AX J0049.5-7323, with ASCA. *PASJ*, 52:L73–L76, December 2000.

[124] J. Yokogawa and K. Koyama. AX J0049-729. *IAU Circ.*, 6835:1, April 1998.

[125] Y. B. Zel'dovich and I. D. Novikov. Reviews of Topical Problems: Relativistic Astrophysics. Ii. *Soviet Physics Uspekhi*, 8:522–577, April 1966.

Appendix A

Technical Information on the ROTSEI-IIa telescope

The ROTSEIII information presented here is taken from [2]. The basic optics of the ROSTEIII type of telescope are built around a 450.0 mm Cassegrain telescope design with a focal ratio of f/1.80 and a field corrector for total focal length of 850.0 mm. This works out to a plate scale of 3".28 per pixel and a total field of view of 2°.62.

The ROTSEIII telescopes use a Marconi Applied Technologies CCD42-40-2-343 type Charged Couple Device (CCD). It is 2048 pixels by 2048 pixels, each pixel being 13.5 μm on a side. It has an 8 e^- readout noise at 20° C and 1MHz clock rate.

Figure A.1 contains the Spectral Response of the CCD from the manufacturer's technical specifications [64]:

Table A.1: Spectral response of the Marconi Applied Technologies CCD42-40-2-343 type CCD

Wavelength (nm)	Minimum QE (%)		Typical QE (%)		Photo response
	midband	broadband	midband	broadband	non-uniformity (in %)
350	15	20	25	40	5
400	40	52	55	75	3
500	85	90	75	84	3
650	85	90	75	77	3
900	30	42	30	38	5

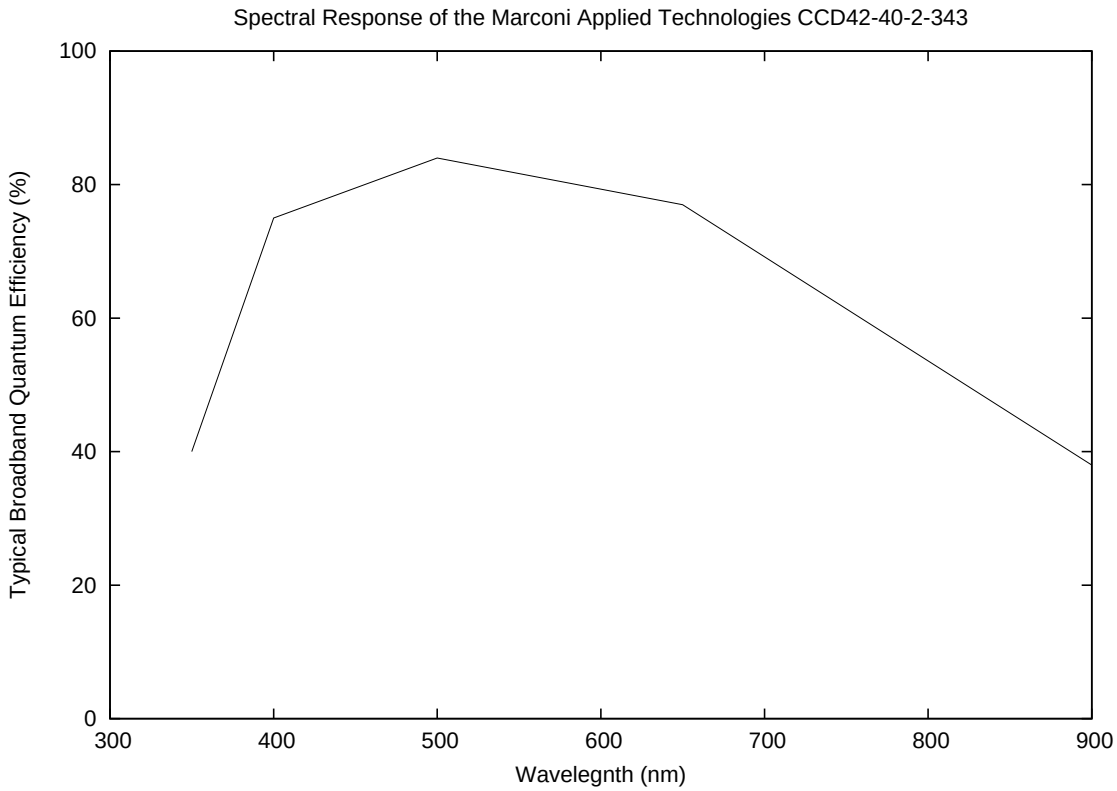

Figure A.1: Spectral response of the Marconi Applied Technologies CCD42-40-2-343 type CCD

Appendix B

Basics of IRAF Photometry

Here we list the specific IRAF[1] tasks used to manage the very large volume of data encountered in this study.

- daofind: This task finds stars on the plate by measuring the statistics of the pixel counts and selecting the centre of regions that deviate by more than a given Full Width Half Maximum (FWHM). These are the stars on the image.

- phot: This task takes the stars found by the previous task and does a very simple annular photometry to obtain a rough magnitude, sky value and error.

- pstselect: The output of the last step is used to select 30 stars that are a minimum of 11 pixels away from any other star and can be used to build a point-spread function (PSF) which will allow a much more precise magnitude and error to be determined for all stars.

- psf: This actually builds the PSF function. Moffat25 was selected for this study.

- allstar: This uses the PSF model derived by psf for 30 stars to measure the magnitudes of all stars in the field. It also sorts and removes stars as it goes through the files of the preceding steps and the image so that it can manage crowded star fields like the SMC and LMC.

B.1 Differential Photometry and Multiphot

These programs were used or written to control the large amount data from the dense plates containing about 30,000 stars per field.

- Multiphot: Multiphot is an external program that is accessed via a script inside the command language of IRAF. It groups stars that are in similar positions on different plates and of similar magnitudes as one star. It allows rapid comparison of an individual star's magnitude across multiple plates which is essential for building lightcurves. Multiphot would not return files if the whole data set from IRAF was used at once. So a shell script was written to select a section of the output from allstar and run Multiphot on that section.

[1]IRAF is distributed by the National Optical Astronomy Observatories, which are operated by the As- sociation of Universities for Research in Astronomy, Inc., under cooperative agreement with the National Science Foundation

- dpsetup: This program provides all the set-up files for dp (differential photometry) to work. This software was written by Gordon Sarty.
- dp: This program provides the actual differential photometry that the lightcurve is based on. This software was written by Gordon Starty.

After these steps the result is a light curve for the star of interest as well as light curves for the comparison star and check star(s).